Modelling scenarios of contaminant transport in an equivalent porous medium

Department of Civil, Environmental, Land, Building Engineering and Chemistry
RISK AND ENVIRONMENTAL, TERRITORIAL AND BUILDING DEVELOPMENT
Ph.D. Program
SSD: ICAR/02– HYDRAULIC AND MARINE CONSTRUCTION AND HYDROGEOLOGY

Final Dissertation

Modelling scenarios of contaminant transport in an equivalent porous medium

---

by
Alessandra Campobasso:

Supervisors:

Prof. Alberto Ferruccio Piccinni

Prof. Vito Iacobellis

Coordinator of Ph.D. Program:
Prof. Michele Mossa

Course n°34, 01/11/2018-31/01/2022

Politecnico di Bari

Department of Civil, Environmental, Land, Building Engineering and Chemistry

RISK AND ENVIRONMENTAL, TERRITORIAL AND BUILDING DEVELOPMENT

Ph.D. Program

SSD: ICAR/02– HYDRAULIC AND MARINE CONSTRUCTION AND HYDROGEOLOGY

Final Dissertation

Modelling scenarios of contaminant transport in an equivalent porous medium

by

Alessandra Campobasso:

Referees:

Geol. Vito Specchio

Ing. Michele Vurro

Supervisors:

Prof. Alberto Ferruccio Piccinni

Prof. Vito Iacobellis

Coordinator of Ph.D Program:

Prof. Michele Mossa

Course n°34, 01/11/2018-31/01/2022

EXTENDED ABSTRACT

Groundwater represents the largest supply of drinking water in the world (25-40%). Increasing urban development and increasing industrial activities, growing water demand due to climate change, and the consequent increase in urban runoff volumes due to the presence of sealed surfaces are causing adverse effects on groundwater both quantitatively and qualitatively. To address water stress, Managed Aquifer Recharge (MAR) represents an engineered approach to water security. MAR techniques aim to recharge the aquifer under controlled conditions for the purpose of subsequent recovery or as a barrier to prevent seawater intrusion. The reuse of urban water to implement this strategy is adopted from the perspective of environmental sustainability. However, the presence of residual contaminants in the injected stream challenges the feasibility of this solution because it may affect human health. In this context, the site modeled in the present work is located adjacent to the municipality of Avetrana, a place in which a confluence will be built from a channel in order to collect stormwater and floodwater thus protecting the town. The case study has a high level of hydraulic disturbance that makes it necessary to evaluate the vulnerability to pollution of the karst aquifer, which is characterized by a low anti-pollution capacity and therefore very fragile. As a result, it was necessary to perform a numerical simulation of groundwater flow and mass transport in the affected area. FEFLOW software, based on the finite element method, was used to determine the three-dimensional numerical groundwater model. The groundwater flow field was obtained by inputting boundary conditions and parameters derived from hydrogeological field surveys and literature review. Specifically, the methodology involved developing the conceptual hydrogeologic model of the aquifer and then modeling the mass transport of a hypothetical contaminant under different scenarios.

Considering that the input conditions in the transport model represent extreme and occasional situations, the modeling performed showed that the geologic structure represents a potential barrier to pollution.

To sum up, the purpose of this study was to make the model a good approximation of the groundwater system and to provide reference to prevent pollution in karst aquifers.

key words: Contaminant transport, Karst aquifer, Equivalent Porous Media, Vadose zone, Numerical modelling, FEFLOW.

EXTENDED ABSTRACT

Le acque sotterranee rappresentano la maggiore risorsa per l'approvvigionamento delle acque per l'uso potabile nel mondo (25-40%). Il crescente sviluppo urbano, l'aumento delle attività industriali, la crescita della domanda di acqua dovuta al cambiamento climatico e il conseguente l'aumento dei volumi di runoff urbani dovuti alla presenza di superfici impermeabilizzate stanno determinando effetti negativi nei confronti delle acque sotterranee sia da un punto di vista quantitativo che qualitativo. Per affrontare lo stress idrico, la ricarica gestita delle falde acquifere (MAR) rappresenta un approccio ingegneristico alla sicurezza idrica. Le tecniche MAR mirano a ricaricare l'acquifero in condizioni controllate allo scopo di un successivo recupero o come barriera per prevenire l'intrusione di acqua marina. Il riutilizzo delle acque urbane per attuare questa strategia è adottato dal punto di vista della sostenibilità ambientale. Tuttavia, la presenza di contaminanti residui nel flusso iniettato pone attenzioni particolari a questa soluzione perché può influenzare la salute umana. In questo contesto, il sito modellato nel presente lavoro è posto in adiacenza al comune di Avetrana, luogo dove si è prevista la confluenza da parte di un canale di imbrigliamento e raccolta delle acque meteoriche e alluvionali a protezione dell'abitato. Il caso studio ha un alto livello di disturbo idraulico che rende necessario valutare la vulnerabilità all'inquinamento dell'acquifero carsico, che è caratterizzato da una bassa capacità antinquinamento e quindi molto fragile. Pertanto, è stato necessario eseguire una simulazione numerica del flusso e del trasporto di massa delle acque sotterranee nell'area interessata. Il software FEFLOW, basato sul metodo degli elementi finiti, è stato utilizzato per determinare il modello numerico tridimensionale delle acque sotterranee. Il campo di flusso delle acque sotterranee è stato ottenuto inserendo condizioni al contorno e parametri derivanti da indagini idrogeologiche di campo e revisio-

ne della letteratura. In particolare, la metodologia ha comportato lo sviluppo del modello idrogeologico concettuale dell'acquifero e successivamente la modellazione del trasporto di massa di un ipotetico contaminante in diversi scenari.

Considerando che le condizioni di input nel modello di trasporto rappresentano situazioni estreme e occasionali, le modellazioni effettuate hanno dimostrato che la struttura geologica rappresenta una potenziale barriera all'inquinamento. Per riassumere, lo scopo di questo studio è stato quello di rendere il modello una buona approssimazione del sistema idrico sotterraneo e di fornire riferimenti per prevenire l'inquinamento negli acquiferi carsici.

key words: Trasporto di contaminanti, Acquifero carsico, Mezzo Poroso Equivalente, Zona vadosa, Modellazione numerica, FEFLOW.

INDEX

1. INTRODUCTION

The concept of aquifer vulnerability is now a major issue, which has interested researchers and policy makers from all over the world in order to raise awareness and find ways to protect groundwater from pollution. In fact, due to overexploitation, increased pollution and thus growing development activities, the protection of this vital resource is threatened. The need to protect aquifers arises from the need to use groundwater as a source of supply in domestic, agricultural, industrial and other sectors, as well as to sustain ecosystems in many countries around the world. In addition, some studies predict that the demand for groundwater supply will tend to increase in the future due to numerous factors such as intensification of agriculture, land use changes, population growth, rapid growth in urbanization and industrialization resulting in increased emission of pollutants. In addition, climate change and global warming will have profound repercussions on the qualitative and quantitative condition of groundwater. In order to cope with these problems and therefore to manage groundwater resources in a sustainable way through effective policies and decision-making processes, it is necessary to assess the vulnerability of groundwater. This assessment allows for efficient management strategies to mitigate groundwater pollution and to determine appropriate land use patterns and practices.

When referring to aquifer vulnerability, we are referring to the susceptibility of an aquifer to be adversely affected by a contaminant load imposed from the

land surface (Foster et al., 2013), in other words it is defined as the probability that contaminants will percolate and diffuse from the land surface into the groundwater system. Karst aquifers are the hydrogeologic structures with the greatest exposure to this risk because they are characterized by rapid infiltration into the subsurface through a network of discontinuities. In fact, the presence of discontinuities, conduits and karst caves represent the main means of contaminant infiltration. The water, quickly infiltrating into the soil and subsoil, rapidly travels considerable distances through unknown paths. Within these dynamics the transportation and release of pollutants occurs. These specific characteristics make karst aquifers very vulnerable to pollution sources. For this reason, it is of great necessity to develop appropriate techniques to manage karst landscapes and protect karst resources.

In this context, a groundwater management strategy can be introduced, namely MAR managed aquifer recharge, whose purpose is to protect and improve water quality and secure stressed groundwater systems. MAR is the intentional recharge of an aquifer for subsequent recovery or environmental benefits and is a valuable method for sustainable water resource management (Dillon et al., 2009; Ringleb et al., 2016). On the one hand, this results in increased groundwater storage in order to ensure the supply of drinking and irrigation water at any time of the year, but also contributes in terms of flood prevention. Other benefits from this assisted recharge were also evaluated such as reducing saltwater intrusion into coastal aquifers, preventing soil subsidence, and improving source water quality by treating soil aquifers. A study by Dillon et al. (2018) found that MAR implementation has accelerated at a rate of 5% per year over the past few decades, and currently MAR has reached an estimated 10 km3 per year. The International Groundwater Resources Assessment Center has compiled the main techniques for managing groundwater recharge by identifying the sources used, i.e., surface water from rivers or lakes, stormwater runoff, and reclaimed water. Among the techniques used, the most applied are those involving recharge through wells and infiltration methods: wells allow di-

rect recharge of the aquifer, which can often be overlain by surface layers with low permeability, while through diffusion methods recharge occurs with the infiltration of water in the unsaturated zone. Despite the apparent simplicity this technique requires an understanding of the response of the system with respect to field conditions, as ineffectiveness issues may occur due to the complexity of site-specific hydrogeologic conditions to processes occurring at various scales. Through numerical modeling that includes scenario analysis and forecasting, it is possible to estimate the feasibility of a MAR method applied to a given site. However, being a topic of recent interest, there are not many specific review studies about the applications of this technique in terms of the choice of modeling software for each technique and the best conditions for implementation (Ringleb et al., 2016).

The lack of systematic and comprehensive studies has also been found with regards to understanding the mechanism of clogging, the likely presence of damage to the aquifer, and the imperfection of theory in calculating infiltration (Zhang et al., 2020) One of the most concerning issues is clogging as it results in a reduction in permeability over time (Bouwer, 2002; Ventura Country, 2011). Clogging also can occur when infiltrating water mobilizes colloidal clay present on the surface of solid soil particles or when clay particles are dispersed by infiltrating water with low electrolyte levels (Torkzaban et al., 2015; Bradford et al., 2015). Although this problem will not be evaluated during the research study, it is always necessary to evaluate the appropriate location of charging devices (Edwards et al, 2016). In addition to this issue, another issue of great interest is the impact that this assisted recharge may have result in on groundwater quality. Several studies including those by Mason et al. (1999), Datry et al. (2004), and Tedoldi et al. (2016) have shown that the vadose zone can result in a slowing of pollutant propagation through pollutant retention and biodegradation processes. Aquifer filtration and sorption processes may contribute to the improvement of water quality during transport and storage in the subsurface by removing organics, nutrients, and metals from the source water. However, it

has not been possible to elucidate upon the factors influencing this process and thus assess the actual efficiency of these biochemical processes. Furthermore, recent studies (Fakhreddine et al., 2021; Standen et al., 2020) have shown that these same processes can also cause non-intentional degradation of water quality through the mobilization of potential naturally occurring toxic contaminants. Specifically, the mode of managed aquifer recharge could after geochemical and hydrological conditions, resulting in the release of geogenic contaminants (e.g., arsenic, fluoride, molybdenum, manganese, and iron) through desorption and dissolution processes (Fakhreddine et al.,2021). This issue presents a challenge in the MAR strategy approach that is likely to be ineffective in terms of water improvement. The impact that these contaminants can have on groundwater quality depends on both the design and operation of infiltration systems and the hydrogeochemical characteristics of aquifers. It is necessary in the design phase to carefully evaluate the strategies adopted for the mitigation of contamination. The most widely used tool for solving problems related to water resources management is numerical modelling. Models allow us to test different real situations, estimate hydraulic parameters, and predict aquifer responses to changes of various types. Modelling in karst aquifers, however, is problematic. These aquifers are characterized by different permeabilities and flow paths and are dominated by secondary porosity such as fractures and tertiary porosity (for example: conduits). Some studies have shown the ineffectiveness of numerical models in representing the real behaviour of karst aquifers, which requires a deep knowledge of the distribution of subsurface fracture and conduit systems. The high degree of heterogeneity and anisotropy in the hydrogeological properties of karst aquifers represents a limitation in the validity of numerical models. In that regard, the approach used in the present study was the Equivalent Porous Medium (EPM) to simulate the flow and transport of contaminants in the karst aquifer considered. The EPM approach assumes that the rock matrix, including fractures and conduit networks can be represented by an equivalent porous medium with equivalent hydraulic conductivity in a given ar-

ea (Anderson et al., 1992). Although some studies have shown that contaminant transport in these aquifers is primarily influenced by the karst conduit network rather than the hydraulic conductivity of the matrix, this approach still allows for representative results depending on the degree of karstification of the aquifer and the scale of the modelling effort. However, questions remain about the actual reliability of this approach and with what temporal resolution groundwater level fluctuation in karst can be replicated (Ghasemizadeh et al., 2015).

In this context comes the following research project that aims to evaluate the propagation of a hypothetical pollutant with a concentration of 100 mg/l in the area where it is expected the confluence of water from a channel of harnessing and collection of rainwater and floodwater to protect the adjacent town is expected. Specifically, the objective will be to create a 3D model that can simulate groundwater flow and pollutant transport within the unsaturated zone. The modelling software used will be FEFLOW (Finite Element subsurface FLOW and transport system), based on the finite element method.

The case study has a strong practical relevance as it manages to fully represent the above issues in a field of application of great hydrogeological complexity. The geology of the site where the collected water is expected to be delivered consists of two structural units having respectively homogeneous hydrogeological characteristics. The first superficial hydrogeological unit is constituted by calcarenites averagely cemented with cemented levels with vacuoles and little cemented levels weakly silty with very variable thicknesses between 0,2 up to 28 meters from the campaign plan (variability can be attributable to the different dislocation of the limestones in the subsoil). The second unit, on the other hand, consists of organogenic limestone and grey-white limestone. This unit is intensely affected by primary and secondary discontinuities. Through the investigations carried out on site it was possible to attribute the values of the hydraulic characteristics related to the two geological units, through the approach of the equivalent porous medium.

Since the value of the equivalent porosity of the limestone layer was not investigated in the borehole tests, it was decided to perform a sensitivity analysis of the porosity in the various transport simulation scenarios, evaluating how much the variation of this characteristic affects the modelling. Chapter 2 will highlight the methodologies and therefore the theory behind the constructed model, while Chapter 3 will present the results obtained with relation to the case study. The construction of the model will be illustrated with the relative simulations in the several cases analysed and finally the results will be discussed.

2. METODOLOGY

This chapter embodies the methodological underpinnings of the present work.

2.1. EQUIVALENT POROUS MEDIUM

Karst aquifers provide 40% of drinking water sources. In the Apulia Region these structures represent the only potable water resource present in the territory determining a great influence on morphological, hydrological, and hydrogeological characters. Karst waters are and will increasingly be a pillar of sustainable development in terms of water resources for human consumption (National days of Speleology, sponsored by the Italian Committee for 2002 Aim) thus the protection of these sources is of fundamental importance.

Karst aquifers are hydrogeological structures characterized by the rapid infiltration of water into the subsoil due to the presence of discontinuities. Discontinuities, conduits and karst caves represent main diffusion pathways also for pollutants that can infiltrate into the soil. These hydrogeological structures are characterized by the propensity for rapid transfer of pollutants and therefore the propensity to be subject to pollution. Specifically, exposure to contamination by karst aquifers is due to the presence of the interconnected network of voids to springs through which contaminants travel rapidly. A topic of great re-

flection related to the vulnerability of karst aquifers is the extreme difficulty or rather the near impossibility of restoring the pristine condition once contamination has occurred (Parise, 2007).

It is very difficult to simulate the flow of water and the transport of harmful substances in karst aquifers because of their heterogeneous structure.

This situation is further complicated by the fact that karst aquifers have very variable characteristics under different hydrological conditions. Karst aquifers are volumes composed of carbonate rocks, such as limestones and dolomites, influenced by karstification processes. The phenomenon of karstification is determined by chemical dissolution by acidic waters on soluble rocks. Because of this process different forces of discontinuity are determined, both on the surface through the formation of sinkholes and in the subsurface assuming forms of interconnected voids and cavities. Large volumes of water are stored within these voids and cavities created by karstification. An issue related to the inherent heterogeneity and anisotropy of rock clusters is the difficulty in predicting the distribution of flow velocity, both in space and time, which would allow the definition of respect zones with chronological criteria (Berkowitz, 2002; Lipfert et al., 2004). In addition, the characteristic structure of the discontinuities results in an increase in the ensemble value of indirect transmissivity capacity.

Indeed, the karst aquifer is characterized by high transmission rates. The heterogeneity of the medium and the divergent flow to undetermined areas generates a complexity in understanding the karst system that manifests itself in an anisotropy towards the mechanisms of groundwater infiltration and circulation. Consequently, the interpretation of hydrological parameters, such as porosity and hydraulic conductivity, is also problematic. The different structures such as tectonic fracturing filled with residual materials, in the case of Apulia consisting of red soil, and the most pronounced karst voids, determine porosity of various orders. Specifically, three types of structures can be defined in karst systems as a result of different formation processes: micropores through the formation of carbonate rocks, fractures as a result of tectonic phenomena and

finally karst ducts following the process of karstification. These structures are interconnected determining the flow of water between the surface layers and the sub-layer. In order to define effective porosity for the purpose of hydrogeology studies in the particular Apulian context, it is convenient to neglect the intergranular porosity of the matrix altogether, the latter being understood as the porosity of the underlying limestone (Cotecchia et al., 2017).

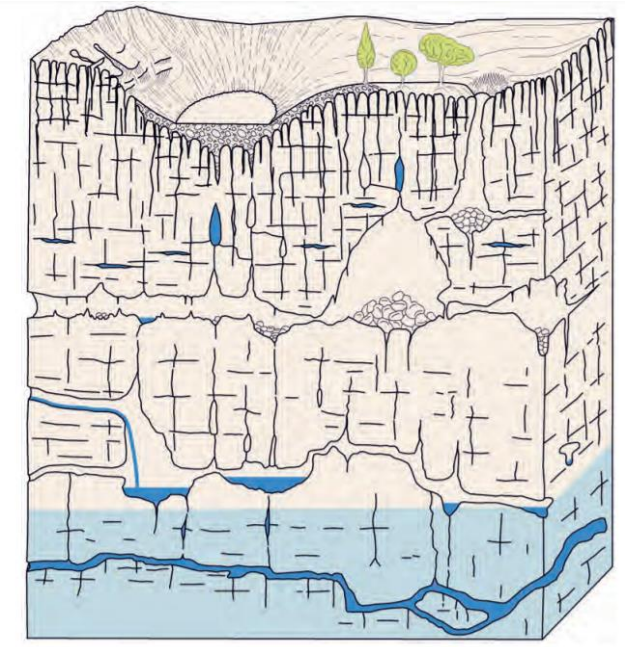

Fig. 2.1.1 – Representation of an ideal karst massif

In order to model the behaviour of the pollutant in the soil, and therefore to determine the most effective remediation intervention, it is necessary to identify the modelling approach that best represents the groundwater flow to be analysed. The presence of karst discontinuities conditions groundwater flow, which is channelled into preferential flow paths and water levels. This complex structure determines a complexity in terms of reconstruction of the water model as it is difficult to attribute the parameters that represent the flow within the fis-

sure network and therefore the real geological structure. In addition, the conduits present in karst aquifers are difficult to locate and spatially distribute, which affects the validity of the results through numerical models (Chen Z. et al., 2014). Regarding the flow characteristics in karst aquifers, the flow varies from laminar to turbulent, with laminar flow in the rock matrix and predominantly turbulent flow in the conduits.

Numerical modelling can enable the representation of water flow and pollutant transport in these complex systems. This can occur if there is equivalence between the conceptual model and the numerical model, and if the conceptual model is representative of the actual situation. Numerical models refer to several approaches to represent the fractured system:

- Equivalent continuous porous medium approach, through which karst features are approximated with a conceptualized equivalent continuous medium.
- discrete approach, in which the system is represented through individual families of discontinuities.
- dual-porosity model, in which filtration occurs both in the discontinuities and within the porous matrix.

The equivalent porous medium approach assumes that the behaviour of the fractured system is equivalent to the behaviour of porous media and can be represented by an equivalent porous medium with equivalent hydraulic conductivity in a given area.

As for the discrete approach, this allows the determination of a crack lattice to which appropriate boundary conditions are applied. Discrete models developed both in two dimensions (Long and Witherspoon, 1985; Robinson, 1982) and in the three-dimensional domain (Hung and Evans, 1985; Rasmussen, 1988; Andersson and Dverstorp, 1987; Dverstorp and Andersson, 1989), explicitly simulate the flow in each individual fracture using, for example, the Navier-

Stokes equation (Bear, 1993). This approach allows the analysis of water circulation conditions as a function of individual discontinuities and their parameters, while the effects produced by the presence of true fracture bands are generally neglected.

Double-porosity models (introduced by Barenblatt et al. in 1960 and later implemented by Warren and Root in 1963 and by Kazemi in 1969) try to combine the simplification of continuous models with the complexity of discrete ones, considering simultaneously but separately the water motion inside the intact rock (primary porosity) and the one in the crack network (secondary porosity). In double porosity models, in fact, the equations governing both media (continuous and fractured) are implemented, between which flow exchanges at the interface are evidently possible.

The approach used in the present study for numerical modelling of flow and transport is the Equivalent Porous Medium (EPM) approach, explained below. This approach was chosen because the modelling was supported by the implementation of data collected from field analyses. From the reconstructions determined through the survey activities, it was possible to attribute the values of the hydrogeological and hydraulic parameters in the area of interest of this study. The EPM approach allows the characteristics of fractured rock behaviour to be approximated to a continuous medium by mediating the properties of the rock matrix over a statistically representative volume. The more fractured the aquifer the more this approach is justified. REV (Representative Elementary Volume) is defined as the minimum volume of the porous medium that allows statistically significant averaging of the properties required in the continuous approach (J. Bear, 1972) and for which the macroscopic laws are valid. Figure 2.2.1 shows a diagram of a hypothetical graphical representation of the porosity of a medium measured on samples of increasing volume V1, V2, . . ., at a point P. Below this volume, there is no single value that can represent the porosity at point P. Volume V3 is the REV or the minimum volume that includes a sufficient number of pores in the continuous approach.

The size of the mediation volume depends on the soil. Within the REV, fracturing is assumed to be pervasively distributed, i.e., random and uniform (Piccinini et al., 2014). There are numerous examples in the literature regarding the use of the EPM approach for both flow and transport simulation, which is also considered effective on regional-scale karst aquifers (Scanlon et al., 2003).

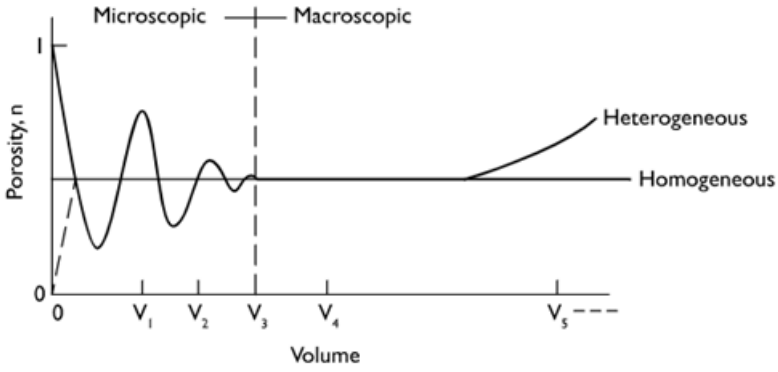

Fig. 2.1.2 – V_3 Representative element volume (Bear 1982)

EPM models do not directly account for preferential flow in fractures, but approximate the large-scale conductivity of the fracture network, often with anisotropy in plan view and vertical perspective. Through the model equivalent to the actual medium, properties related to the fractured aquifer can be determined that are difficult to identify through tectonic and geophysical studies that fail to detect discontinuities at depth. Thus, this approach allows solving pollutant flow and transport problems when information about these structures is not available. The flow equations underlying flow principles apply at a macroscopic scale. However, some flow and mass transport phenomena cannot be analyzed at this scale but considering a macroscopic approach.

The main disadvantage of this approach results from the lack of information on the spatial variation of hydraulic loading and groundwater flow directions. Modeling through this approach is performed in a stochastic and probabilistic

framework and not through a deterministic simulation approach. Therefore, it is necessary to set parameters relevant to the case study.

It is emphasized that the conceptual model constitutes a systematisation of the physical system finalized to idealize the real situation. Such simplification is necessary due to the fact a complete reconstruction of the real domain would need an excessive number of necessary information.

2.2. FEFLOW

FEFLOW (Finite Element subsurface FLOW and transport system) is one of the most sophisticated numerical codes available for the simulation of flow and transport processes in porous media, under saturated and unsaturated conditions. The modelling platform features an advanced graphical environment to simulate subsurface flow dynamics in complex situations and contaminant transport in the aquifer.

The use of a finite element approach (as opposed to the finite difference method used by classical numerical groundwater flow models) provides extreme flexibility in the spatial discretization of the domain, improved representation of natural elements and anisotropy conditions. In addition to the better representation of the calculation domain, compared to the most common simulation codes, FEFLOW offers other important advantages and potentialities in the representation of the local dynamics, among these the possibility of complete desaturation of the calculation layers, of strategic importance in the case of high gradients.

Through the interactive groundwater modelling system promoted by FEFLOW, it is possible to determine three-dimensional and two-dimensional models, with horizontal, vertical and axisymmetric representations of the model. The obtained models can analyse groundwater fluxes and mass and heat transport in various saturated situations, analysing transient or stationary con-

ditions. In addition, the software enables multi-species reactive transport in groundwater environments with or without one or more free surfaces.

FEFLOW is effectively used to analyse the spatial and temporal distribution and allows modelling the reactions of groundwater contaminants. It also allows the simulation of geothermal processes, the estimation of the duration and travel time of chemical species in aquifers, the planning and designing of remediation strategies and interception techniques and assisting in the design of alternative solutions and effective monitoring schemes. Model implementation is enabled through interfaces to GIS and CAD data and through specific plug-ins that allow the addition of external codes and programs.

FEFLOW's modelling is based on the finite element method (FEM). This type of modelling approach is a very versatile numerical resolution tool because it allows simplifying the numerical resolution of irregular domains by discretizing them into regular shaped subdomains that are subsequently merged. In this way, conservation and behaviour laws are assigned for each subdomain without altering the differential equations related to each of the finite elements. The FEM allows functions to be assigned within each of the finite elements into which the domain has been divided. The functions are assigned by identifying the values of relative variables in the nodes around the element. This allows the number of unknowns to be reduced to a finite value within the discretized domain, expressing the field in terms of approximate functions. This methodological approach is very useful in cases where there are internal constraints such as faults in the models or to simulate seepage surfaces or source or loss points.

In FEFLOW the domain discretization operation is performed through the "Supermesh" operation, through which the finite element mesh is determined. In 2D modelling the mesh is composed of an arbitrary number of polygons, lines and points, while in 3D it is defined by layers, solids or lines and points. The denser the mesh, the better the numerical accuracy and the greater the computational effort. During simulation, the results are computed on each node of the

mesh and interpolated within the finite elements. There are many different strategies for discretizing complex domains into triangles and quad elements (FEFLOW 7.0 user guide, 2016):

- Advancing Front is a simple triangle meshing algorithm. With this, no lines or points are supported in the supermesh, which, if present, are ignored during the generation process. Its main advantages are its speed and its ability to produce very regular shaped elements.
- GridBuilder is a triangulation algorithm that supports polygons, lines and points in the supermesh.
- Triangle is an extremely fast triangulation code that supports very complex combinations of polygons, lines and points in the supermesh. It also allows you to specify a minimum angle for all finite elements created.
- Transport mapping is the algorithm used in FEFLOW to generate meshes of quadrilateral elements. During this meshing, lines and points are ignored and all generated polygons are defined by four nodes.

The mathematical modelling underlying the FEFLOW computational code is based on the following basic physical principles:

- Conservation of fluid mass and solid continuous media.
- Conservation of the mass of chemical constituents and contaminants.
- Conservation of the moment of the fluid and of the continuous medium.
- First law of thermodynamics or energy conservation law.

2.3. PRINCIPLES

The unsaturated flow principles

The vertical distribution of groundwater is characterized by the aeration zone or unsaturated zone. The aeration zone, or the unsaturated zone, consists of pores filled partially with water and partially with air. In the saturation zone all pores are occupied by water under hydrostatic pressure.

Soil water retention depends on capillarity and molecular attraction of particles. As the amount of pore water in the soil increases, gravity increases and capillarity decreases. Thus, even after infiltration has ceased, percolation can continue. When the water rate decreases and the soil becomes dry, capillarity plays an important role. No further percolation can occur after the capillary and gravitational forces are balanced.

The upper surface of the saturated zone is the water table, or the phreatic surface, that is characterized of atmospheric pressure. The area above the water table is called capillary zone, or capillary fringe, where, due to capillary attraction, water is held at less than atmospheric pressure.

Water retention in soils is due to a combination of capillarity caused by surface tension at the air-water interface and by molecular attraction at the interface solid-liquid interface. If we consider a capillary tube to represent pore space, capillary rise h_c can be derived from a balance between the surface tension of the water and the weight of the raised water.

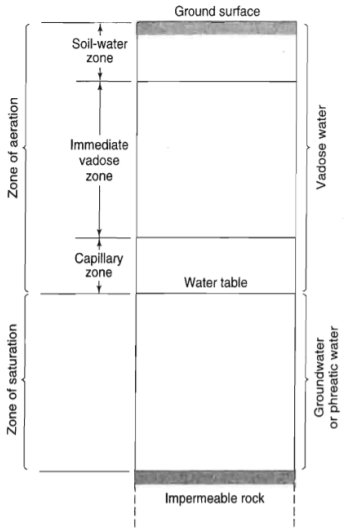

Fig. 2.3.1 – Divisions of subsurface water

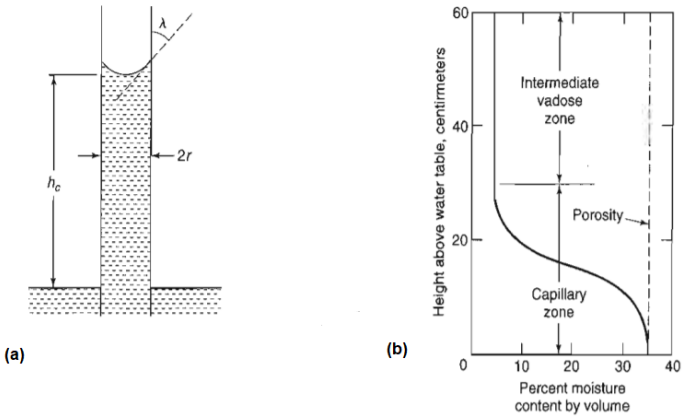

Fig. 2.3.2 – (a) Rise of water in a capillary tube. – (b) Distribution of water in a coarse sand above the water table after drainage

The thickness of the capillary zone varies inversely with the pore size of the soil or rock.

$$h_c = \frac{2-\sigma}{\rho g d} cos\alpha \qquad (1)$$

σ: water surface tension $[N/m]$

ρ: water density $[kg/m^3]$

d: micropore diameter $[m]$

α: wetting angle $[deg]$

The fraction of void space in the porous material is defined by porosity ratio (Orzechowski at al.,1997):

$$\eta = \frac{V_v}{V_t} \qquad (2)$$

η: porosity ratio $[-]$

V_v: void volume $[m^3]$

V_t: total volume of soil $[m^3]$

The amount of water contained in soil may be characterized by water content or moisture content. Volumetric water content θ is defined as:

$$\theta = \frac{V_w}{V_t} \qquad (3)$$

θ: volumetric water content $[m^3/m^3]$

V_w: volume of water contained in soil $[m^3]$

Thus, gravimetric water content θ_m is defined:

$$\theta_m = \frac{m_w}{m_t} \qquad (4)$$

θ_m: gravimetric water content $[kg/kg]$

m_w: mass of water contained in soil $[kg]$

m_t: mass of soil $[kg]$

The degree of saturation is the fraction of actual volumetric content to the volumetric water content of tested soli in saturated conditions (Kowalik, 2007)

$$S = \frac{\theta_a}{\theta_s} \qquad (5)$$

S: degree of saturation

θ_a: actual volumetric water content $[m^3/m^3]$

θ_s: saturated volumetric water content $[m^3/m^3]$

The hydraulic head is comprised of two portions, the pressure head that represents the internal energy of water and the elevation:

$$h = \frac{p}{\rho g} + z \qquad (6)$$

In the expression of total head, there is no term for velocity head because the velocities are small.

A general form of the governing equation of the groundwater flow is:

$$\pm W + \frac{\partial}{\partial x}\left(k_x \frac{\partial h}{\partial x}\right) + \frac{\partial}{\partial y}\left(k_y \frac{\partial h}{\partial y}\right) + \frac{\partial}{\partial x}\left(k_z \frac{\partial h}{\partial z}\right) = S_s \frac{\partial h}{\partial t} \qquad (7)$$

k_x, k_y and k_z are components of the hydraulic conductivity tensor. The hydraulic conductivity depends on the material of the soil.

$\pm W$: is a general sinks/sources terms that are positive or negative and define the volume of inflow or outflow to the system per unit volume of aquifer per unit of time.

S_s: specific storage. About confining aquifers, total pores are fuel with water and Specific Storage is:

$S_s = (\alpha + n\beta)\rho g$

α: compaction of the soil

β: expansion

The governing equation is derived by mathematically combining the conservation of mass equation with Darcy's Law. Consider flow in an infinitesimal control volume.

This cube of porous material in known as a representative elementary volume or REV. Its volume is equal to $\Delta x \Delta y \Delta z$.

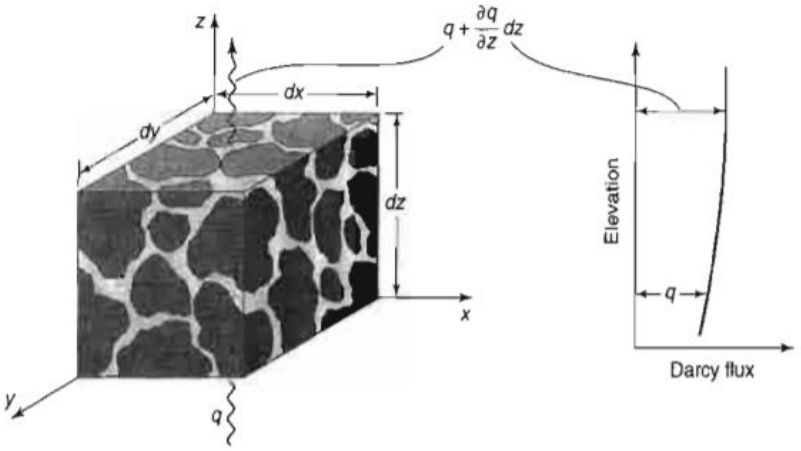

Fig. 2.3.3 – Control volume for development of the continuity equation in porous medium.

The flow of water through the representative elementary volume is the discharge rate Q:

$$Q = q_x i_x + q_y i_y + q_z i_z \qquad (8)$$

q_x, q_x, q_x: components of the Q vector

i_x, i_x, i_x: unit vectors along the x, y, and z axes.

The conservation of mass or the water balance equation states that inflow less outflow is equal to the change in storage and is expressed as:

$$\sum [\Delta(Q_{in} - Q_{out})] = \Delta_{storage} \qquad (9)$$

$\Delta_{storage}$ is represented by specific storage S_s, that is the volume of water released from storage per unit change in head per unit volume of aquifer:

$$S_s = -\frac{\Delta V}{\Delta h \Delta x \Delta y \Delta z} \qquad (10)$$

Combining these equations with the Darcy's law the governing equation is obtained.

Darcy's Law states that the flow rate divided by an area is directly proportional to the hydraulic gradient. The constant of proportionality is the hydraulic conductivity ks.

$$FLUX\ [LT-1](m/s) = \frac{Q}{A}\frac{(m^3/s)}{m^2} = q = -ks\frac{\Delta h}{\Delta x} \qquad (11)$$

Darcy's law in three dimensions is written as follows:

$$q_x = -K_x\frac{\partial h}{\partial x} \qquad (12)$$

$$q_y = -K_y\frac{\partial h}{\partial y} \qquad (13)$$

$$q_z = -K_z\frac{\partial h}{\partial z} \qquad (14)$$

In the unsaturated zone the flow equation is:

$$\pm W + \frac{\partial}{\partial x}\left(k_x\frac{\partial h}{\partial x}\right) + \frac{\partial}{\partial y}\left(k_y\frac{\partial h}{\partial y}\right) + \frac{\partial}{\partial x}\left(k_z\frac{\partial h}{\partial z}\right) = \frac{\partial h}{\partial t} \qquad (15)$$

The pores are partially filled with air and partially filled with water. The only water that you can take out from storage is by decreasing the saturation. Water

through the electrostatic forces between the polar bonds of the water molecules and the particle surfaces is bound to the particle surfaces in the soil.

Since the soil is dry and therefore water flows with more difficulty, the hydraulic conductivity K will not depend on saturation but on pressure.

$$k(\theta), \qquad \theta(P), \qquad therefore\ k(P)$$

Darcy's law for unsaturated flow can be expressed as:

$$q = -k_u(\theta)\frac{\Delta h}{\Delta z} \qquad (16)$$

$k_u(\theta)$: hydraulic conductivity as a function of the moisture content θ.

The suction head (or matric potential) ψ in the unsaturated flow is the energy caused by soil suction forces. Total head is the sum of the matric potential; that varies with moisture content, and gravity head:

$$h = \psi + z \qquad (17)$$

Darcy's law can be rewritten as:

$$q = -k_u(\theta)\frac{\Delta(\psi + z)}{\Delta z} \qquad (18)$$

It is possible to correlate the saturation gradient with the hydraulic conductivity, which is a function of the suction head. Because soil suction head varies with moisture content and moisture content varies with elevation, the suction gradient is defined as:

$$\frac{\partial \psi}{\partial z} = \frac{d\psi}{d\theta}\frac{\partial \theta}{\partial z} \qquad (19)$$

$\frac{\partial \theta}{\partial z}$: wetness gradient

$\frac{d\psi}{d\theta}$: specific water capacity

Darcy's law now is:

$$q = -k(\theta)\left(\frac{\partial \psi}{\partial z} + \frac{\partial z}{\partial z}\right) = -k\left(\frac{d\psi}{d\theta}\frac{\partial \theta}{\partial z} + 1\right) = -\left(k(\theta)\frac{d\psi}{d\theta}\frac{\partial \theta}{\partial z} + k(\theta)\right) \quad (20)$$

Defined the soil water diffusivity D $[L^2/T]$ as ratio of hydraulic conductivity to the water capacity of soil:

$$D = k(\theta)\frac{d\psi}{d\theta} \quad (21)$$

one can rewrite the above equation as:

$$q = -\left(D\frac{\partial \theta}{\partial z} + k(\theta)\right) \quad (22)$$

Whence Richard's equation in a one-dimensional form for unsaturated flow in a porous media is:

$$\frac{\partial \theta}{\partial t} = -\frac{\partial q}{\partial z} = \frac{\partial}{\partial z}\left(D\frac{\partial \theta}{\partial z} + k(\theta)\right) \quad (23)$$

The constitutive relationship of the hydraulic parameters in the unsaturated flow are the water retention curve and the hydraulic conductivity of soils.

Both moisture content θ and hydraulic conductivity k are functions of matric potential ψ.

Regarding moisture content, this in the soil is caused by the surface tension forces present between the meniscus curvature radius of the soil grains. for larger curvature radius there will be a higher moisture content, hence lower surface tension forces and lower tension loads.

Considering the soil-water retention constitutive relationship, the curve shows a different pattern depending on whether the soil is wet or dry, resulting in hysteresis behaviour. Hysteresis occurs, therefore, due to the entrapment of air in pockets connecting different pore sizes during humidification. Secondary hysteretic loops are determined when humidification and drying cycles alternate.

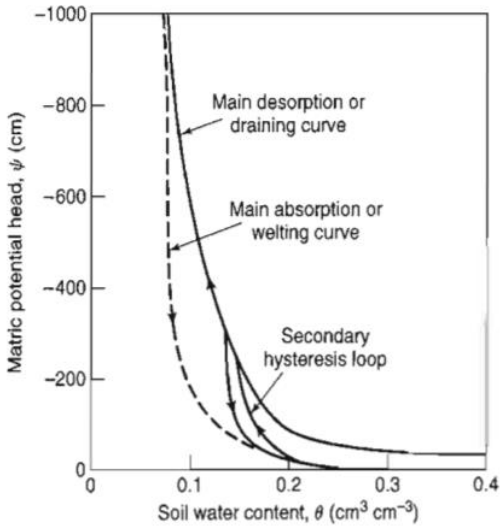

Fig. 2.3.4 – The effect of hysteresis on the function $\psi(\theta)$ of sandy loam topsoil during wetting and drying

The most widespread mathematical description of the shape of the water retention curve was presented by Van Genuchten (1980):

$$\theta = \frac{\theta_s - \theta_r}{[1 + (\alpha h)^n]^m} + \theta_r \qquad (24)$$

θ_r: residual volumetric water content

α, n, m: fitting parameters

The table below shows the values of the fitting parameters for water retention curve in the Van Genuchten's model:

Soil type	Saturated soil moisture θ_s	Residual soil moisture θ_r	Fitting parameters	
			α	n
	[m³/m³]	[m³/m³]	[1/cm]	[-]
Sands (average for Sand, Loamy Sand, Sandy Loam, Sandy Clay Loam)	0.396	0.052	0.0263	2.23
Loams (average for Loam and Clay Loam)	0.512	0.056	0.0407	1.19
Silts (average for Silty Loam and Silt)	0.428	0.031	0.0120	1.38
Clays (average for Clay, Sandy Clay, Silty Clay and Silty Clay Loam)	0.512	0.098	0.0178	1.30
Sand	0.380	0.110	0.0260	7.700
	0.250	0.153	0.0079	10.400
Silt loam	0.550	0.161	0.0367	1.572
Loam	0.500	0.060	0.0261	1.441
	0.520	0.218	0.0115	2.030
Sandy loam	0.042	0.010	0.0094	1.632
	0.335	0.074	0.0153	1.265
Fine sand	0.380	0.030	0.0226	7.339
Sandy loam	0.335	0.074	0.0153	1.265
Silt loam	0.388	0.173	0.0471	1.461
	0.469	0.190	0.0050	7.090
	0.369	0.131	0.0042	2.060
Sandy clay loam	0.402	0.112	0.0082	1.275
Clay	0.589	0.109	0.0007	1.419
	0.446	0.000	0.0015	1.170

Fig. 2.3.5 – Exemplary parameters of water retention curves for various soils.

Van Genuchten's model can also be presented in a form based on the degree of saturation applied in FEFLOW (Diersch, 2005):

$$S = \frac{S_s - S_r}{[1 + (\alpha\psi)^n]^m} + S_r \qquad (25)$$

S_r: residual saturation

The hydraulic conductivity in unsaturated conditions is defined as:

$$k_r = \frac{k}{k_s} \qquad (26)$$

k_r: relative hydraulic conductivity of soil

k: hydraulic conductivity

To model water movement and pollutant transport in soil as correctly as possible, knowledge of hydraulic conductivity under unsaturated conditions is necessary.

Due to the variation in soil saturation by water and soil pressure, defining the value of hydraulic conductivity in unsaturated soil is complex. Therefore, empirical models are used to calculate the value of hydraulic conductivity, the most common of which are listed below, which consider the following factors: the head of air inlet pressure, the degree of saturation, and the fitting parameters a, b, α, n, m, l.

Name	Formula
Brooks and Corey (1964)	$K_r = K_s, h \geq h_a$ $K_r = (\frac{h_a}{h})^{-n}, h < h_a$
Rijtema (1965)	$K = K_s, h \geq h_a$ $K_r = e^{\alpha(h-h_a)}, h_1 \leq h \leq h_a$ $K = K_1 \left(\frac{h}{h_1}\right)^{-n}, h < h_1$
Wind (1955)	$K = \alpha\lvert h\rvert^{-n}$
Gardner (1958)	$K_r = e^{ah}, K = \frac{a}{\lvert h\rvert^n + b}$
Van Genuchten (1980)	$K = K_s S^l \left[1 - \left(1 - S^{\frac{1}{m}}\right)^m\right]^2$

where: h_a – air entry pressure head [m], S – degree of saturation [-], a, b, α, n, m, l – fitting parameters.

Fig. 2.3.6 – The most popular formulas of unsaturated hydraulic conductivity empirical models.

Below are graphs of the trends in the constitutive relationships for soil water retention and hydraulic conductivity of two contrasting soil textures. Regarding the water retention curve, in figure a) clay soil retains more water than sandy soil. Figure b), on the other hand, shows the trend in hydraulic conductivity. This function does not vary linearly with the volumetric water content of the soil and varies with soil texture. For both soils, the curve decreases as the water content decreases.

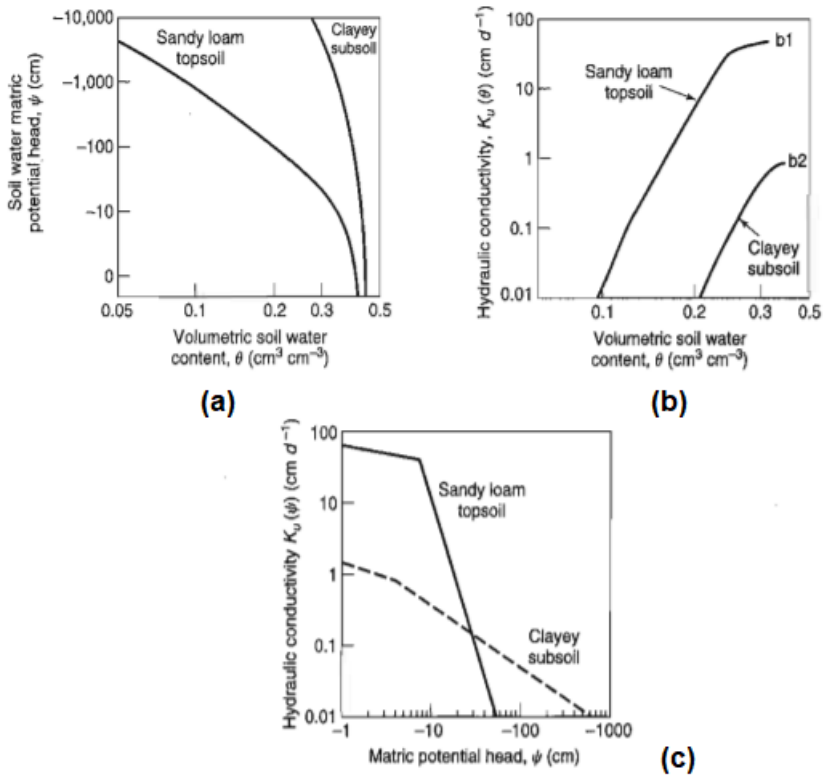

Fig. 2.3.7 – (a) $\psi(\theta)$ relationship – (b) $k(\theta)$ relationship – (c) $k(\psi)$ relationship of sandy loam and clayey horizons.

Figure c) outlines the hydraulic conductivity versus matric potential head curve: the trend for sandy soil decreases more rapidly than for clay as the ma-

tric potential head decreases. Furthermore, for low values of the matric potential head, which refers to higher suctions, the hydraulic conductivity of the clay loam is higher.

Below is a table of the constitutive relationships for soil water retention and hydraulic conductivity proposed by Brooks and Corey, Campbell, and Van Genuchten.

Hydraulic soil characteristic	Parameters	Parameter correspondence
	Brooks and Corey[13]	
Soil water retention $\frac{\theta-\theta_r}{\phi-\theta_r}=\left(\frac{h_b}{h}\right)^{\lambda}$	λ = pore-size index h_b = bubbling capillary pressure θ_r = residual water content ϕ = porosity	$\lambda=\lambda$ $h_b=h_b$ $\theta_r=\theta_r$ $\phi=\phi$
Hydraulic conductivity $\frac{K(\theta)}{K_s}=\left(\frac{\theta-\theta_r}{\phi-\theta_r}\right)^{n}=(S_e)^{n}$	K_s = fully saturated conductivity ($\theta=\phi$) h = matric potential S_e = effective saturation $n=3+\frac{2}{\lambda}$	$K_s=K_s$ $h=\psi$
	Campbell[16]	
Soil water retention $\frac{\theta}{\phi}=\left(\frac{H_b}{\psi}\right)^{1/b}$	ϕ = porosity H_b = scaling parameter with dimension of length b = constant	$\phi=\phi$ $H_b=h_b$ $b=\frac{1}{\lambda}$
Hydraulic conductivity $\frac{K(\theta)}{K_s}=\left(\frac{\theta}{\phi}\right)^{n}$	n = 3 + 2b	
	Van Genuchten[102]	
Soil water retention $\frac{\theta-\theta_r}{\phi-\theta_r}=\left[\frac{1}{1+(\alpha h)^{n}}\right]^{m}$	ϕ = porosity θ_r = residual water α = constant n = constant m = constant h = absolute value of matric potential	$\phi=\phi$ $\theta_r=\theta_r$ $\alpha=(h_b)^{-1}$ $n=\lambda+1$ $m=\frac{\lambda}{\lambda+1}$ $h=\lvert\psi\rvert$
Hydraulic conductivity $\frac{K(\theta)}{K_s}=\left(\frac{\theta-\theta_r}{\phi-\theta_r}\right)^{1/2}\left\{1-\left[1-\left(\frac{\theta-\theta_r}{\phi-\theta_r}\right)^{1/m}\right]^{m}\right\}^{2}$		

θ = water content; ψ = capillary suction, cm; $K(\theta)$ = hydraulic conductivity for given water content, cm/h

Fig. 2.3.8 – Soil water retention and hydraulic conductivity relationships.

Mass transport in soil

To determine the differential equation for solute transport in porous materials, we consider an elementary volume within the study domain characterized by internal and external solute flow. Given an elementary volume, the mass conservation equation:

$$\begin{bmatrix} Rate\ of\ change \\ of\ solute\ mass \\ within\ the\ element \end{bmatrix} = \begin{bmatrix} Solute\ flow\ out \\ of\ \text{the}\ element \end{bmatrix} - \begin{bmatrix} Solute\ flow\ within \\ the\ element \end{bmatrix} \pm \begin{bmatrix} Solute\ mass \\ loss\ or\ gain \end{bmatrix}$$

$$\frac{\partial C}{\partial t} = \frac{\partial}{\partial x_i}\left(D_{ij}\frac{\partial C}{\partial t}\right) - v_i\frac{\partial C}{\partial x_j} \pm Q_C \qquad (27)$$

x_{ij}: a curvilinear coordinate direction taken along the flowline,

v_i: the average linear groundwater velocity,

D_{ij}: the coefficient of hydrodynamic dispersion in the longitudinal direction)

C: the solute concentration.

This differential equation is called the advection-dispersion equation (ADE) and is valid in both the saturated and unsaturated zones.

Hydrodynamic dispersion and advection are the physical processes that determine the flow out of and into the elementary volume. The last term in the mass conservation equation considered can occur due to radioactive decay.

As a result of mechanical mixing and molecular diffusion, hydrodynamic dispersion is determined. The mechanical dispersion term in the equation is only considered for materials that are isotropic with respect to the dispersion properties of the medium.

Advection (or convection) is the component related to transport by the water table in the process of solute movement. The transport velocity is equal to the average linear groundwater velocity $\bar{u}$,

$$\bar{u} = v/n \qquad (28)$$

v= specific discharge

n= porosity

About the ADE equation, the coefficient of hydrodynamic dispersion can be expressed in terms of two components:

$$D_{ij} = a_{ij} v + D^* \qquad (29)$$

a_{ij}: a characteristic property of the porous medium known as the dynamic dispersivity, or simply as dispersivity

D^*: the coefficient of molecular diffusion for the solute in the porous medium.

The concentration versus time relation of the outflow is known as the breakthrough curve.

At a low velocity, diffusion is the important contributor to the dispersion, and therefore the coefficient of hydrodynamic dispersion equals the diffusion coefficient D*. At a high velocity, mechanical mixing is the dominant dispersive process, in which case $D_{ij} = a_{ij} v$. Larger dispersivity of the medium produces greater mixing of the solute front as it advances.

The dimensionless parameter ($\bar{v}$ d/D) is known as the Peclet number, where the average particle diameter is denoted by d. The exact shape of the relation between the Peclet number and D_{ij} = D* depends on the nature of the porous medium and on the fluid used in the experiments.

One of the characteristic features of the dispersive process is that it causes spreading of the solute, if the opportunity is available, in directions transverse to the flow path as well as in the longitudinal flow direction. The process of mechanical dispersion is directionally dependent even though the porous medium is isotropic with respect to textural properties and hydraulic conductivity.

3. RESULTS

In this chapter, after an overview of the case study, the steps for building the model, the results obtained from the model, and the analysis of the output data are described.

3.1. THE CASE STUDY

The case study concerns an area adjacent to the town of Avetrana located in southern Italy, in the region of Puglia, in the province of Ta-ranto (TA). The area represents the destination of a channel for the harnessing and collection of water coming mainly from the basins located along the western side of the considered site. The development of the channel represents an intervention aimed at the mitigation of hydrogeological risk related to the municipality of Avetrana. The destination is three disused quarries hydraulically connected, which have a volume of water accumulation and disposal capacity compatible with the estimated inflow for different return times.

Thanks to the reconstruction of the geomorphological and litho-stratigraphic evidence that allowed the detailed geological survey around interest of the project infrastructure work, it was possible to define and identify the main geomorphological, hydrogeological, and litho-stratigraphic conditions and therefore the main pathologies of discontinuity and degradation of geo-structural characters at the scale of the in-situ survey. The investigation plan included several geo-gnostic surveys, sampling of environmental samples for the deter-

mination of some chemical parameters, prospections with the methodological approach of surface refraction seismic in P-waves and seismic prospections for the determination of shear waves (S).

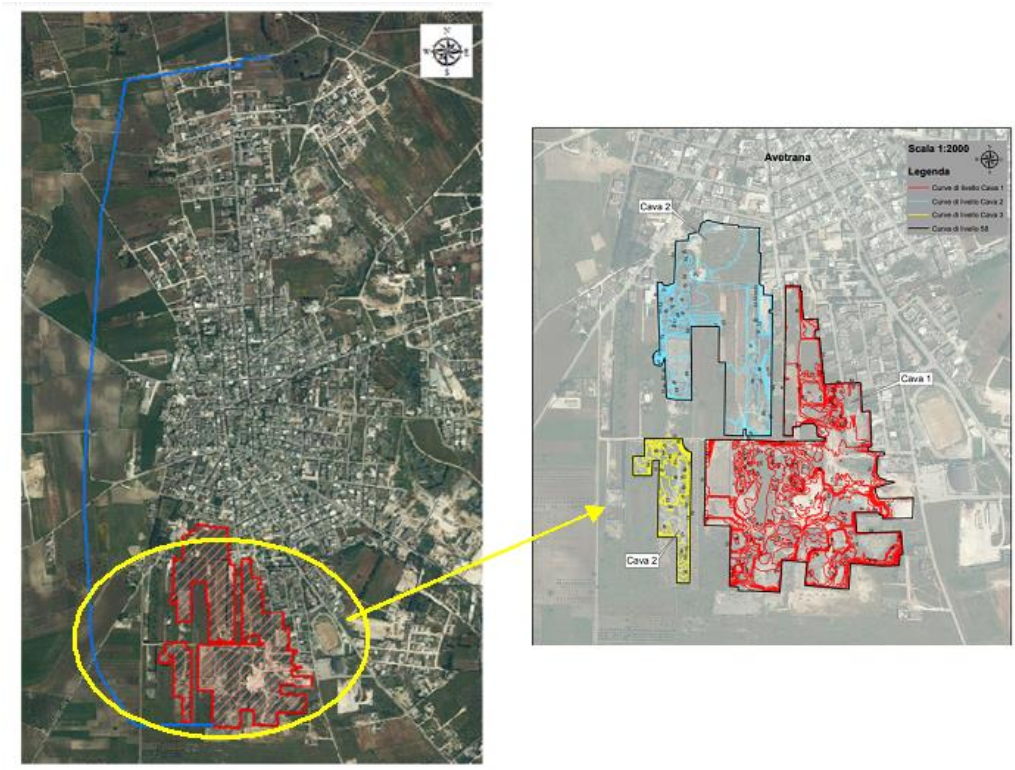

Fig. 3.1.1 - Planimetry of the study area

The municipal territory of Avetrana is morphologically characterized by mainly flat areas interrupted by the presence of endoreic areas of accumulation of flood volumes and by a superficial, undeveloped hydrographic network not very developed.

From a the morphostructural point of view the territory is strongly conditioned by the geological and morphostructural conditions of a graben system, consisting of two calcareous ridges faulted NNE-SSW that show a low morphological quaternary filling. On this calcareous-nitic apparatus, due to further stress-and-strain complexes, an interconnected basin condition was created,

filled by a successional sedimentation of poorly cemented calcareous sands (Pliocene Calabrian Sup) with intercalated banks, as well as blue-gray clayey sands (averaging a few meters), with basal levels of greenish-gray clays (clay thicknesses in the area can exceed 10 meters).

Fig. 3.1.2 - The official geological cartography

This allows the highlighting of a western area outside the urban fabric (but connected to it) that presents all the characteristics of a plate area, vascularized by a paleo surface drainage system, with delivery in depressed and interlocked areas. This wide and disordered system, with an outcropping lithology clearly clayey or sandy-loamy overlying a clayey horizon, actually favors the creation of fields of existence of surface hydrostructures strongly conditioned by rainfall events of marked intensity. The photogeological analysis has provided a detailed system of geo thematic information levels, allowing later comparison with the results of the geological survey in the field, as it can provide information of lithostructural characters. As far as the hydrogeological aspects are concerned, in the central sector of the territory, in correspondence to the built-up area of Avetrana, there is the presence of an aquifer, which given its depth can be defined as intermediate, supported in bed by an extensive horizon of clayey silts. These silts, having a rather low permeability, do not allow the meteoric infiltration waters to arrive in the limestone, but they establish the conditions for the existence of this aquifer, which circulates in the basal layers of the

limestone. The recharge of the surface aquifer is conditioned by the regime of meteoric events, i.e., in relation to reference rainfall periods; therefore, this supply fluctuates strongly in relation to events and is cumulative. It is plausible to admit that the discrete permeability of the limestone clouds causes the aquifer potential to be discrete during wetter periods. During drier periods the aquifer potential decreases significantly. In contrast, a powerful aquifer is found within carbonate lithologic units. The interpretation of recharge modes and, above all, of groundwater circulation and outcropping is complex: in fact, it cannot be simplistically assumed that water infiltrated into surface aquifer flows undisturbed towards the natural outlet constituted by the deep aquifer (which is located in carbonate rocks). It is important to underline how these considerations have a purely indicative character, as it was not possible to extend the study area in order to allow the quantification of the actual recharge capacity of the phenomena described above.

On the basis of the sedimentological and geological-structural characteristics described above, two distinct hydrogeological environments are identified in the examined area: an upper environment, characterized by an essentially sandy-calcarenitic aquifer, strongly seasonal, and another environment, below the previous one, characterized by an aquifer located within the Cretaceous carbonate basement. The cretaceous basement soils are affected by primary and secondary discontinuities that constitute the site of the powerful deep aquifer. The discovery level of this aquifer proceeds from sea level at the coastline to the innermost areas with a piezometric gradient on the order of 1 -2°/oo. Therefore, the calcarenitic and sandy terms and the clay intercalations determine a hydrogeologically complex soil pattern, with modest sorption aptitude, the presence of weak layers suspended on silty clay sediments, the development of pseudocarst or paracarst phenomena, all with final deliveries in the deep aquifer. This is the most important from the point of view of potential, and that confined in the limestones. The depth of discovery of the aquifer is in cor-respondence of the agglomerations (for the available data) is generally rep-

resented by a static level stabilized at an altitude above sea level between 1-3 meters.

Considering the investigations carried out in the area under consideration, it was possible to determine the characteristics of the subsoil in correspondence to the soils that will constitute the project bed. In the area, the presence of a lens of silty-sandy clay deposits was found to be present for most of the channel route. Considering the length of the channel from upstream to downstream, this lens extends from the 700th meter to the 2400th meter, with a thickness varying from a few centimeters to 4-5 meters and resting directly on the calcarenites present for a thickness of at least about 28 meters. The limestone formation was surveyed through a 28-meter depth survey. However, it is possible to determine the depth of the limestone bedrock in other areas from the seismic surveys performed. In fact, from the S-wave velocity profiles, a jump in velocity is observed at depths varying between 15 meters and 20 meters from the survey plane. This variability can be attributed to the different dislocation of the limestones in the subsurface.

Through in situ testing, it was possible to determine the permeability coefficient. Considering the difficulties and uncertainties in the determination of this parameter, except in the case of homogeneous and isotropic soils located in areas whose boundary conditions are known, the choice of test method must be made according to the type of soil and the desired degree of accuracy. Experimental measurement of the permeability of a soil can be done either in the laboratory or in situ: for natural soils, in situ measurements are generally more significant and therefore preferable (since permeability is also strongly influenced by macrostructural characters). In-hole tests by injecting water into the hole itself allow determination of the permeability of the soils at the bottom of the holes above or below the water table and can be performed at either constant or variable load. The general stratigraphy of the borehole is: 0 meters to 0.2 meters from the topsoil level; 0.2 meters to 1 meter from the topsoil level highly altered calcarenites; 1 meter to 28 meters from the topsoil level moder-

ately cemented calcarenites with cemented levels with vacuoles and weakly cemented levels; 28 meters to 29 meters organic limestone and gray-white limestone.

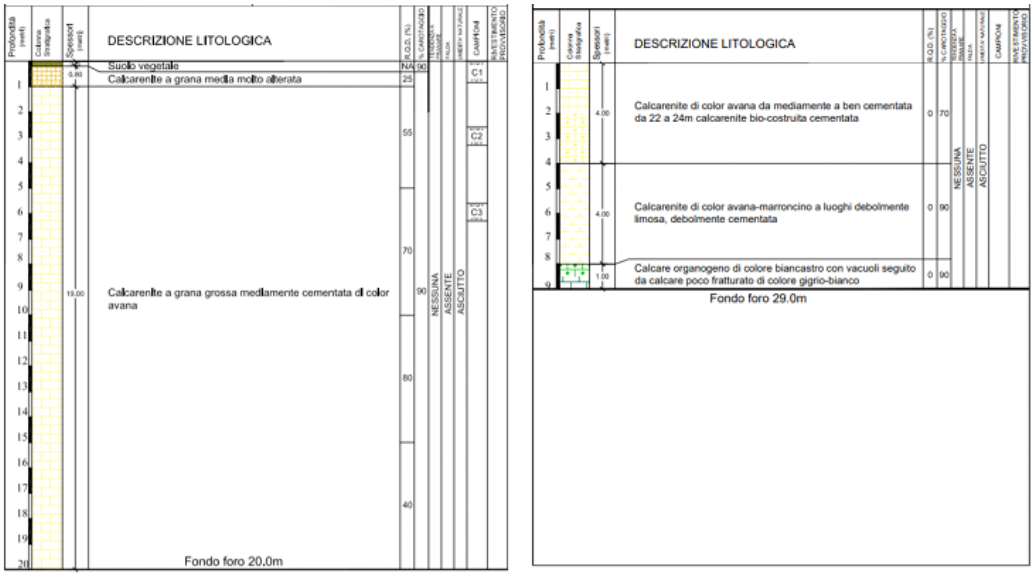

Fig. 3.1.3 - Stratigraphic survey from 0 to 29 meter

As a result of the permeability tests carried out at variable load, it was possible to identify the average values of the permeability coefficients of the two hydrogeological units: calcarenite with an average permeability value of k=4.35E-06 m/s, and limestone with an average k value of 5.50E-04 m/s.

The quarries that are expected to be used as final destination, cover a total area of about 20 hectares, with a minimum height of 47 meters above sea level and a maximum height of 58 meters above sea level. The channel coming from west will be inserted in the first quarry with a 125 meters long section with a final height of 54,81 meters above sea level. The work foresees the realization of a system of dispersing wells that together with the gorge, located inside the second quarry, will ensure the disposal of water for infiltration and the simulta-

neous recharge of the water table. All wells will have a depth of 30 m and a diameter D = 400 millimeters, reaching 5 meters in the fractured limestone under the calcarenite layer. Assuming an average permeability for limestones K = 5*10-4 m/s, precautionary value with respect to literature ones and assuming an average head of 4 meters in the quarries (hydraulic head H = 34 meters), it is possible to estimate the absorption capacity of a single well equal to Q = 0,0145 m^3/s.

The well mouth will consist of a metal sleeve with a total length of 5 meters, of which 2,5 meters will be ground with respect to the bottom of the tank and 2,5 meters will be inside the hole. The part above ground will have a lateral break with a 90° bend pointing downwards, grafted at 1,4 meters from the bottom of the tank, so as to create a real siphon that allows the water accumulated inside the tank to be fished not from the upper free surface, but from 0,4 meters below, i.e. from 1 meter from the bottom of the tank. This solution prevents any floating objects (such as leaves, plastic bottles, refuse, etc...) that may accidentally reach the bottom of the tank from entering the well and clogging it. This device also provides a higher level of environmental protection as it prevents any floating oils on the water from entering the well, and thus the surface layers of the soil and subsoil. Approximately 0,5 meters above the lateral detachment, the liner will be closed with a slanted flange to prevent water pooling. A 40 mm diameter vent pipe will also be provided inside the liner, which will descend 5.0 meters from the bottom of the reservoir and rise above the closing flange of the liner by 4,5 meters, corresponding to the threshold limit of filling the reservoir, ending with a bend so as to prevent anything from entering from above.

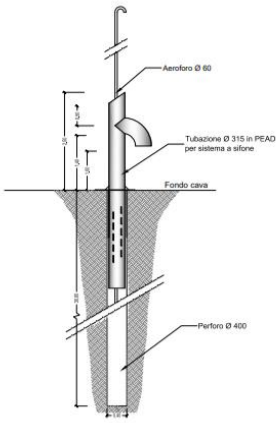

Fig. 3.1.4 - Detail of the injection well

Therefore, the hydrogeological structure present in the area of the quarries adjacent to the municipality of Avetrana is made up of distinct units which present substantially homogeneous hydrogeological characteristics identifiable as follows

- Vegetated land from 0 meters to 0,2 meters above ground level;
- A surface hydrogeological unit consisting of averagely cemented calcarenites with cemented levels with vacuoles and weakly cemented silty levels with highly variable thicknesses between 0,2 and 28 meters from ground level (variability can be attributed to the different dislocation of limestones in the subsoil), average permeability value equal to k=4,35E-06 m/s;
- A second unit consisting of organogenic limestone and gray-white limestone. This unit is intensely affected by primary and secondary discontinuities, average permeability value equal to k=5,50E-04 m/s.

The depth of discovery of the aquifer is generally represented by a stabilized static level at an elevation above sea level between 1-3 meters.

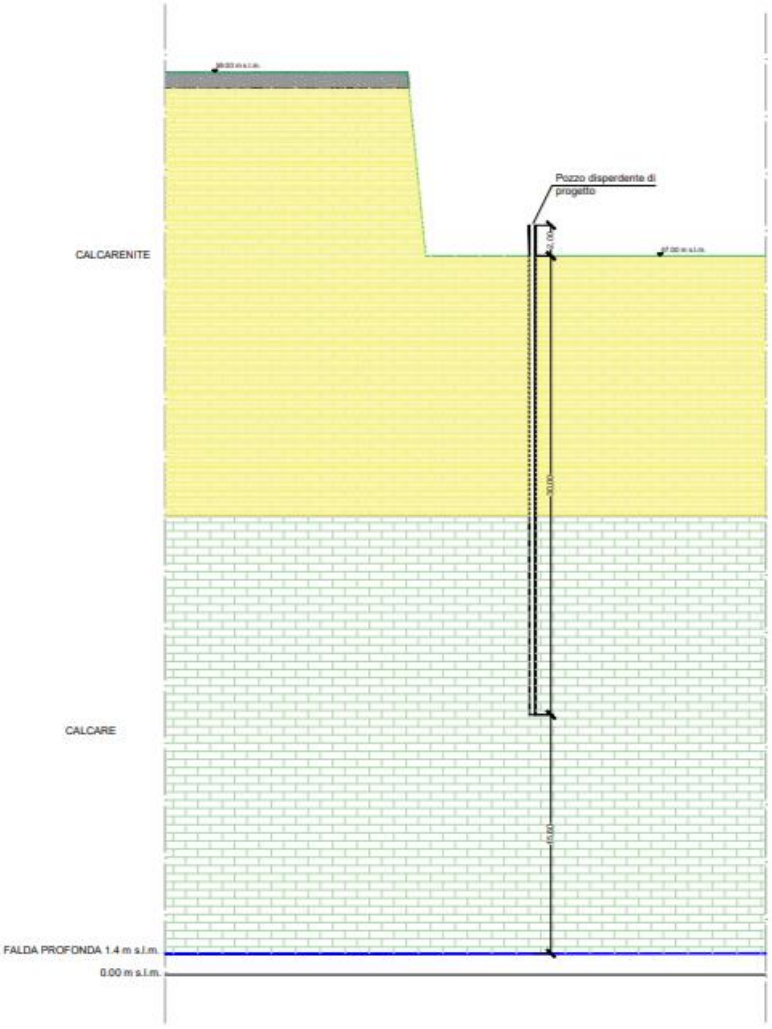

Fig. 3.1.5 - Representative stratigraphic section of the site

3.2. MODELLING OUTPUTS

The objective of the modelling was to simulate groundwater flow and transport of a leached pollutant within the unsaturated zone, evaluating the infiltration capacity into the soil and thus the possibility of deep aquifer contamination.

The modelling was divided into several phases:

1. flow simulation under steady state conditions.
2. simulation of the transport in steady state conditions.
3. simulation of the transport in steady state conditions with the injection well.
4. simulation of the transport in transient mode.

The simulations carried out wew started considering the flow in steady state mode, to then be implemented with the transport model both in steady state and transient conditions. Through these last simulations it was been possible to consider a specific time period within which to carry out the model, having therefore an ultimate term and starting from an initial condition (also temporal discretization). By contrast, a model solution under steady state conditions was obtained by representing the state of the system at fixed boundary conditions and material properties for an infinite period of time. In the specific case, a combination of the steady state flow with a transient transport simulation was finally performed. The FEFLOW simulation program allowed this combination by

setting the steady state solution of the flow simulation as an initial condition for the steady state flow and transient transport mode.

Three different scenarios were considered for each transport simulation, depending on the different porosity value attributed to the limestone layer (50%, 70%, 90%). This sensitivity analysis of the equivalent porosity with respect to the aquifer layer was conducted because the borehole tests performed in situ did not investigate the value of this hydraulic parameter.

Considering the different geological units (Fig. 3.1.5, in the previous chapter) of the considered site, the 3D model was constructed with FEFLOW, software based on the finite element method.

MODEL SCENARIO

After defining the domain (mesh) we discretized the model (super-mesh).

Each active node of the mesh during the simulation generated calculations on the basis of which the results were determined, and then interpolations within the finite elements. In areas where more numerical precision was required, the area of interest was refined locally by thickening the mesh to determine a denser mesh. In this case, it was decided to thicken the area on the first slice where the pollutant release is considered and thus where the injection well was then placed. FEFLOW has allowed to discretize the model in different layers: the unsaturated zone is divided into 10 layers, characterized by a thickness of 5 meters each, while the saturated zone, under the water table is characterized by a single layer having 10 meters of thickness. Each layer has two slices, one upper and one lower, characterized by the value of the corresponding elevation. The study model, considering the geological situation previously analysed, consists of 12 slices: the first slice at an altitude of 50 m above sea level and the last slice at -10 m above sea level. The layers between the first slice and the slice at 25 m above sea level represent the calcarenite layer, while the layers below represent the limestone geological unit.

This discretization of the model into the layers can be seen in the following figure, characterized by the elevation values of the respective slices.

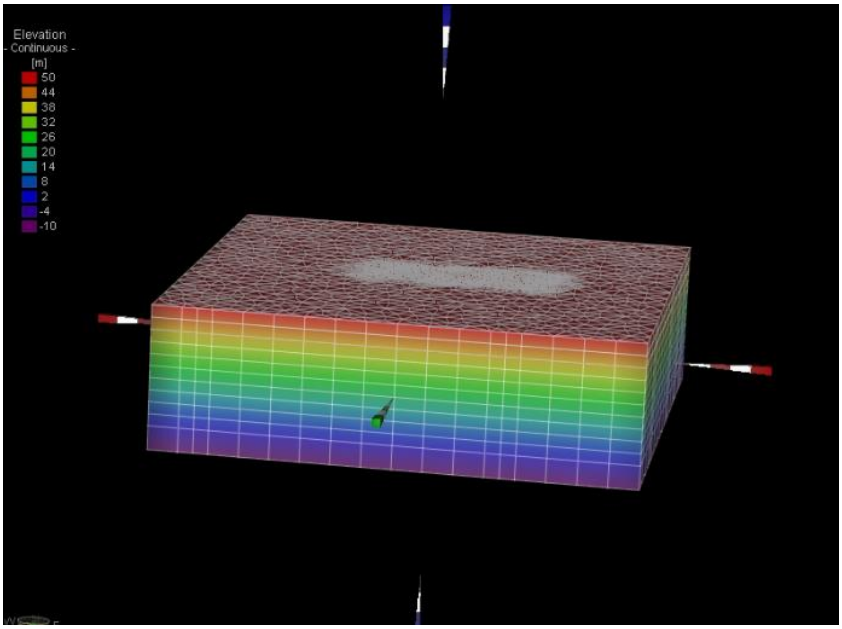

Fig. 3.2.1 – Elevation's model

1: SIMULATION OF THE FLOW IN STEADY STATE CONDITIONS

The first simulation carried out represents the flow in steady state conditions in the unsaturated zone. Below are the settings set in this first phase (Fig. 3.2.2) through the "problem setting" function of the software. As can be seen from the image X has been set:

- simulation: Richards' equation
- fluid flow: steady.

The reason why the Richards' equation was chosen for the simulation is that it generally governs the flow in an unsaturated zone. In fact, one of the features of FEFLOW is to simulate flow (and mass transport processes) in both a saturat-

ed zone, with the Darcy equation, and in a variably saturated or unsaturated zone, with the Richards' equation.

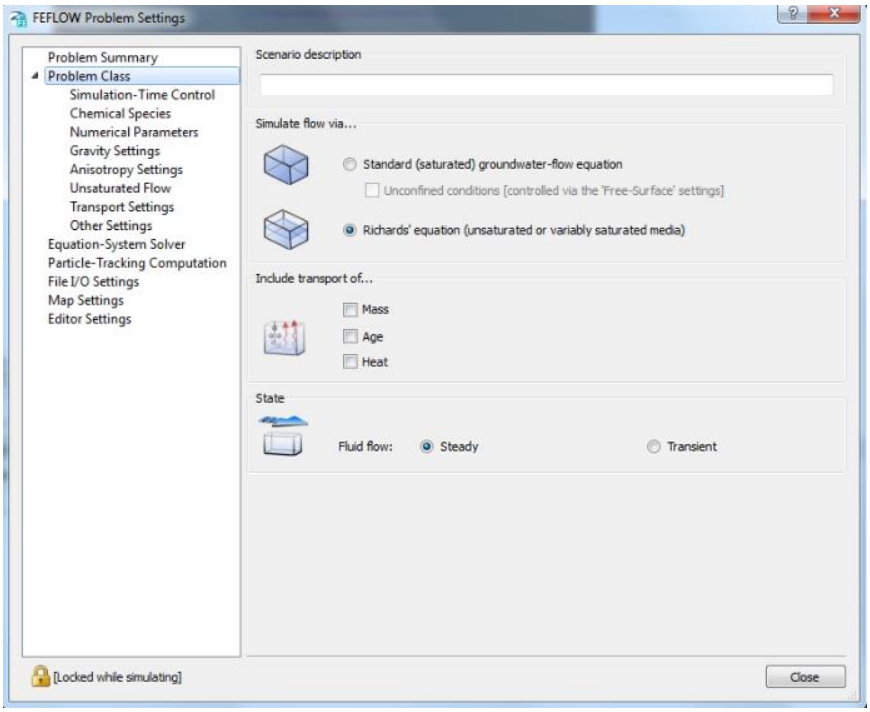

Fig. 3.2.2 – Problem settings for a steady-state unsaturated 3D flow model

The Richards' equation, in the formulation used by the software, is obtained by combining the conservation of mass equation with Darcy's equation:

$$\frac{\partial \theta}{\partial t} = -\frac{\partial q}{\partial z} = \frac{\partial}{\partial z}\left(D\frac{\partial \theta}{\partial z} + k(\theta)\right)$$

$D = k(\theta)\frac{d\psi}{d\theta}$

ψ : pressure head

MODEL PROPERTIES

Once the basic simulation conditions were set, the model properties were identified by determining the initial conditions, boundary conditions, and material properties. In order to positively influence the convergence behavior of the simulation, the hydraulic head was set. Considering the mean value of phreatimetry obtained through field investigations and thanks to the PTA (Water Protection Plan of the Puglia Region - Piano regionale di Tutela delle Acque -, that is the act that regulates the government of water on the territory. This is a dynamic instrument of knowledge and planning, which has as its objective the integrated protection of the qualitative and quantitative aspects of water resources, in order to pursue a healthy and sustainable use.), values updated in 2015 (Fig. 3.2.3), a hydraulic gradient was set through the determination of two hydraulic head values present at opposite edges of the section. As shown in Fig. 3.2.4, boundary conditions were set for the hydraulic head along the edges of the model. The left edge was set with a hydraulichead of 1.4 meters above sea level and the right edge with a value of 1.5 meters above sea level.

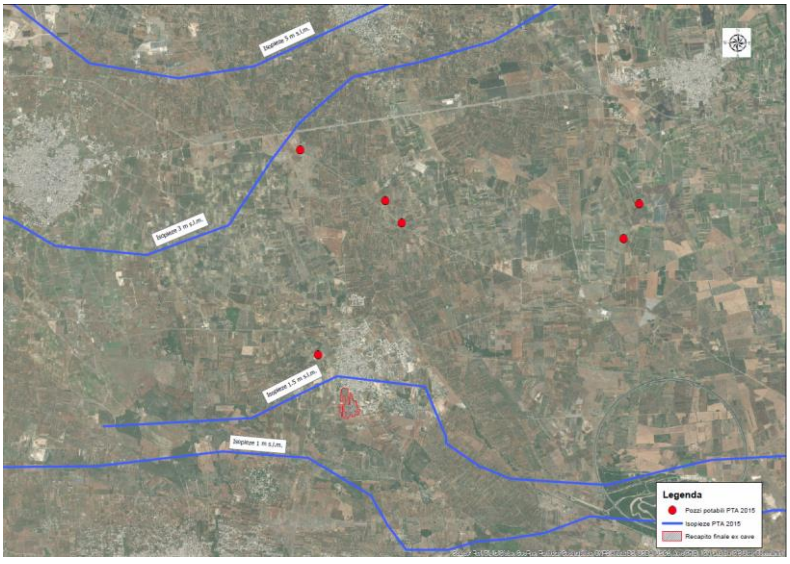

Fig. 3.2.3 – Equipotential lines (PTA)

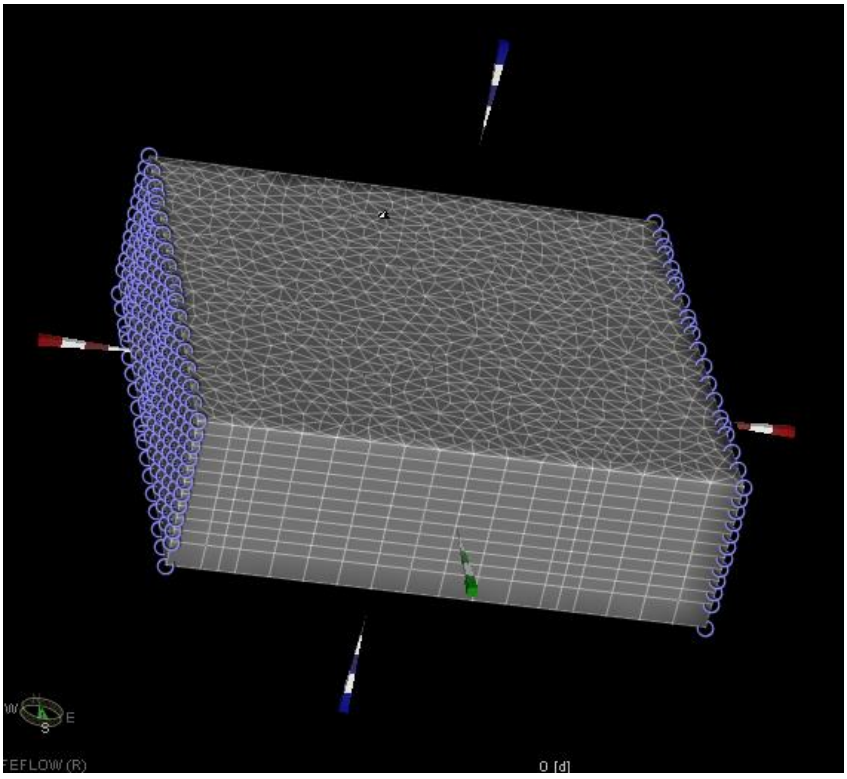

Fig. 3.2.4 – Hydraulic-head boundary condition

Considering the values related to the analysis of the rainfall network data provided by the Civil Protection of Puglia Region with respect to the site under study and evaluating the average annual rainfall values revealed by the reports published by Ispra Ambiente Puglia Region, a rainfall frequency value of 500 mm/year was set. This value was set as the recharge value (inflow at the top) on the first slice. This setting can be visualized in Fig. 3.2.5, where the first slice is in red and represents the layer invested by diffuse rainfall.

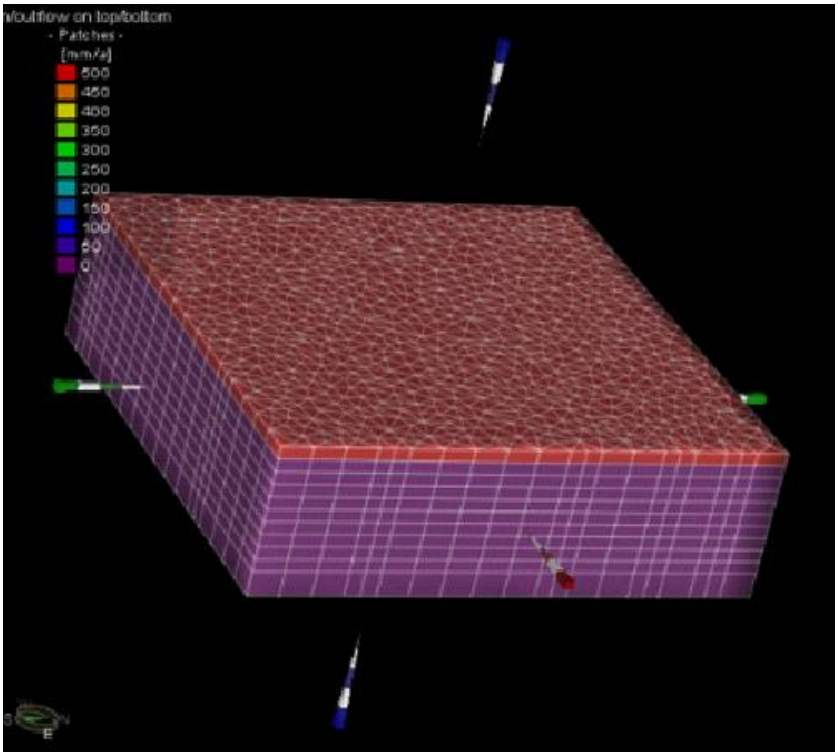

Fig. 3.2.5 – Recharge 500mm/anno

MATERIAL PROPERTIES

After analyzing the geology of the area considered in this study, two different hydrogeological environments were identified. The upper environment, characterized by a modest aptitude for absorption, is the seat of the calcarenite layer, and the lower environment, the seat of the deep aquifer, characterized by primary and secondary discontinuities, is the seat of the limestone layer. Different values of permeability and porosity were attributed to the attested calcarenite for the first 5 layers of the model and to the underlying limestone.

The hydraulic conductivity (K) was considered isotropic (Kx=Ky=Kz) according to the equivalent porous model, and after evaluating the results of the evidence from surveys, the average value of the calcarenite layer K tensor was attributed as 4.35E-6 m/s, and the average value of the limestone layer K as 5.50E-04 m/s.

This difference can be visualized in Fig. 3.2.6 where the respective value of the calcarenite layer is fixed in red and that of the underlying limestone in purple.

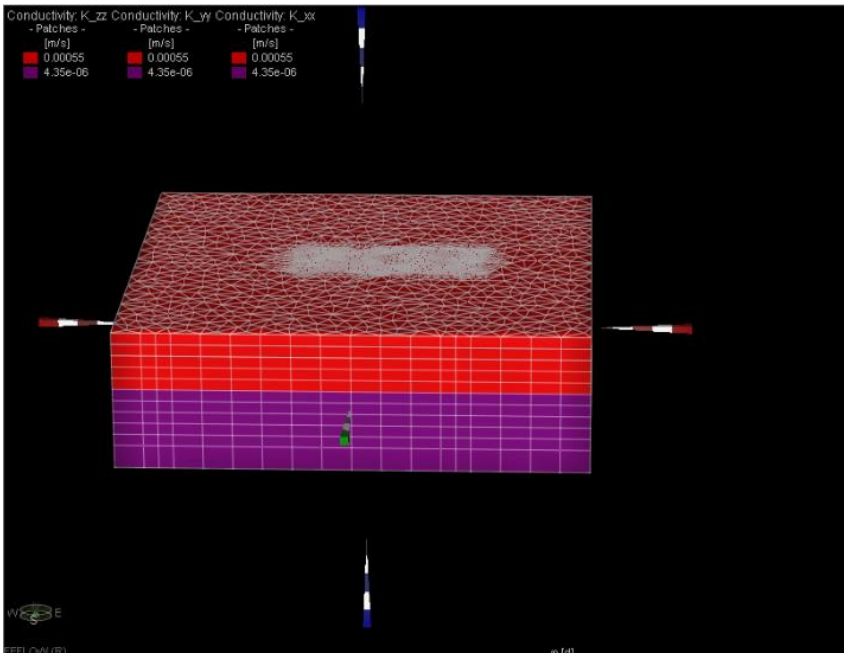

Fig. 3.2.6 – Conductivity K

Regarding the porosity value of the respective layers, from the sounding tests it was possible to use only the value related to the calcarenite layer equal to 40%. As already mentioned, a sensitivity analysis was carried out for the porosity value of the limestone layer, while the value of the calcarenite layer was not determined by the evidence from surveys carried out. Starting from the values of the porosity present in the literature characteristic of the "Altamura limestone", equal to 50% (“The groundwater and the seawater intrusion in Apulia: from research to the emergency in the safeguard of the water resource”, V.Cotecchia), it was decided to consider two increasing values 70% and 90% (extreme condition) to assume the most representative behavior regarding the porosity of a fractured limestone.

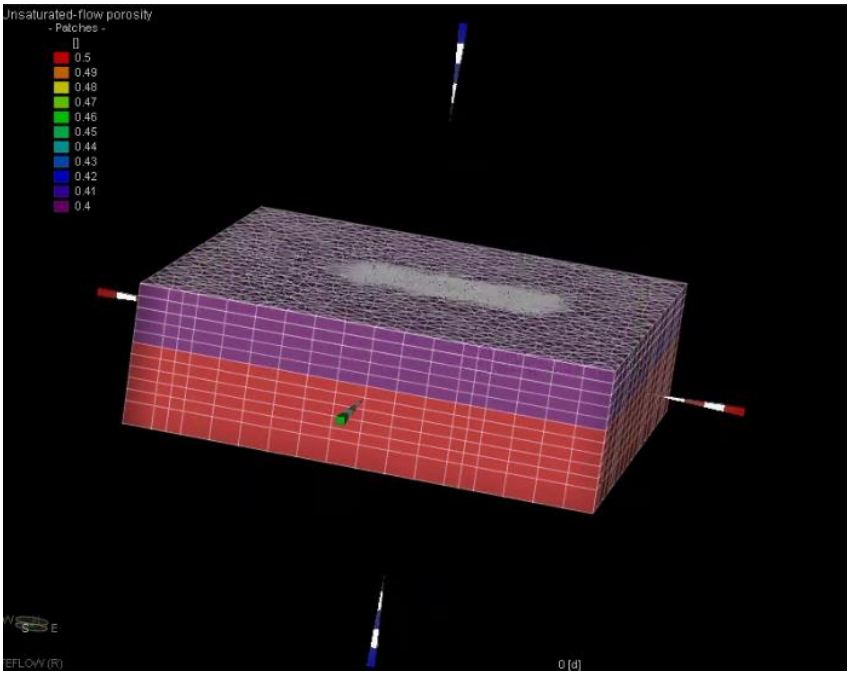

Fig. 3.2.7 – Unsaturated flow porosity – 50%

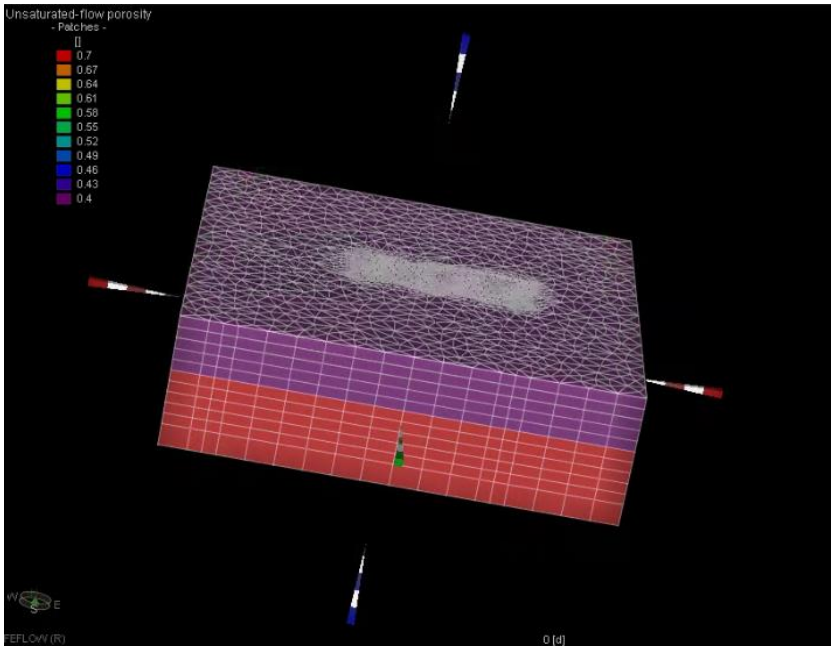

Fig. 3.2.8 – Unsaturated flow porosity – 70%

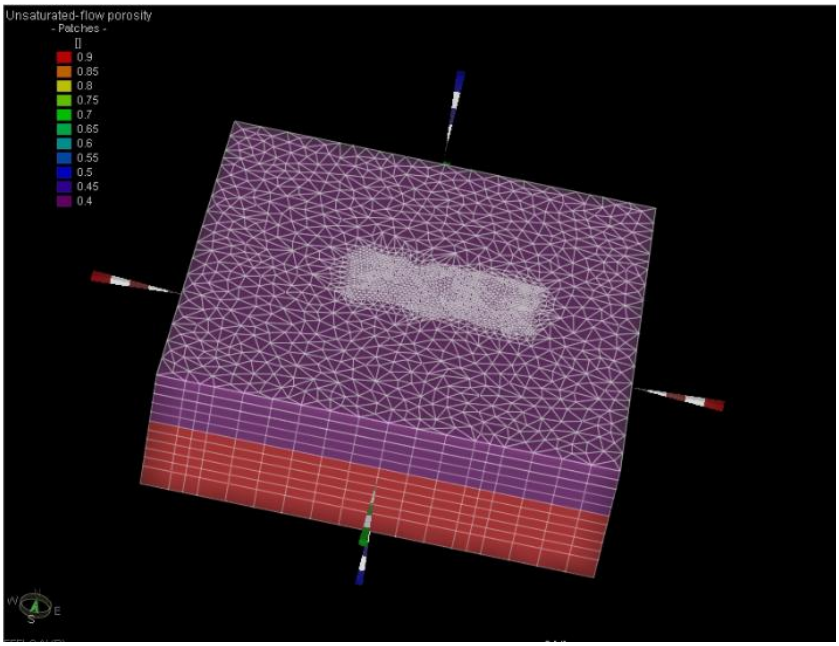

Fig. 3.2.9 – Unsaturated flow porosity – 90%

In figures 3.2.7, 3.2.8, 3.2.9 different values of porosity are indicated with respect to the limestone layer in red. In the first figure, according to what is reported by the values in the legend, the equivalent porosity assumes a value of 50%, in the second equal to 70% and finally that relative to 90%. The value relative to the limestone layer in purple remains constant in the different scenarios.

CONSTITUTIVE RELATIONSHIPS OF HYDRAULIC PARAMETERS IN UNSATURATED FLOW.

The Richards' equation incorporates constitutive relationships to describe the di-slope between (capillary) pressure head Ψ and saturation S (water retention curve), and between saturation S and relative permeability k. These relationships are described by empirical parametric models (such as van Genuchten) or spline tables.

To parameterize the soil water retention function, we considered values related to the Mualem model (modified van Genuchten model), given below (Fig.

3.2.10), since the parameters related to the van Genuchten equation do not correspond to the soil situations present in the study. For calcarenite, the values used by the Mualem model are those related to TOPSOIL MEDIUM, and for limestone those related to TOPSOIL COARSE.

		θ_r	θ_s	α	n	m	l	K_s
Topsoils	Coarse	0.025	0.403	0.0383	1.3774	0.2740	1.2500	60.000
	Medium	0.010	0.439	0.0314	1.1804	0.1528	-2.3421	12.061
	Medium Fine	0.010	0.430	0.0083	1.2539	0.2025	-0.5884	2.272
	Fine	0.010	0.520	0.0367	1.1012	0.0919	-1.9772	24.800
	Very Fine	0.010	0.614	0.0265	1.1033	0.0936	2.5000	15.000
Subsoils	Coarse	0.025	0.366	0.0430	1.5206	0.3424	1.2500	70.000
	Medium	0.010	0.392	0.0249	1.1689	0.1445	-0.7437	10.755
	Medium Fine	0.010	0.412	0.0082	1.2179	0.1789	0.5000	4.000
	Fine	0.010	0.481	0.0198	1.0861	0.0793	-3.7124	8.500
	Very Fine	0.010	0.538	0.0168	1.0730	0.0680	0.0001	8.235
	Organic*	0.010	0.766	0.0130	1.2039	0.1694	0.4000	8.000

* There was no topsoil/subsoil distinction among organic soils.

Fig. 3.2.10 – The Mualem-van Genuchten parameter

The following are images related to the execution of the flow simulation under steady-state conditions. Fig. 3.2.11 shows the hydraulic head values along the first slice. The hydraulic head trend, orthogonal to the equipotential lines justifies the values fixed with the model properties, i.e., the value of the diffuse rainfall and the values of the boundary conditions.

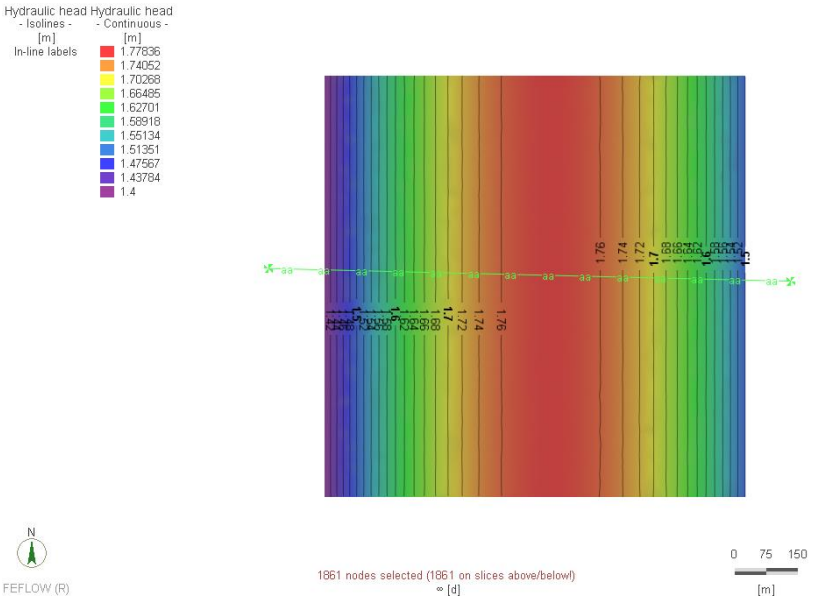

Fig. 3.2.11 – Hydraulic head

In images 3.2.12 and 3.2.13, the trends of pressure distribution and saturation in the model cross section can be seen (aa). By evaluating the pressure distribution values, one can see if the hydraulic head values have been correctly assigned. In an unconfined model, a pressure of zero commonly reflects the interface between the saturated and unsaturated zones and thus the groundwater level. Thus, in the images of pressure values and saturation distribution relative to a cross-section (aa), the groundwater line relative to the groundwater surface is shown in white. In the figure 3.2.12 related to the pressure trend, it can be seen that, according to the legend, the pressure values in the vadose zone are characterized by negative expressions, while the values in the saturated zone are positive. In the figure 3.2.13 related to the saturation distribution, the zone related to the capillary fringe is displayed in green, immediately above the surface of the water table. This figure shows the values under the water table of a saturation equal to 1.

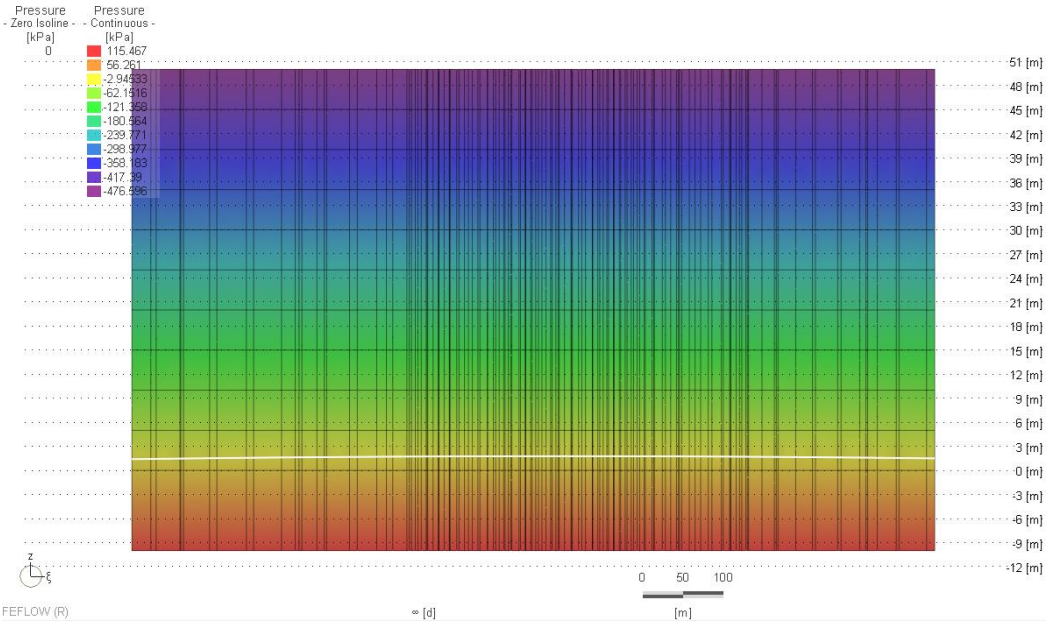

Fig. 3.2.12 – Pressure – cross section view (aa)

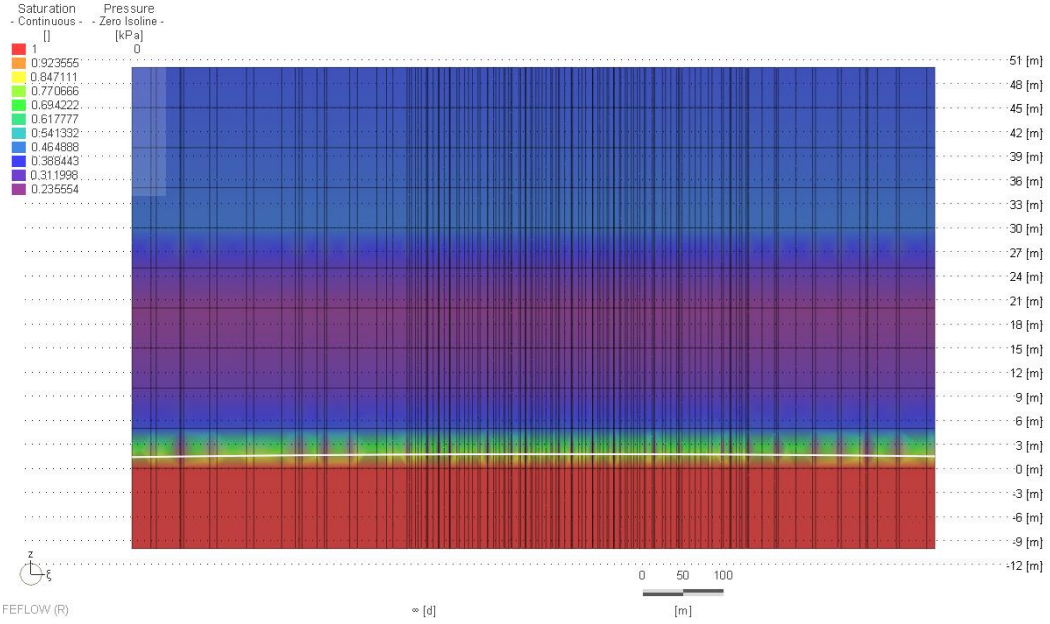

Fig. 3.2.13 – Saturation distribution – cross section view (aa)

2: SIMULATION OF TRANSPORT UNDER STEADY STATE CONDITIONS

The 3D flow model was extended to a 3D transport model. The settings of the first transport simulation are in steady state mode in the unsaturated aquifer (Fig. 3.2.14).

The two steady-state transport simulations were performed to represent two different situations, both of which have the potential to affect groundwater quality. In the first model, contamination occurs at the field level (first slice), at the infiltrated zone of the model mesh involving 10 nodes, and considering a hypothetical contaminant concentration of 100 mg/l. In the second transport model, the introduction of the 100 mg/l contaminant concentration occurs through a recharge well located in the infiltrated zone of the model mesh.

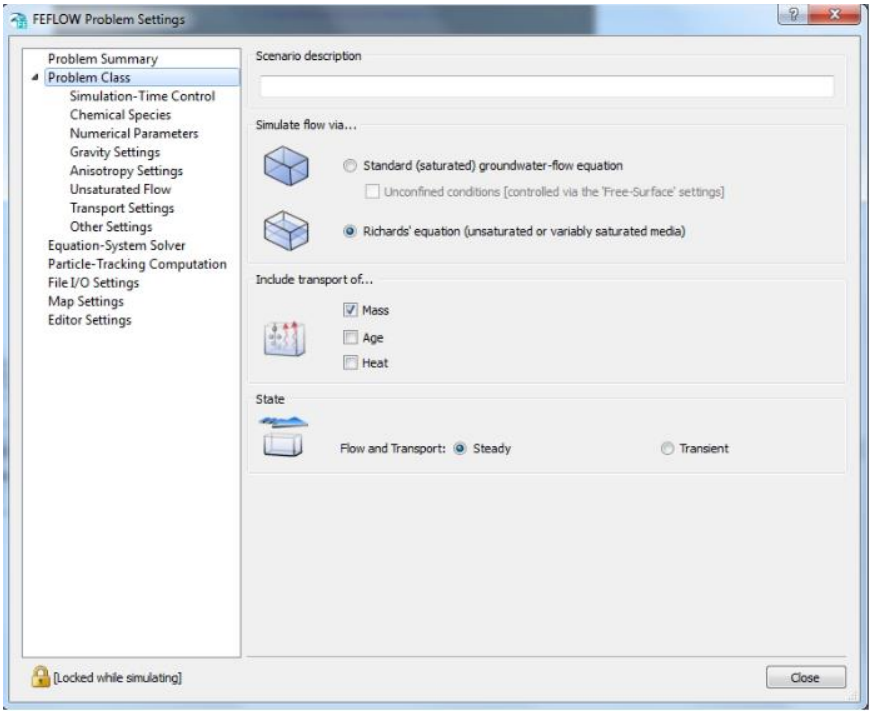

Fig. 3.2.14 – Problem settings for a steady-state unsaturated 3D mass concentration model

For both simulations, we set the setting conditions of the problem on Richard's equation, including mass transport and considering the simulations under steady-state conditions. The hydrodynamic parameters set in both models were the same. The mass transfer in the aquifer system was modelled by the advection-dispersion-equation (ADE).

In general, for the simulation of a mass transport problem, it is necessary to set the porosity and dispersivity values to local conditions.

The longitudinal dispersivity is calculated using the following formula (Xu&Eckstein, 1995):

$$\alpha_x = 0.83 \cdot (\log_{10} L_p)^{2.414}$$

where Lp is the scale of the phenomenon (length of the plume)

Therefore, the longitudinal dispersivity was set equal to 3 m, while the transversal dispersivity, 1/10 of the first, equal to 0.3 m.

Regarding the porosity value, we proceeded in both simulations with the sensitivity analysis of the equivalent porosity related to the limestone layer considering three porosity values equal to 50%, 70% and 90%. The superior layer of calcarenite that is attested for the first 5 layers of the model, instead, is characterized by a constant value of the porosity equal to 40%.

In Figures 3.2.15 and 3.2.16, the zone where contamination occurs is identified in red. There are 10 affected nodes located on the first slice of the model.

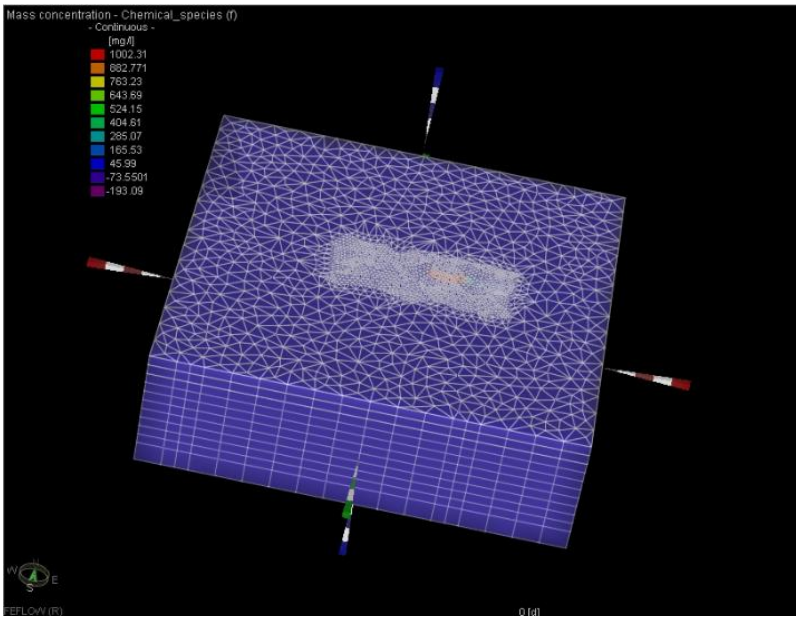

Fig. 3.2.15 – 3D view of mass concentration

The results of model point contamination of the pollutant on soil under the three equivalent porosity scenarios are shown below.

The first figure represents the trend of the pollutant along the first slice. It can be seen how, at the beginning of the simulation, the pollutant extends into adjacent nodes, affecting a larger area (in red).

Figures 3.2.17, 3.2.18 and 3.2.19 represent the scenarios considering the three values of the equivalent porosity along the slice. Please refer to the next chapter for a detailed description of the results obtained.

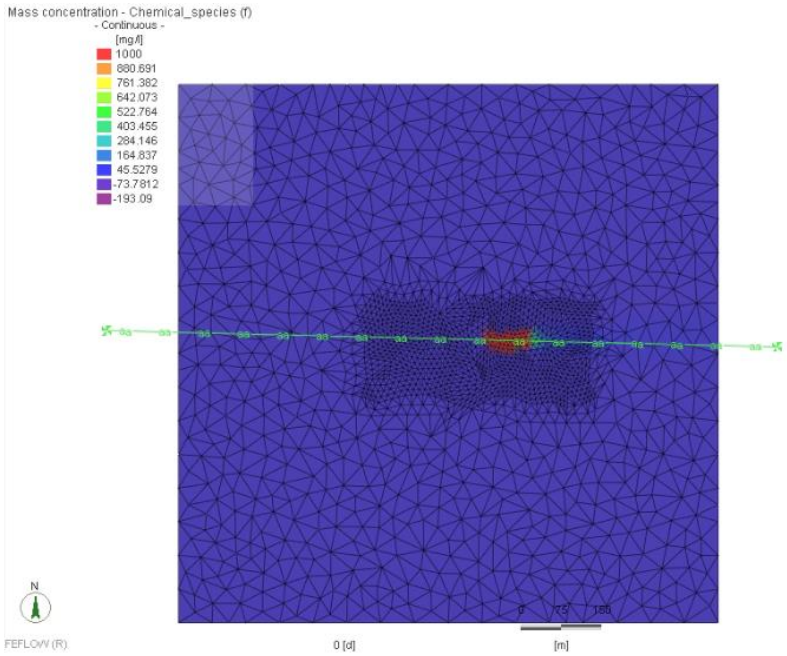

Fig. 3.2.16 – First slice view of mass concentration

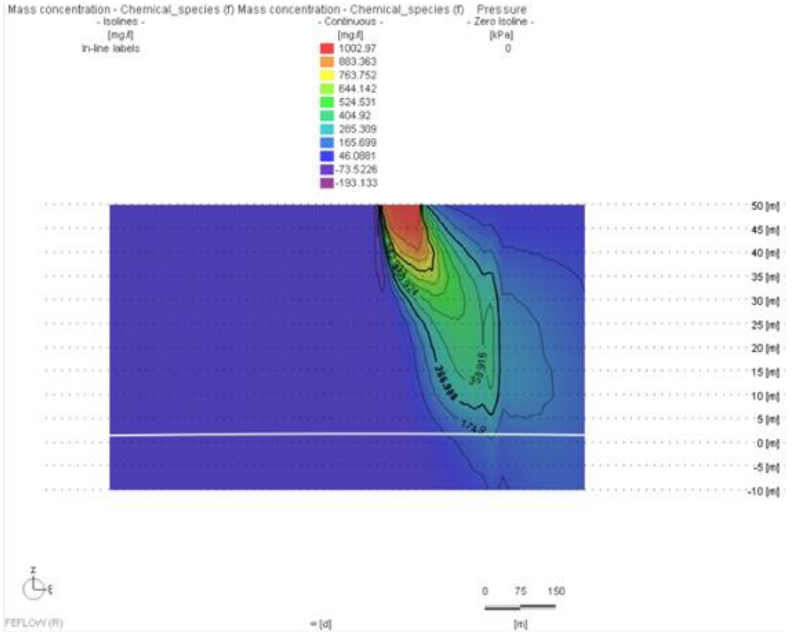

Fig. 3.2.17 – Mass concentration (aa) - 50% limestone porosity

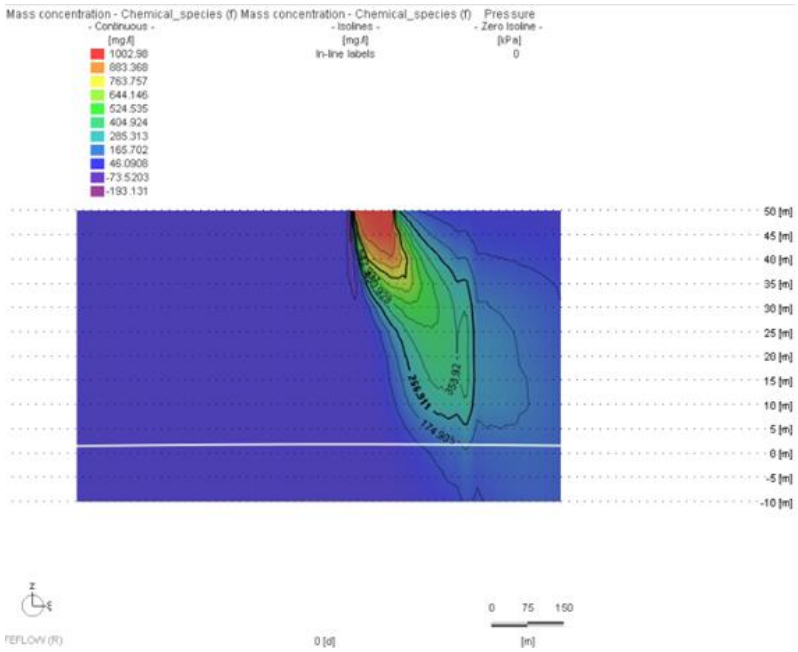

Fig. 3.2.18 – Mass concentration (aa) - 70% limestone porosity

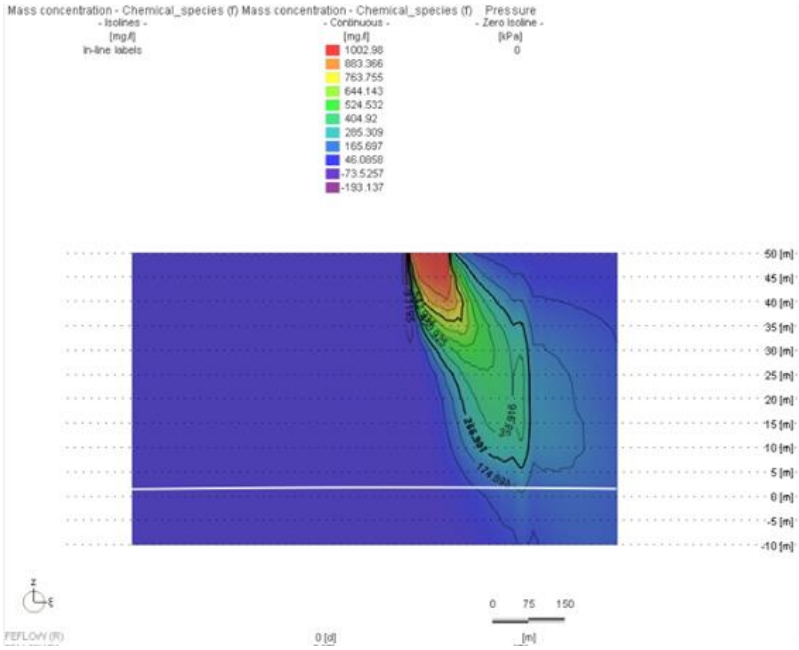

Fig. 3.2.19 – Mass concentration (aa) - 90% limestone porosity

3: SIMULATION OF TRANSPORT UNDER STEADY-STATE CONDITIONS WITH THE INJECTION WELL.

In the second mass transport model, an injection well was provided. In FEFLOW, it is possible to simulate the water injection through the function "Multilayer well". To define the boundary conditions of the well, we have considered the project related to the channel of embankment and collection of rainwater and alluvial water for the protection of the municipality of Avetrana, which requires the presence of wells for the disposal of collected water. The well, located in the area characterized by a dense mesh, is up to 20 meters deep, affecting part of the limestone layer. The radius of the well is 0.20 meters, and the depth is 30 meters. The flow rate is 1252 m3/d. To set the injection well in FEFLOW, the negative value relative to the capacity of the wall was considered (Fig. 3.2.20). The flow within the well along the screened interval was simulated by the FEFLOW software using the Hagen-Poiseuille law.

The input of the hypothetical pollutant at a concentration equal to 100 mg/L was enacted through the considered well and the model was performed in the three scenarios related to limestone porosity equivalent 50%, 70% and 90%.

The hydrodynamic parameters set were the same as in the pre-existing simulation.

In figure 3.2.21 the node affected by the well is located both in the 3D visualization and along the first slice and the coordinates can be seen in Fig. 3.2.20.

The following figures (Fig. 3.2.23, 3.2.24, 3.2.25) show the values for the simulation results in the three scenarios considered. Please refer to the next chapter for a detailed description of the results obtained.

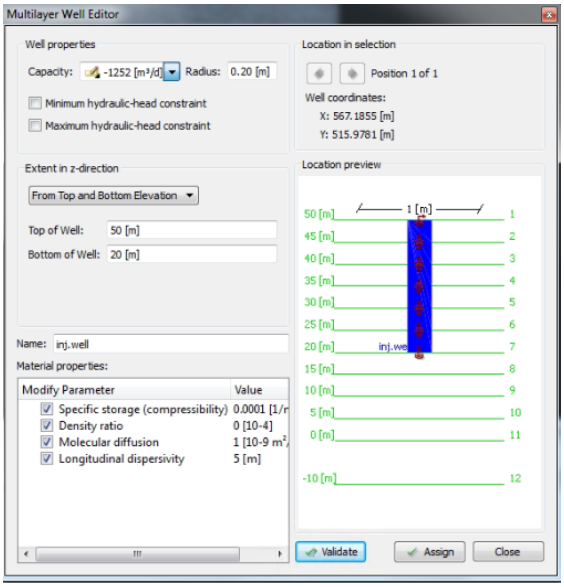

Fig. 3.2.20 – Injection well setting

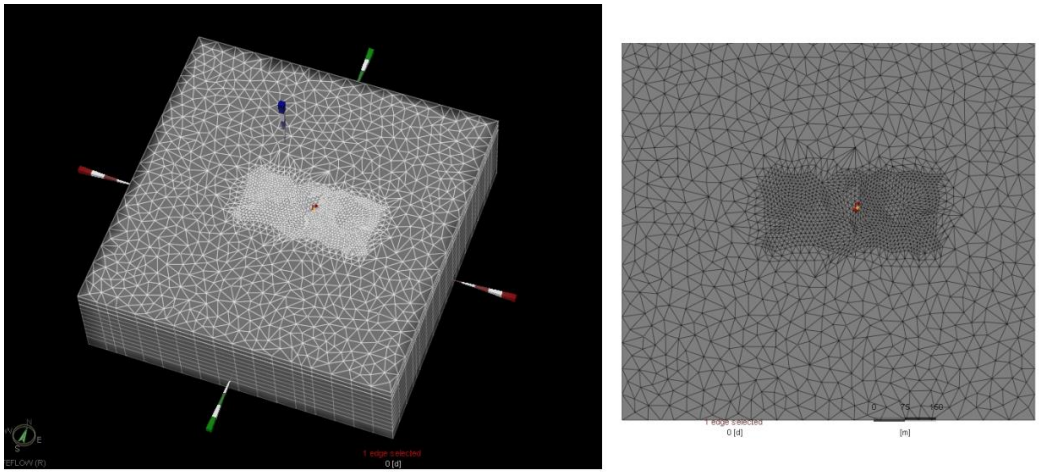

(a) (b)

Fig. 3.2.21 – (a) 3D view of injection well; (b) first slice view of injection well

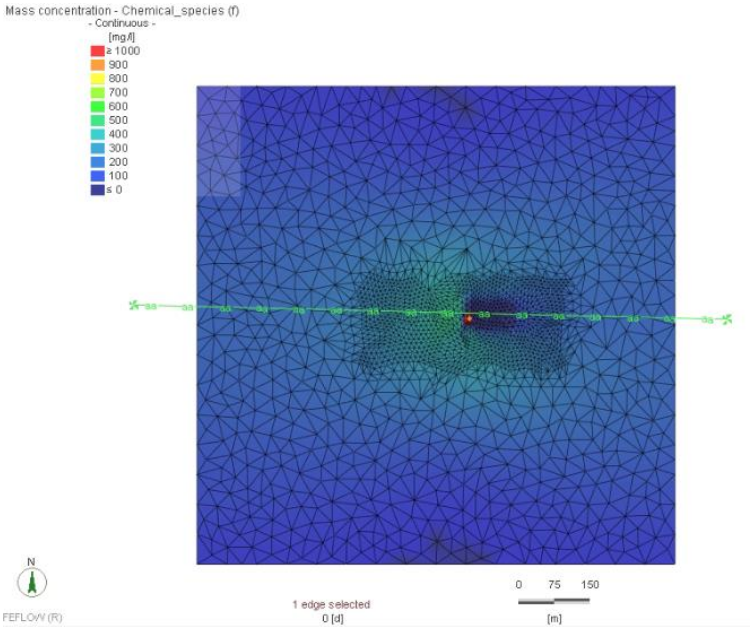

Fig. 3.2.22 – First slice view of mass concentration with injection well

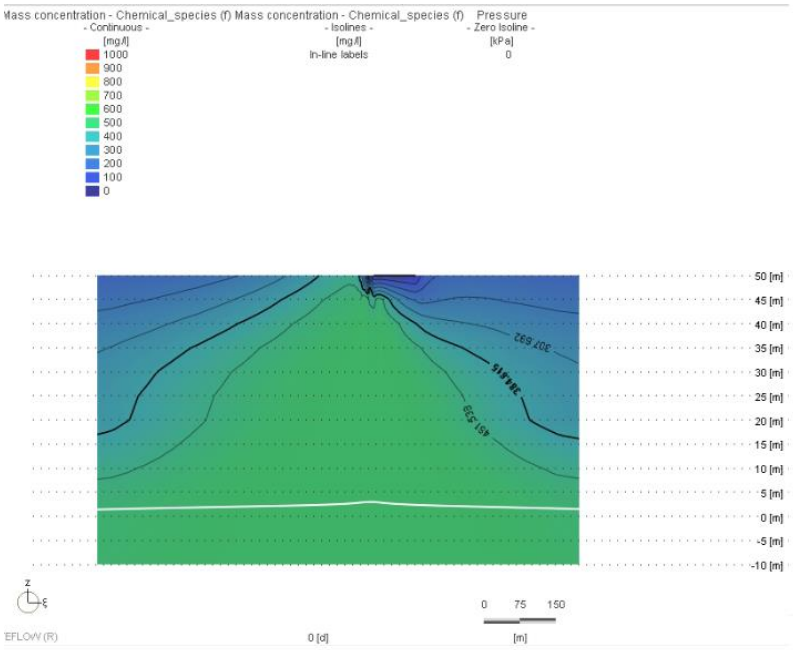

Fig. 3.2.23 – Mass concentration (aa) - 50% limestone porosity

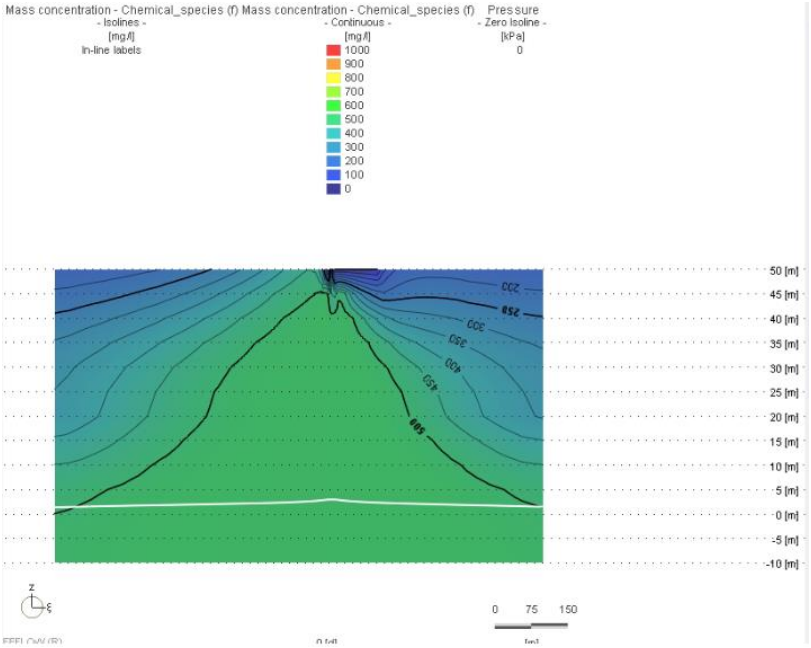

Fig. 3.2.24 – Mass concentration (aa) - 70% limestone porosity

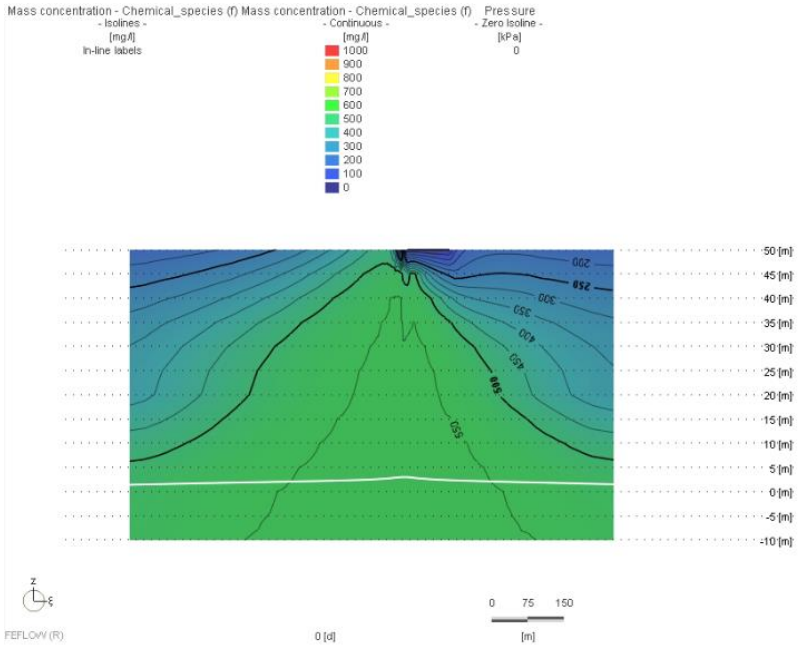

Fig. 3.2.25 – Mass concentration (aa) - 90% limestone porosity

4: SIMULATION OF TRANSPORT UNDER TRANSIENT CONDITIONS

In the last analysis we proceeded with the simulation of transport under transient conditions. The model has predicted the local contamination on the first slice involving 10 nodes, considering the value of a hypothetical pollutant equal to 100 mg/l.

Through the simulation under transient conditions, it was possible to evaluate the trend of mass transport during and after a given period of time. The simulation is based, like the previous ones, on the steady-state flow solution. The following are the settings set for this simulation. The time considered is 5 years (1825 days).

The hydrodynamic parameters set in the previous transport models remained unchanged (longitudinal dispersivity equal to 3 m, while the transverse dispersivity, 1/10 of the former, equal to 0.3 m).

Regarding the porosity value, we proceeded in both simulations with the sensitivity analysis of the equivalent porosity related to the limestone layer considering three porosity values equal to 50%, 70% and 90%. The upper layer of calcarenite, on the other hand, is characterized by a constant porosity value of 40% for the first 5 layers of the model.

The results of the scenarios for the latter case are shown below (Fig. 3.2.27, 3.2.28, 3.2.29)

We refer to the next chapter for a detailed description of the results obtained.

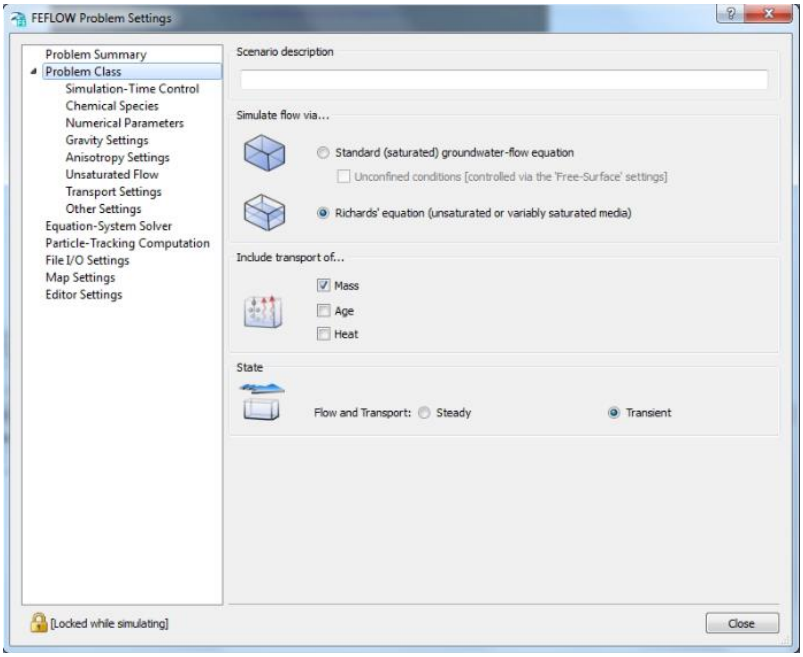

Fig. 3.2.26 – Problem settings for a transient unsaturated 3D mass concentration model

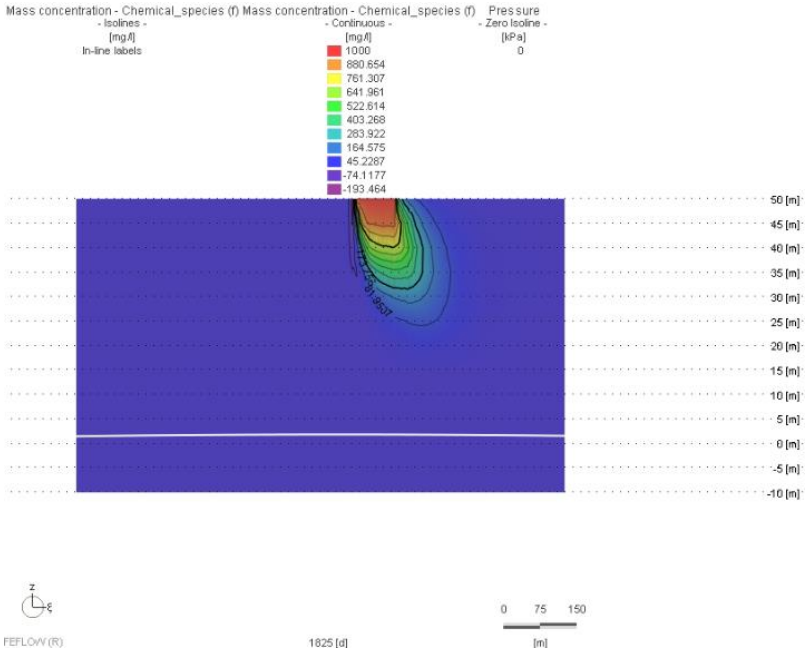

Fig. 3.2.27 – Mass concentration (aa) - 50% limestone porosity

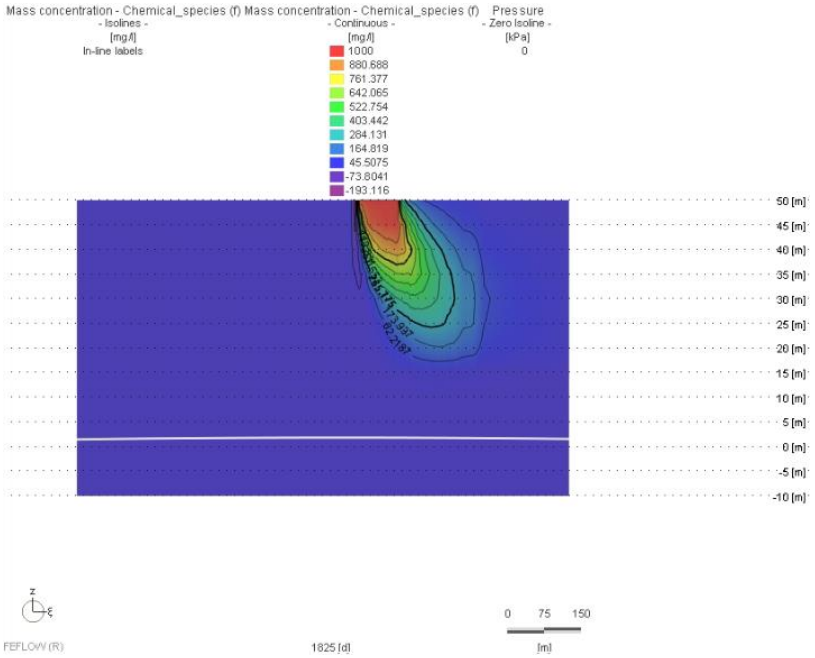

Fig. 3.2.28 – Mass concentration (aa) - 70% limestone porosity

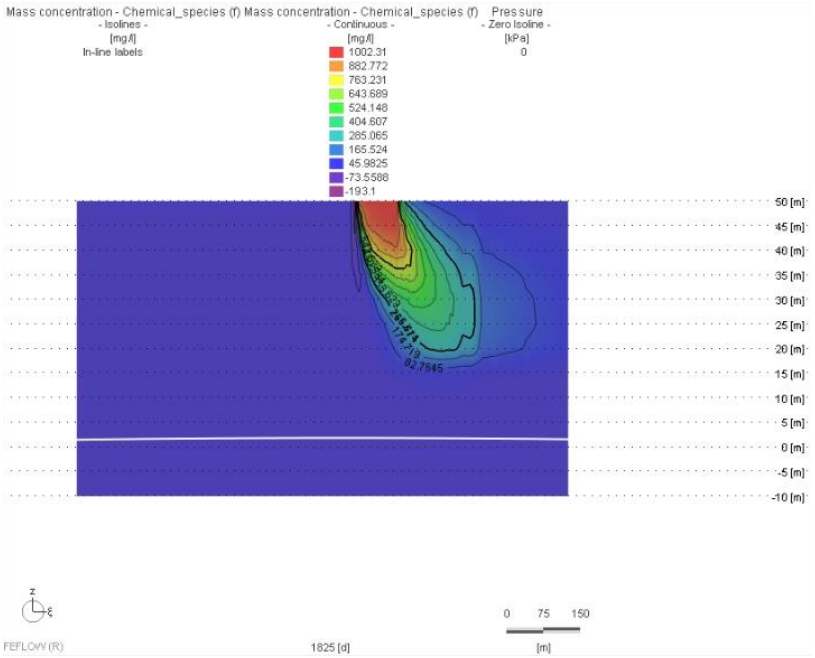

Fig. 3.2.29 – Mass concentration (aa) - 90% limestone porosity

3.3. DATA ANALYSIS

This chapter discusses the results obtained from the transportation simulations with respect to the various scenarios considered.

SIMULATION OF TRANSPORT UNDER STEADY-STATE CONDITIONS

Through the first steady-state transport simulation, results were obtained in the three scenarios considered with respect to the equivalent porosity values attributed to the limestone layer. It can be seen from Figure 3.3.1, in which the trends of the mass concentration along the cross-section in the different equivalent porosity scenarios are shown, that the plume increases as the percentage value of the equivalent porosity considered increases. This trend will also be confirmed in the subsequent figures. The value of the mass concentration decreases along the different layers of the model in all three scenarios analyzed. It can be seen that in the first layers (between the second and third slice) the concentration values remain very high, and this is represented by the red value present in the plume. After this slice, having an elevation of 40 meters above sea level, the concentration value starts to decrease up to the water table (white line).

50% limestone porosity	70% limestone porosity	90% limestone porosity
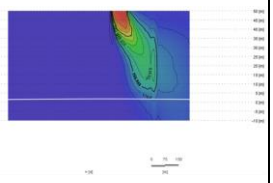	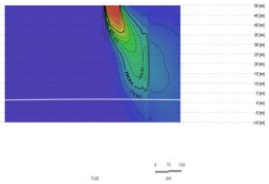	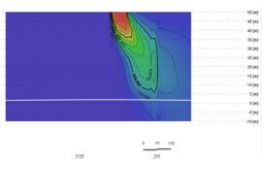

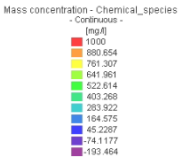

Fig. 3.3.1 – Scenarios of the plume trend

In order to have a more effective graphical and analytical resolution of the mass concentration trends both in the different scenarios and in the various layers, the trends under investigation were extrapolated into three slices: two in the calcarenite and one in the limestone. From these three layers, placed respectively at 45 meters above sea level (slice 2), 30 meters above sea level (slice 5) and 20 meters above sea level (slice 7), the graphs tabulated in the next figure 3.3.2 were obtained. The results from the slices with respect to the scenario of limestone with a porosity equivalent to 50% are shown in the first line. In the second line the scenario of equivalent porosity at 70% and finally the last scenario at 90%.

Analysing the results, considering the trend of the pollutant along the slices, it is possible to infer that there are preferential directions for the path of the contaminant particles. The graphs for each slice show that the isochrones close within the area where maximum concentrations occur. At shallow depths (slice 2) the contamination appears to be substantially contained within the contamination area, while at greater depths (slice 5 and slice 7), the propagation of contamination invades adjacent areas. Therefore, the values of the maximum concentrations decrease along the slices, investing however areas adjacent to the contamination area.

This trend is also reconfirmed in the other two scenarios with equivalent limestone porosity of 70% and 90%. Since we wanted to attribute a numerical value to the mass concentration along the layers to identify and quantify the propagation of the pollutant, we extrapolated from FEFLOW the databases containing the model outputs with reference to the values of the mass concentration along all the slices. Considering the three slices previously analyzed (slice 2, slice 5 and slice 7), the maximum concentration values were tabulated (TAB 3.3.1). It can be seen that the maximum concentration values decrease as we descend along the soil layers.

Both from the graphs obtained for each slice (Fig. 3.3.2) and from the table representing the maximum concentration values (Tab. 3.3.1) it can be observed that for higher porosity values the concentration value increases in the slices considered. Bypassing slice 2 in which the maximum value remains 1000 mg/l in all three situations of equivalent porosity, it can be seen that in slice 5 and slice 7 the value of the maximum concentration increases as the value of equivalent porosity increases.

	45m s.l.m. – slice 2	30m s.l.m. – slice 5	20m s.l.m. – slice 7
50 %	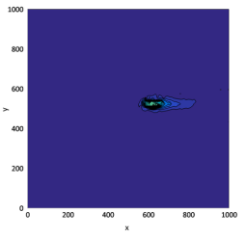	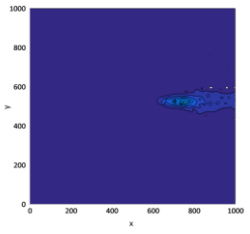	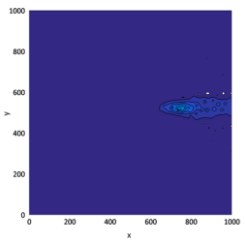

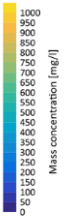

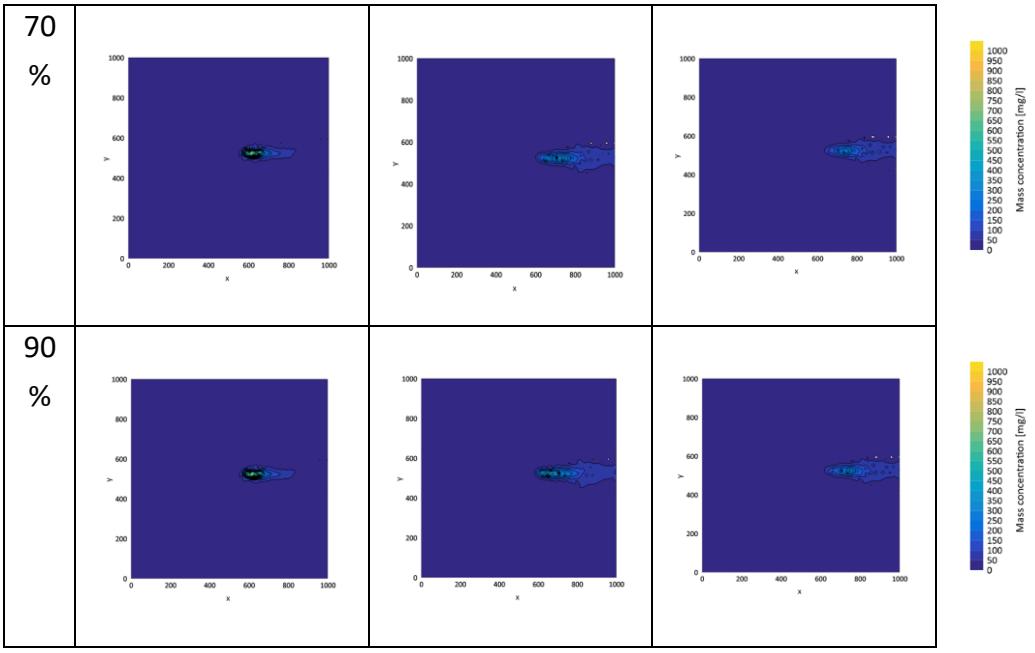

Fig. 3.3.2 – Mass concentration scenarios

Tab. 3.3.1 – Maximum values of mass concentration

	45m s.l.m. – slice 2	30m s.l.m. – slice 5	20m s.l.m. – slice 7
50%	1000 mg/l	452 mg/l	399 mg/l
70%	1000 mg/l	525 mg/l	423 mg/l
90%	1000 mg/l	722 mg/l	452 mg/l

A relationship between mass concentration and mass transport velocity was found from the scientific literature.

FEFLOW enabled the extrapolation of the process variables downstream of the simulations, defined as auxiliary variables, which support the evaluation and visualization of the results.

Through the "Darcy flux" function it has been possible to extrapolate the value of the mass transport velocity inside the flow. However, this setting, which cannot be used to implement the input parameters, allowed the identification

of the transport and the calculation of the trajectories. The results of extrapolating this variable for the three equivalent porosity scenarios are shown below (Fig. 3.3.3, 3.3.4, 3.3.5). The trajectory of the pollutant particle is made evident through the representation by means of the “bullets”. The values of the velocities decrease along the layers of the model, and this is evident from the colours present through the legend. It is also possible to notice a clear contrast between the two different geological units, evident in the passage between the two slices having an elevation respectively equal to 24 meters above sea level and 20 meters above sea level.

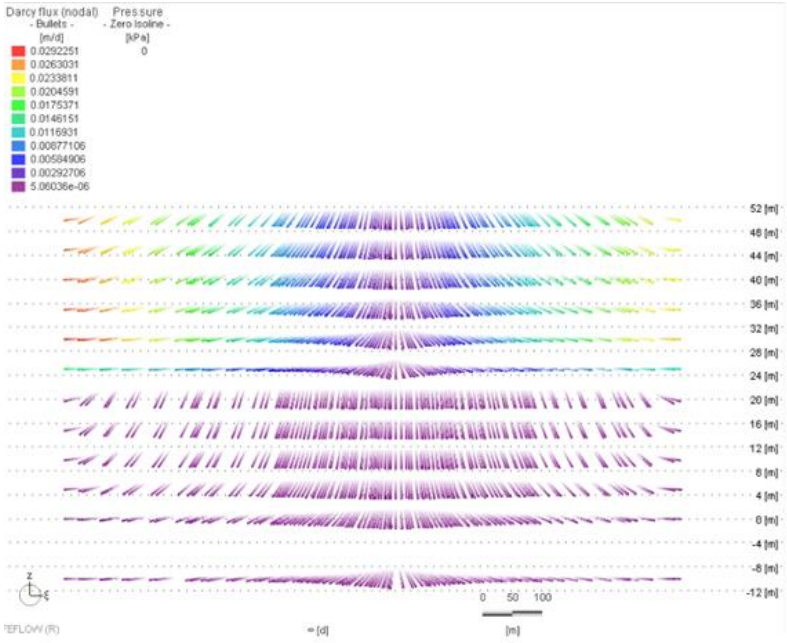

Fig. 3.3.3 – Darcy flux (nodal) (aa) - 50% limestone porosity

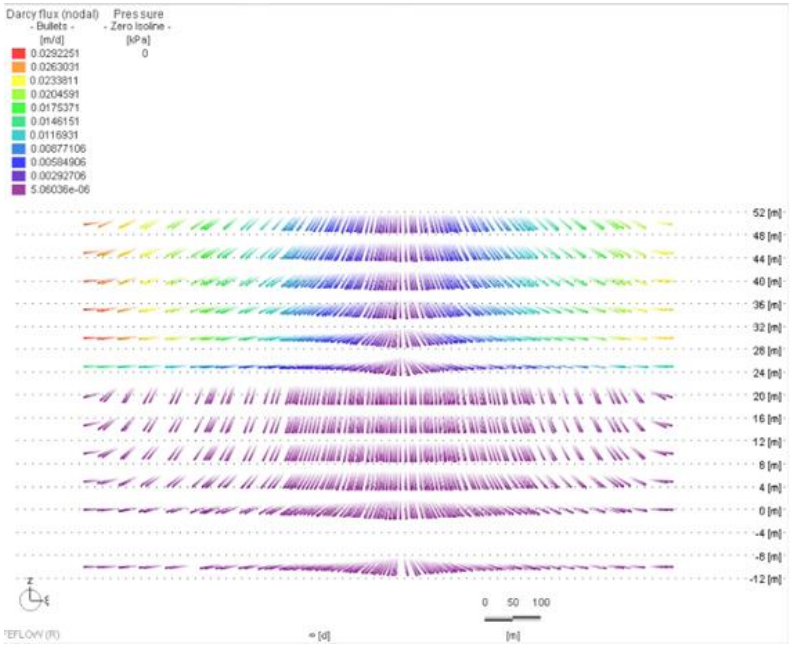

Fig. 3.3.4 – Darcy flux (nodal) (aa) - 70% limestone porosity

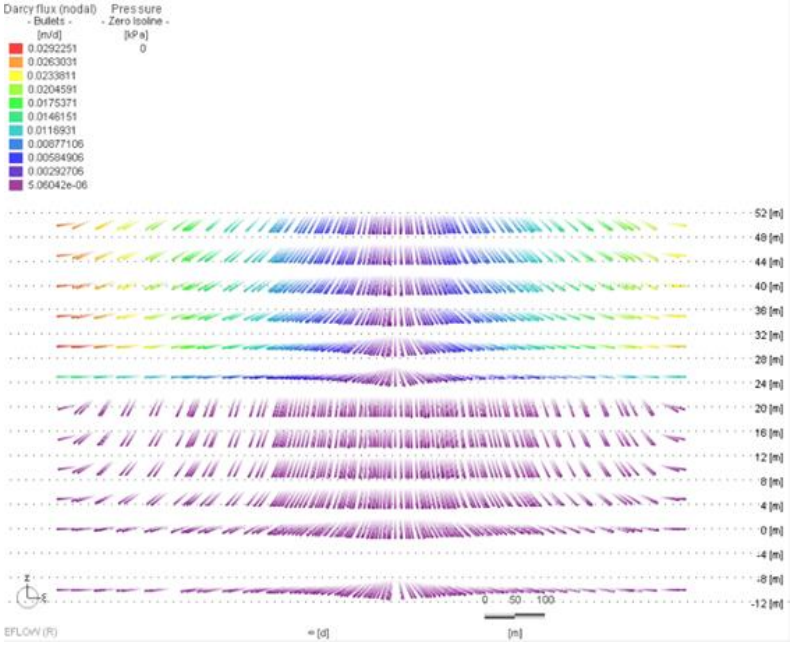

Fig. 3.3.5 – Darcy flux (nodal) (aa) - 90% limestone porosity

50% limestone porosity	70% limestone porosity	90% limestone porosity
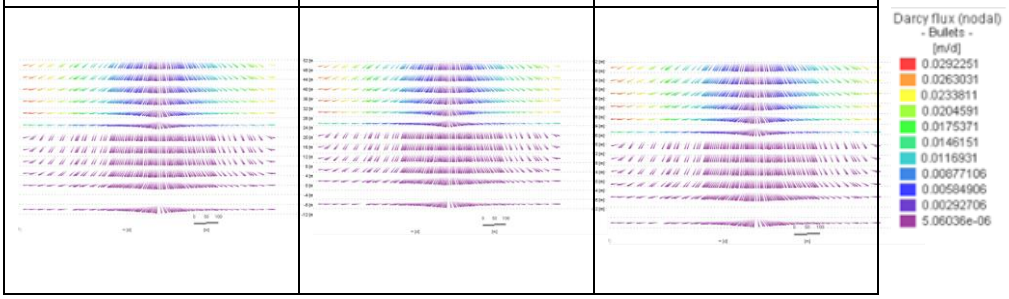		

Fig. 3.3.6 – Scenarios of Darcy flux (nodal)

In order to have an easier understanding of the data regarding this speed value, we proceeded through the extrapolation of the FEFLOW data base. Below is the graph (Fig. 3.3.7) obtained from the analysis of the data with respect to the average speed relative to the value of the "Darcy flux". This data base is composed of all the mass transport velocity values for each node of the model. From the three slices (slice 2, slice 5 and slice 7) it was possible to plot a graph showing the trend of the average speed through the data analysis with Excel, starting from the output data of Feflow. The decreasing trend is explained by the decrease in pollutant along the various depths. A divergent decline in velocity between a limsone porosity of 70% and 90% can also be observed. It is recalled that the first two slices are in the first geological unit (calcarenite), while the last slice under consideration (slice 7) is related to the limestone layer. From the trend of the three scenarios, it was possible to identify the different average values of the velocities throughout the three scenarios. It can be seen that the average mass transport velocity in the scenario related to 90% limestone porosity has higher values than in the other two scenarios. Moreover, it can be seen in the graph that in the scenario related to 50% limestone porosity, the slope of the curve is constant, and this is justified by the small difference in the value of the porosity of the two geological units. In this scenario, in fact, the porosity of calcarenite has been set equal to 40%, while limestone to 50%.

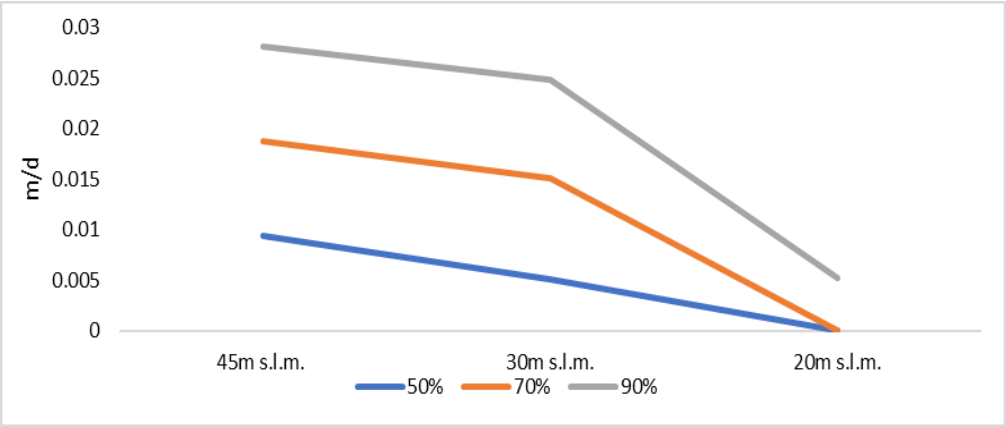

Fig. 3.3.7 – Mass transport velocity scenarios

SIMULATION OF THE TRANSPORT IN STEADY-STATE CONDITIONS WITH THE INJECTION WELL

The second transport simulation considered the presence of an injection well. The results obtained in the three equivalent porosity scenarios are shown below. Differences can be seen with respect to the previous simulation, and this is due not only to the different hypothetical contamination methodologies but also to the amount of pollutant injected. In this condition, in fact, a dilution occurs due to the fact that the hypothetical pollutant is injected through a flow in a dispersant well. Thus, the initial conditions of mass transport will be different. It can be seen from figure 3.3.8 how the area represented by the contamination cone increases as the percentage value of the equivalent porosity in the limestone increases.

50% limestone porosity	70% limestone porosity	90% limestone porosity
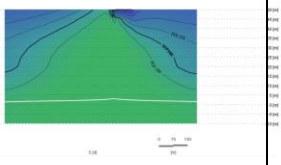	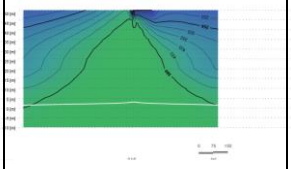	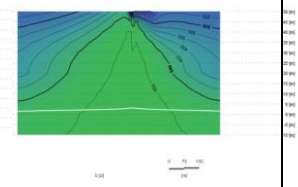

Fig. 3.3.8 – Scenarios of the plume trend

In order to evaluate the scenarios in the most detailed and systematic way possible, the analysis of the second simulation results followed the same steps as the analysis of the previous mass transport simulation. Thus, the trends investigated in three slices (slice 2, slice 5, and slice 7) were extrapolated to the different scenarios of the equivalent limestone porosity (50%, 70%, and 90%) tabulated in the figure 3.3.9 below. The graphs for each slice show that the isochrones join up to form a circular shape within the area where maximum concentrations occur. As the depth of the soil increases, it can be seen that the isochrones' area of action also increases, i.e., the area where the concentration is highest. This trend is also reconfirmed in the other two scenarios having equivalent limestone porosity of 70% and 90%.

In order to quantify the numerical value of the mass concentration in the various scenarios and in the various slices, we proceeded to the numerical extrapolation of the data base containing the outputs of the model. In the table 3.3.2, where the values obtained from the analysis of the data are reported, it can be seen that while increasing the area of propagation of the pollutant, the maximum values of the concentration undergo small decreases going down between slice 2 and slice 5, while between slice 5 and slice 7 the decrease is less marked.

	45m s.l.m. – slice 2	30m s.l.m. – slice 5	20m s.l.m. – slice 7
50 %	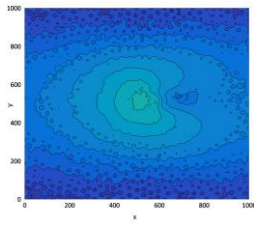	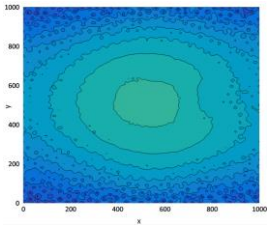	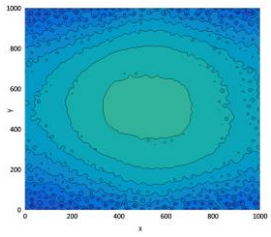
70 %	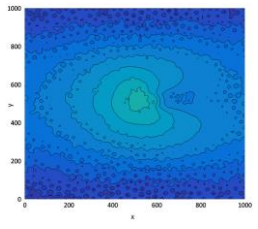	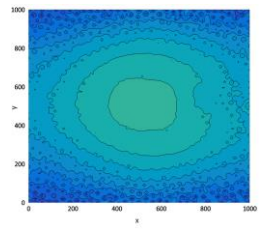	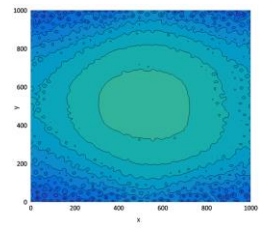
90 %	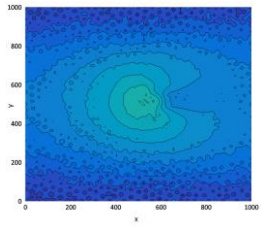	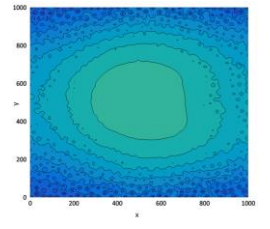	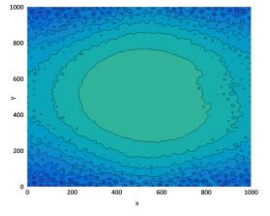

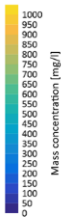

Fig. 3.3.9 – Mass concentration scenarios

Tab. 3.3.2 – Maximum values of mass concentration

	45m s.l.m. – slice 2	30m s.l.m. – slice 5	20m s.l.m. – slice 7
50%	525 mg/l	518 mg/l	518 mg/l
70%	531 mg/l	524 mg/l	524 mg/l
90%	558 mg/l	550 mg/l	550 mg/l

On the other hand, as regards the analysis of the various scenarios, it can be seen from the table 3.3.2 that the higher the porosity of limestone, the higher the concentration of a contaminant. This trend is also confirmed by the figure 3.3.9 in which it is evident the increase in the diameter of the isochones for each slice with respect to the scenarios of increased porosity.

Similarly, proceeding with the analysis of the mass transport velocity, the results of the extrapolation of the process variable for the three scenarios of equivalent porosity, through the function of "Darcy flux" are reported below. From the figures 3.3.10, 3.3.11, 3.3.12, evaluating the distribution of the bullets or the coloration, it can be seen that the value of the mass transport velocity is characterized by a growth in correspondence to the slice having an elevation equal to 20 meters above sea level, or in correspondence to the end of the well.

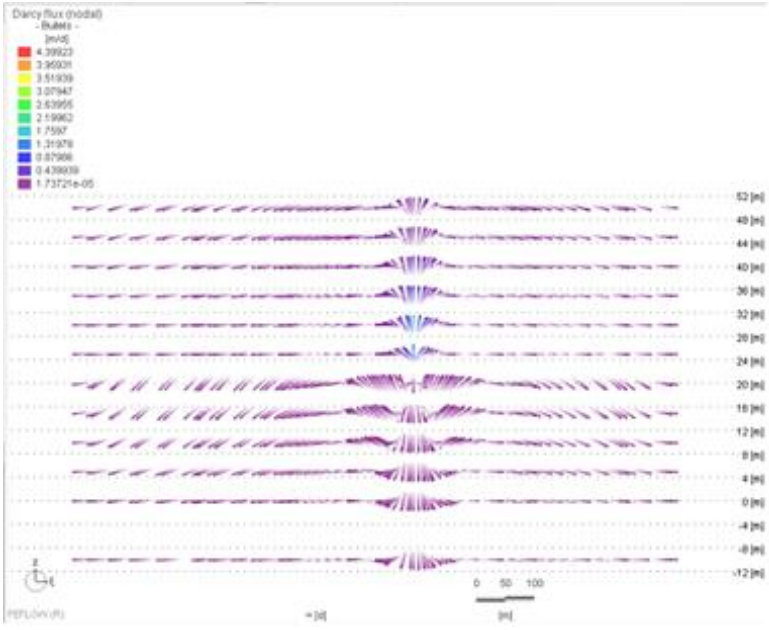

Fig. 3.3.10 – Darcy flux (nodal) (aa) - 50% limestone porosity

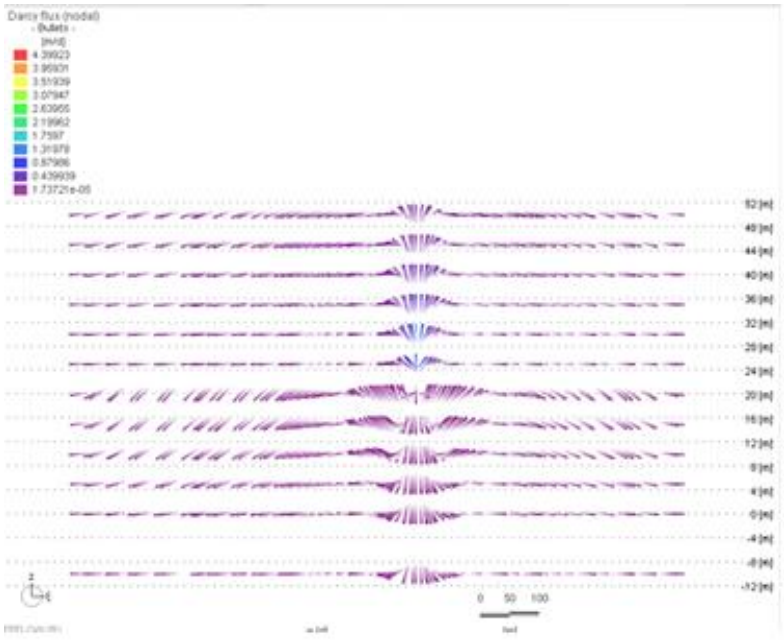

Fig. 3.3.11 – Darcy flux (nodal) (aa) - 70% limestone porosity

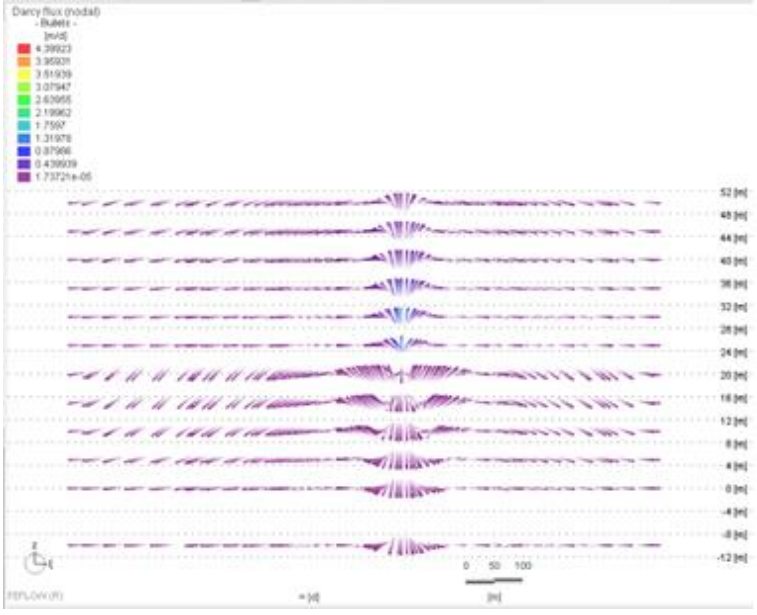

Fig. 3.3.12 – Darcy flux (nodal) (aa) - 90% limestone porosity

50% limestone porosity	70% limestone porosity	90% limestone porosity
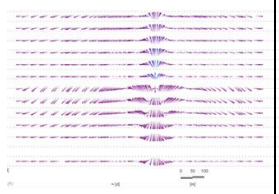	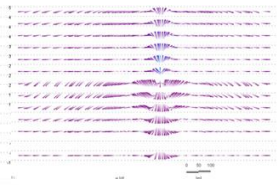	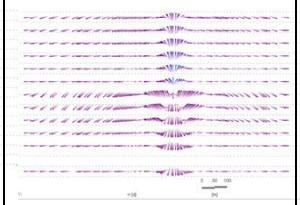

Fig. 3.3.13 – Scenarios of Darcy flux (nodal)

Subsequently, the transport speed value was extrapolated from the FEFLOW data base. Below is the graph obtained from the analysis of the data with respect to the average speed relative to the value of the "Darcy flux" (Fig. 3.3.14). It can be seen that the speed undergoes an initial increase in the average value and then decreases up to slice 7. This trend is justified by the presence of the well up to slice 5, i.e. by the action of the injected flow that causes an increase in the value of the average speed. After slice 5, the pollutant particle slows down due to the passage through the limestone medium and therefore the average of the mass transport velocity decreases. From the trend of the three scenarios, it was possible to identify the different trends in average velocity for each value. It can be noticed that the average speed of the pollutant particle in the scenario related to a limestone porosity of 90% has higher values respectively to the other two scenarios.

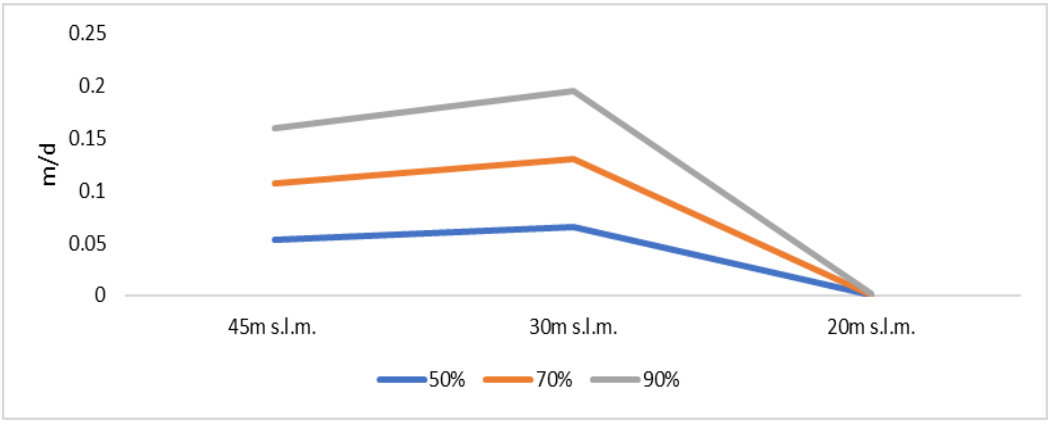

Fig. 3.3.14 – Mass transport velocity scenarios

As a final analysis, downstream of the two mass transport simulations carried out with and without the input well, the values of the average velocities of the results of the two simulations were considered with respect to the scenario of a limestone porosity of 70%. From the graph below (Fig. 3.3.15) it is evident that the average mass transport velocity in the condition of diffusion through the well is greater than the propagation of the hypothetical pollutant without the well.

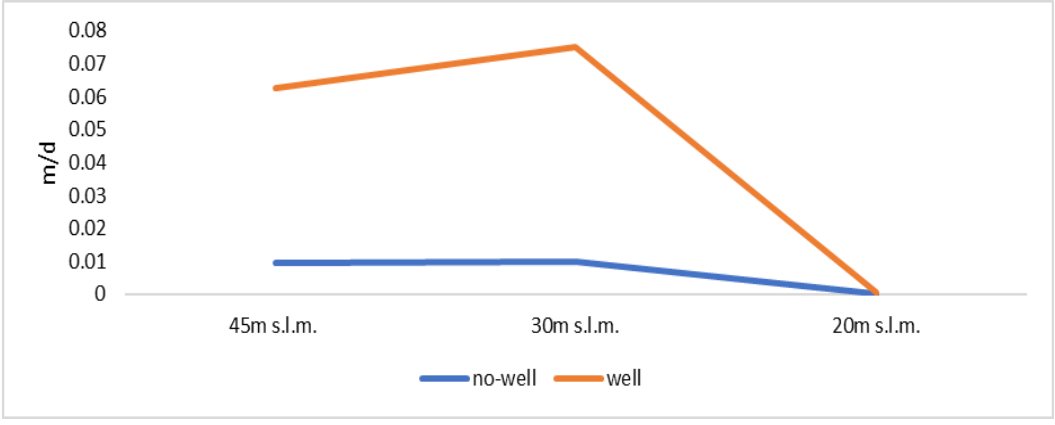

Fig. 3.3.15 – Mass transport velocity scenarios

TRANSIENT TRANSPORT SIMULATION

50% limestone porosity	70% limestone porosity	90% limestone porosity
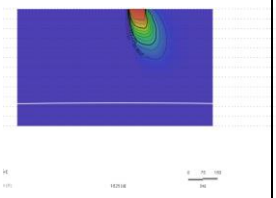	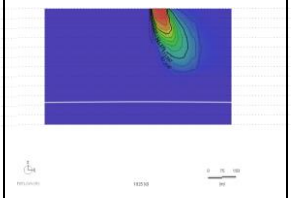	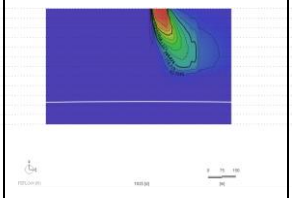

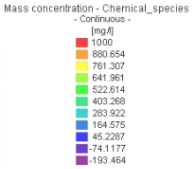

Fig. 3.3.16 – Scenarios of the plume trend

The last simulation analysed was the mass transport assessment under transient conditions. Figure 3.3.16 shows the results obtained under the different scenarios after five years. This simulation enabled the gathering of results and values of mass concentrations relative to a specified time period (1825 days). From the results obtained, it can be seen that the pollutant spreads more as the value of the equivalent porosity attributed to the limestone layer increases. It can also be seen that the pollutant undergoes a clear slowdown from the two layers of soil present. These evaluations are confirmed by the data analysis carried out downstream of the simulations with respect to the trend and value of mass concentrations in different slices (slice 2, slice 5 and slice 7) and in different scenarios (50%, 70% and 90% porosity of limestone) (Fig. 3.3.17).

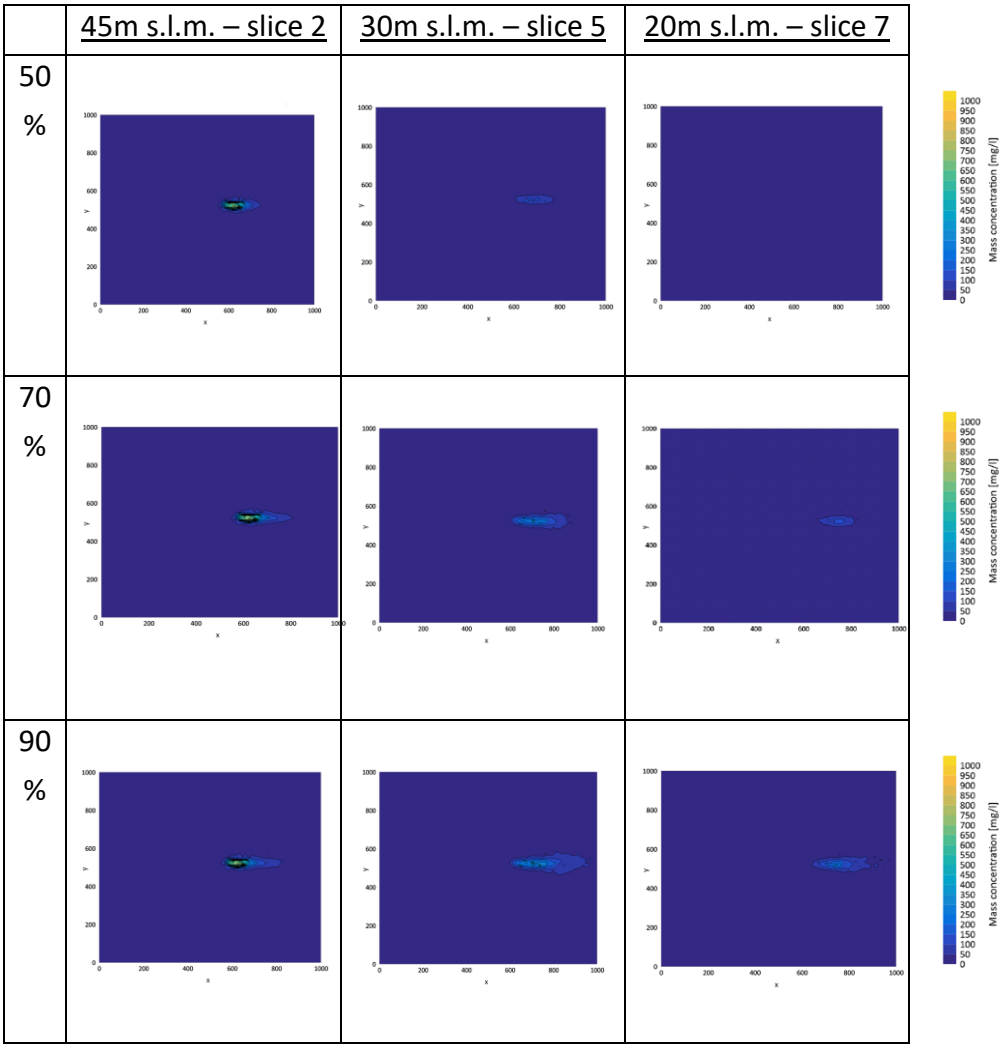

Fig. 3.3.17 – Mass concentration scenarios

Tab. 3.3.3 – Maximum values of mass concentration

	45m s.l.m. – slice 2	30m s.l.m. – slice 5	20m s.l.m. – slice 7
50%	946 mg/l	210 mg/l	32 mg/l
70%	997 mg/l	436 mg/l	172 mg/l
90%	1000 mg/l	505 mg/l	297 mg/l

In this simulation the trend of pollutant propagation is more evident. Considering the first scenario (50% porosity of the limestone) it can be seen that the maximum concentration values diminish as they go down along the soil layers, until they reach a concentration in slice 7 that is not evident (less than 50 mg/l). From the tabulated values (Tab. 3.3.3), in fact, there is a sudden reduction in the various slices until a value of 32 mg/l is reached. This trend mirrors that of the first simulation: the values of the maximum concentrations decrease along the slices but contaminant spreads to areas adjacent to the site of original contamination. This behavior, graphically justified by the trend of the isochrones and the values of the maximum mass concentrations in the table 3.3.3, is also reconfirmed in the other two scenarios having limestone equivalent porosity of 70% and 90%.

With regard to the analysis of the average transport velocities considered, it is possible to verify from the graphs obtained a decreasing trend with respect to the model slices (Fig. 3.3.18, 3.3.19, 3.3.20). This decrease in the velocities can be justified by the decrease of the pollutant along the depths. It is also possible to notice a different rate of decline due to the different porosity of the two geological units. The trend of the mass transport velocity values confirms that of the first transport simulation under steady-state conditions, although assumes different orders of velocity. This is also confirmed by the trend of the three scenarios of limestone porosity: the average of the mass transport velocity in the scenario related to 90% limestone porosity has higher values than in the other two scenarios. Furthermore, the slope of the graph with respect to the scenario of 50% limestone porosity is also constant in the two sections due to the small difference in the porosity values of the two geological units (Fig. 3.3.22).

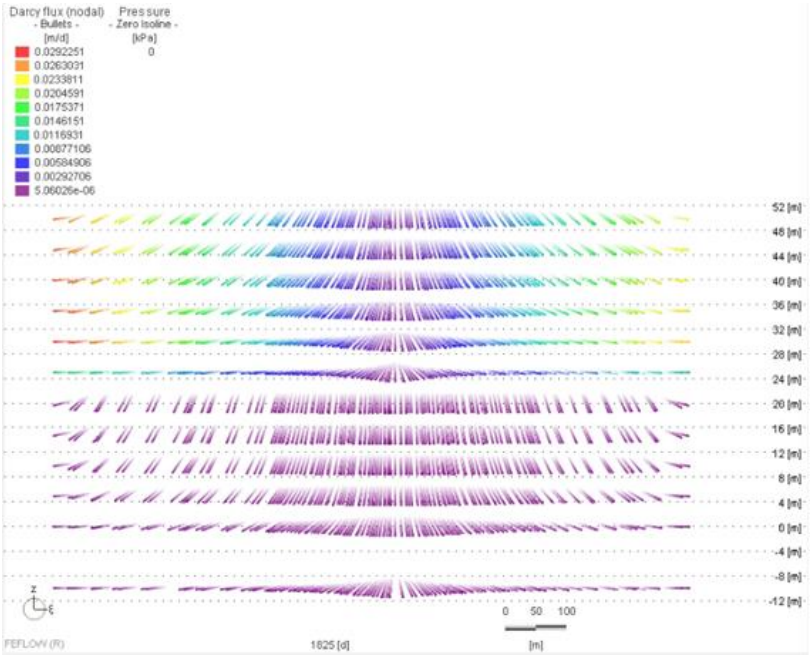

Fig. 3.3.18 – Darcy flux (nodal) (aa) - 50% limestone porosity

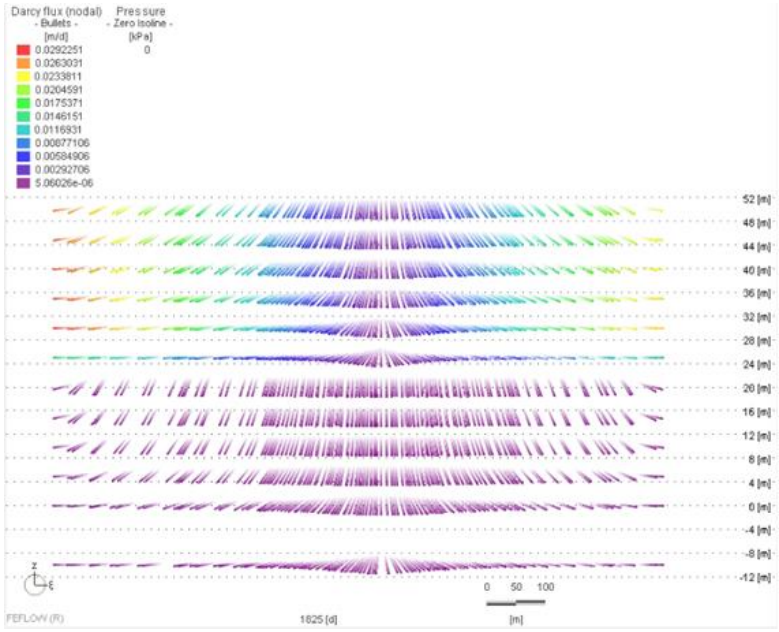

Fig. 3.3.19 – Darcy flux (nodal) (aa) - 70% limestone porosity

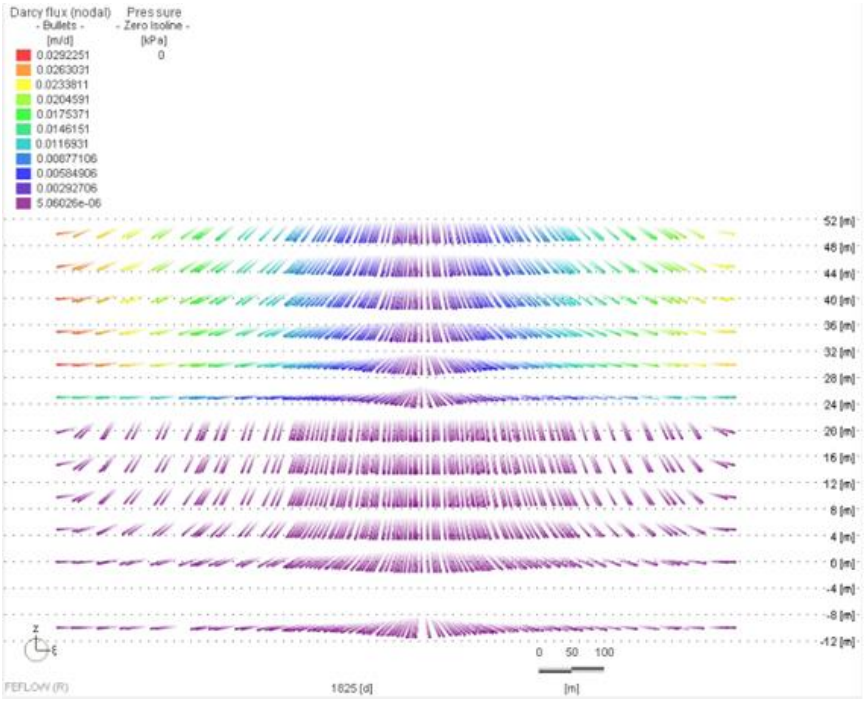

Fig. 3.3.20 – Darcy flux (nodal) (aa) - 90% limestone porosity

50% limestone porosity	70% limestone porosity	90% limestone porosity
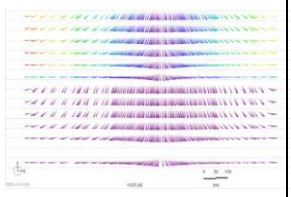	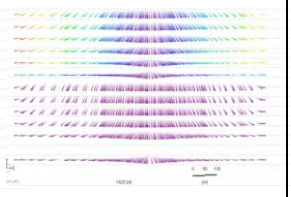	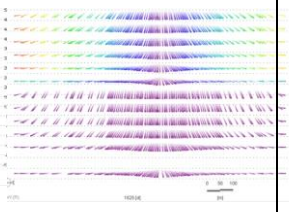

Fig. 3.3.21 – Scenarios of Darcy flux (nodal)

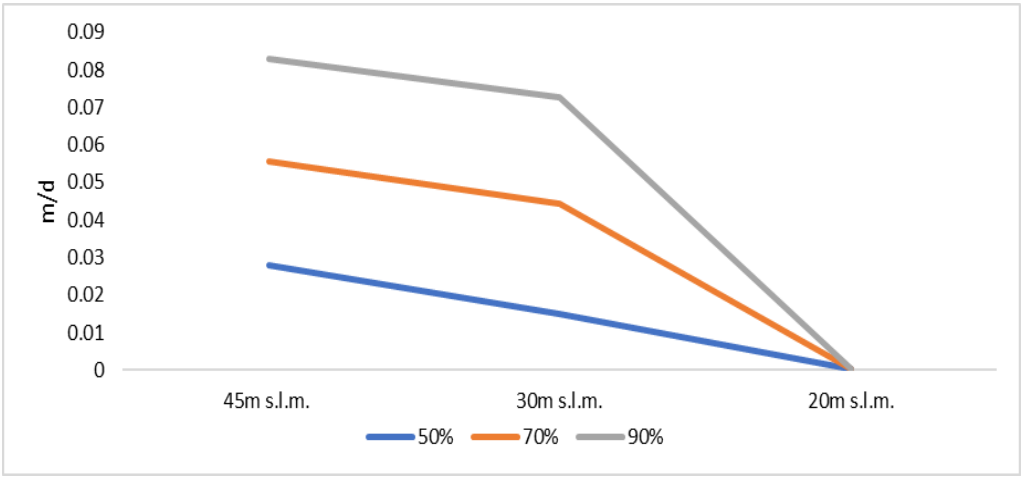

Fig. 3.3.22 – Mass transport velocity scenarios

4. DISCUSSION AND CONCLUSIONS

Increasing urban development, increased industrial activities, increased water demand due to climate change, and the resulting increase in urban runoff volumes due to the presence of impervious surfaces result in negative impacts to groundwater both quantitatively and qualitatively. One of the proposed solutions to mitigate this negative impact is the reuse of urban runoff for groundwater recharge through soil infiltration (USEPA, 2003, Country of Los Angeles Department of Public Works, 2014). Managed aquifer recharge (MAR) techniques aim to re-charge the aquifer under controlled conditions for the purpose of subsequent recovery or as a barrier to prevent seawater intrusion. In many U.S. states, injection wells are used to convey runoff to urban areas and to recharge aquifers in semi-arid regions. However, the presence of residual contaminants in the injected stream problematises this solution because it can affect human health.

This case study has strong practical relevance as it succeeds in fully representing the aforementioned issues in a field of application of great hydrogeological complexity. The site modelled in the present work is located adjacent to the municipality of Avetrana, a place where a channel for the bridging and collection of meteoric and alluvial waters has been planned to protect the built-up area. It is characterized by a high level of hydraulic disturbance that makes it necessary to evaluate the vulnerability to pollution of the karstic aquifer, characterized by a low anti-pollution capacity and therefore very fragile.

Karst aquifers, which provide 40% of drinking water sources, and in the Apulia Region represent the only potable water resource, are characterized by the propensity to rapid transfer of pollutants and therefore the propensity to be subject to pollution. Specifically, exposure to contamination by karst aquifers is due to the presence of the interconnected network of voids to springs through which contaminants travel rapidly. A topic of great reflection related to the vulnerability of karst aquifers is the extreme difficulty or rather the near impossibility of restoring the pristine condition once contamination has occurred (Parise, 2007). In order to model the behaviour of the pollutant in the soil, and therefore determine the most effective remediation, it is necessary to identify the modelling approach that best represents the groundwater flow under analysis. In addition, the conduits present in karst aquifers are difficult to locate and spatially distribute, which affects the validity of the results through numerical models (Chen Z. et al., 2014). Based on this, it was decided, therefore, to adopt the Equivalent Porous Medium approach through which it was possible to approximate the behaviour of fractured rock to a continuous medium through the mediation of the properties of the rock matrix over a statistically minded representative volume. Through the Porous Medium Equivalent model, it was possible to determine properties related to the fractured aquifer otherwise difficult to identify through tectonic and geophysical studies, which are unable to detect discontinuities in depth. Specifically, after analysing the geological state of the territory considered in this study through hydrogeological reports and field tests, two different hydrogeological environments have been identified. The upper environment, characterized by a modest propensity to absorption, seat of the calcarenite layer, and the lower environment, seat of the deep-water table, characterized by primary and secondary discontinuities, seat of the limestone layer. For the definition of the hydrological parameters, in order to build the model, the parameters obtained from sounding tests carried out in situ were evaluated, considering both geological units as isotropic media, resulting in a simulation of the flow and transport of groundwater of the equivalent po-

rous medium. The software FEFLOW (Finite Element subsurface FLOW and transport system), based on the finite element method, was used to determine the three-dimensional numerical groundwater model.

The objective of the model was to simulate the groundwater flow and transport of a leached pollutant within the unsaturated zone, evaluating the infiltration capacity in the soil and therefore the possibility of contamination of the deep aquifer. FEFLOW is one of the most sophisticated numerical codes available for the simulation of flow and transport processes in porous media, in saturated and unsaturated conditions. The modelling platform is equipped, in fact, with an advanced graphical environment that allows the simulation of underground flow dynamics in complex situations and the transport of contaminants in the aquifer. The simulations were carried out considering the stationary flow, and then implemented with the transport model both in stationary and transient conditions. Through the latter it was possible to consider a specified period of time within which to perform the modelling, thus having an end point and starting from an initial condition. On the contrary, a modelling solution in stationary conditions was obtained by representing the state of the system at fixed boundary conditions and material properties for an infinitely long time. In the specific case, a combination of the stationary flow with a transient transport simulation was ultimately performed. The groundwater flow field was obtained by incorporating boundary conditions and parameters derived from hydrogeologic reports, field tests, and literature review. Three different scenarios were considered for each transport simulation depending on the different value of the equivalent porosity attributed to the limestone layer (50%, 70%, 90%). This sensitivity analysis of the equivalent porosity with respect to the aquifer layer was conducted because the sounding tests carried out in situ did not investigate the value of this hydraulic parameter, which is assumed to be high due to the high number of cracks present in the area under study. Through the results obtained from the transport simulations with respect to the various scenarios considered, it was possible to carry out an analysis of i) the data extrapo-

lated from the model outputs with respect to the concentration values and ii) the trend of the transport speed of the pollutant particle in the flow. The different contamination modes, that is from a source on the ground plane or through the injection well, demonstrated different mass transport trends under steady-state conditions. In both simulations (with and without well) the plume increases as the percentage value of the equivalent porosity considered increases.

The differences found in the results of the simulations are not only due to the different hypothetical contamination methodologies but also to the different amount of pollutant input. In the simulation through the injection well, in fact, a dilution of the contamination occurred due to the fact that the hypothetical pollutant is introduced through a flow in the well. Thus, the initial conditions of mass transport were different.

Extrapolating the values of the maximum concentrations, it was possible to evaluate the mass transport trend along three slices of the model (slice 2, slice 5, and slice 7). The outlined isochrones formed a close shape within the area where maximum concentration values were identified. At shallow depths (slice 2), contamination appeared to be substantially contained within the area of contamination, whereas at greater depths (slice 5 and slice 7), the propagation of contamination affected adjacent areas. Thus, maximum concentrations showed a decrease along the slices but spread to areas adjacent to the contamination area. This pattern was confirmed in both simulations.

Downstream of the two mass transport simulations performed with and without an inlet well, the values of the average velocity results of the two simulations were considered with respect to the 70% limestone equivalent porosity scenario.

From the graphs obtained it was possible to observe that the value of the average velocity of transport in the condition of diffusion through the well is greater than the propagation of the hypothetical pollutant without the well. Moreover, the velocities in both simulations increase as the equivalent porosity of the limestone increases. Finally, through the simulation of mass transport

under transient conditions, results and trends in mass concentrations could be obtained relative to a specified time period. The source was identified over an area corresponding to ten nodes of the first slice model, and 1825 days was set as the simulation time. From the results obtained, a greater diffusion of the pollutant was inferred as the value of the equivalent porosity attributed to the limestone layer increased. It can be noticed how the pollutant undergoes a slowdown in correspondence with the passage from calcarenite to limestone.

In conclusion, it can be stated that due to the lithology involved, a slowing down of pollutant propagation in the vadose zone has been shown. Considering that the input conditions in the transport model represent extreme and occasional situations, the modeling performed showed that the geologic structure represents a potential barrier to pollution.

The methodology adopted in this study has determined the development of the conceptual hydrogeological model of the karst aquifer, about the case of study, and then the modelling of mass transport of a hypothetical contaminant in different scenarios. It was therefore possible to represent, with good approximation, the groundwater system and provide references to prevent pollution in karst aquifers, characterized by high intrinsic volatility. Through numerical modelling it is possible to systematise the characteristics of hydrogeological environments that are highly complex and therefore characterized by a high variability of the geo-structural variability. Moreover, these simulations enable the identification of the area that requires safeguarding due to contamination: the plume and the inverse conoid. This approach represents, therefore, a further contribution to the surface study of what are the targets that must be observed when a release is granted. Notably, the methodology that distinguishes this study can also be used for other similar cases. The cases of final deliveries in areas characterized by karst aquifers are numerous and this study represents a useful methodological tool to the problem, determinating an application implication of great interest.

5. ACKNOWLEDGEMENTS

I would like to thank my supervisors Professor A. F. Piccinni and Professor V. Iacobellis for their time and dedication. Particularly Professor A.F. Piccinni for his guidance throughout this process.

Special thanks to my colleagues Rosangela and Virginia for their help, continued support, and time shared together. Finally, I would like to thank Antonello, my parents, my brother, and my friends for their encouragement during this journey.

REFERENCES

Alem, Abdellah, Abdulghadir Elkawafi, Nasre-Dine Ahfir, and HuaQing Wang. 2013. “Filtration of Kaolinite Particles in a Saturated Porous Medium: Hydrodynamic Effects.” Hydrogeology Journal 21, no. 3: 573-86. Accessed May 23, 2019. http://dx.doi.org/10.1007/s10040-012-0948-x.

Alem, Abdellah, Nasre-Dine Ahfir, Abdulghadir Elkawafi, and HuaQing Wang. 2015. “Hydraulic Operating Conditions and Particle Concentration Effects on Physical Clogging of a Porous Medium.” Transport in Porous Media 106, no. 2 (October): 303-21. Accessed May 23, 2019. http://dx.doi.org/10.1007/s11242-014-0402-8.

Anderson MP, Woessner WW (1992) Applied groundwater modeling: simulation of flow and advective transport. Academic Press, New York, 381p

Anderson, M.P., Woesner, W.W., 2002. Applied Groundwater Modeling. Academic Press.

Beliaev A.Y., Schotting R.J., Analysis of a new model for unsaturated flow in porous media including hysteresis and dynamic effects, Computational Geosciences 5: 345–368, 2001.

Berre I., Doster F., Keilegavlen E., Flow in Fractured Porous Media: A Review of Conceptual Models and Discretization Approaches, Transport in Porous Media (2019) 130:215–236 https://doi.org/10.1007/s11242-018-1171-6

Bouchemella S., Ichola I., Séridi A., Estimation of the empirical model parameters of unsaturated soils, E3S Web of ConferenceS, 2016, 10.1051/e3sconf/20160916007

Bouwer, H. Artificial recharge of groundwater: Hydrogeology and engineering. Hydrogeol. J. 2002, 10, 121–142. http://dx.doi.org/ 10.1007/s10040-001-0182-4.

Bouwer, Herman. 2002. "Artificial Recharge of Groundwater: Hydrog ology and Engineering" Hydrogeology Journal 10, no. 1 (February): 121-42. Accessed May 23, 2019. http://dx.doi.org/10.1007/s10040-001-0182-4.

Castiglioni, S., Valsecchi, S., Polesello, S., Rusconi, M., Melisa, M., Palmiotta, M., Manenti, A., Davoli, E., Zuccato, E., 2015. Sources and fate of perfluorinated compounds in the aqueous environment and in drinking water of a highly urbanized and industrialized area in Italy. https://doi.org/10.1016/j.jhazmat.2014.06.007

Chen Z., Goldscheider N., Modeling spatially and temporally varied hydraulic behavior of a folded karst system with dominant conduit drainage at catchment scale, Journal of Hydrology, Volume 514, 6 June 2014, Pages 41-52

Cheng, J., Vecitis, C.D., Park, H., Mader, B.T., Hoffmann, M.R., 2008. Sonochemical Degradation of Perluorooctane Sulfonate (PFOS) and Perfluorooctanoate (PFOA) in Landfill Groundwater: Environmental Matrix Effects. https://doi.org/10.1021/es8013858

Chenini I., Zghibi A., Kouzana L., Hydrogeological investigations and groundwater vulnerability assessment and mapping for groundwater resource protection and management: State of the art and a case study, Journal of African Earth Sciences 109 (2015) 11–26, http://dx.doi.org/10.1016/j.jafrearsci.2015.05.008

Cherubini C., Giasi C., Approccio geostatistico per la simulazione del flusso e del trasporto nel Calcare di Bari, Giornale di Geologia Applicata 2 (2005) 167–172, 10.1474/GGA.2005–02.0–24.0050

Chu J., Liu N., Miao Y., Lin X., Tan H., Liu F. 2020. Numerical simulation and pollution prediction of karst groundwater in water-conducting faults distribution area. 2020 6th International Conference on Energy, Environment and Materials Science.

Cordner, A., De La Rosa, V.Y., Schaider, L.A., Rudel, R.A., Richter, L., Brown, P., 2018. Guideline levels for PFOA and PFOS in drinking water: the role ofscientific uncertainty, risk assessment decisions, and social factors. https://doi.org/10.1038/s41370-018-0099-9

Cotecchia V., Simeone V., Gabriele S., Le acque sotterranee e l'intrusione marina in Puglia, 2017, https://www.isprambiente.gov.it/files2017/pubblicazioni/periodici-tecnici/memorie-descrittive-della-carta-geologica-ditalia/volume-92/memdes_92_1_2_caratteri_idrogeologici.pdf

Delle Rose M., Fidelibus C. 2016. Water resource management in karstic catchments: the case of the Asso Torrent basin (Southern Italy). Springer-Verlag

Delle Rose M., Martano P., Fidelibus C. 2020. The Recent Floods in the Asso Torrent Basin (Apulia, Italy): An Investigation to Improve the Stormwater Management. Water MDPI

Dillon P., Stuyfzand P., Grischek T., Lluria M., Pyne R., Jain R., Bear J., Schwarz J., Wang W., Fernandez E., Sixty years of global progress in managed aquifer recharge, Hydrogeology Journal (2019) 27:1–30 https://doi.org/10.1007/s10040-018-1841-z

Dillon, P., Pavelic, P., Page, D., Beringen, H., Ward, J., 2009. Managed Aquifer Recharge. In an Introduction Waterlines Report Series No. 13. National Water Commission, Canberra, Australia.

Dillon, P., Stuyfzand, P.J., Grischek, T., Liuria, M., et al., 2018. Sixty years of global progress in managed aquifer recharge. Hydrogeol. J. https://doi.org/10.1007/ s10040-018-1841-z.

Edwards, Emily C., Thomas Harter, Graham E. Fogg, Barbara Washburn, and Hamad Hamad. 2016. "Assessing the Effectiveness of Drywells as Tools for

Stormwater Management and Aquifer Recharge and their Groundwater Contamination Potential." Journal of Hydrology 539 (August): 539-53. Accessed May 23, 2019. http://dx.doi.org/10.1016/j.jhydrol.2016.05.059.

Equivalent Porous Media (EPM) Simulation of Groundwater Hydraulics and Contaminant Transport in Karst Aquifers

Fakhreddine S., Prommer H., Scanlon B., Ying S., Nicot J., Mobilization of Arsenic and Other Naturally Occurring Contaminants during Managed Aquifer Recharge: A Critical Review, Environ. Sci. Technol. 2021, 55, 2208−2223, dx.doi.org/10.1021/acs.est.0c07492

FEFLOW 7.0 user guide, 2016.

Felizeter, S., McLachlan, M.S., De Voogt, P., 2012. Uptake of Perfluorinated Alkyl Acid by Hydroponically Grown Lettuce (Lactuca sativa). https://doi.org/10.1021/es302398u

Freeze, R.A., Cherry, J.A., 1979. Groundwater. Prentice Hall.

Gattinoni P., Modellazione degli acquiferi fessurati, Dispensa estratta dalle presentazioni del corso di formazione permanente "Studi idrologici per la gestione delle risorse idriche sotterranee alla luce degli strumenti normativi" Milano 2009

Ghasemizadeh R, Yu X, Butscher C, Hellweger F, Padilla I, Alshawabkeh A (2015) Equivalent Porous Media (EPM) Simulation of Groundwater Hydraulics and Contaminant Transport in Karst Aquifers. PLoS ONE 10(9): e0138954. 10.1371/journal.pone.0138954

Ghisi, R., Vamerali, T., Manzetti, S., 2019. Accumulation of perfluorinated alkyl substances (PFAS) in agricultural plants: A review. https://doi.org/10.1016/j.envres.2018.10.023

Gonzalez-Merchan, Carolina, Sylvie Barraud, Sébastien Le Coustumer, and Tim Fletcher. 2012."Monitoring of Clogging Evolution in the Stormwater Infiltration System and Determinant Factors." European Journal of Environmental and Civil Engineering 16, no.1 (June): 34-47. Accessed May 23, 2019. http://dx.doi.org/10.1080/19648189.2012.682457.

https://doi.org/10.1016/j.jhydrol.2014.04.005

Khilar, K., Fogler, S. 1998. Migration of Fines in Porous Media. Netherlands: Springer Netherlands. Quoted in Torkzaban, Saeed, Scott A. Bradford, Joanne L. Vanderzalm, Bradley M. Patterson, Brett Harris, and Henning Prommer. 2015. "Colloid Release and Clogging in Porous Media: Effects of Solution Ionic Strength and Flow Velocity." Journal of Contaminant Hydrology 181 (October): 161-171. Accessed May 23, 2019. http://dx.doi.org/10.1016/j.jconhyd.2015.06.005.

Lazarova, V., Levine, B., Sack, J., Cirelli, G., Jeffrey, P., Muntau, H., et al. 2001. Role of water reuse for enhancing integrated water management in Europe and Mediterranean countries. Water Sci. Technol. 43, 25–33.

Lechner, M., Knapp, H., 2011. Carryover of Perfluorooctanoic Acid (PFOA) and Perfluorooctane Sulfonate (PFOS) from Soil to Plant and Distribution to thr Different Plant Compartments Studied in Cultures of Carrots (Daucus carota ssp. Sativus), Potatoes (Solanum tuberosum), and Cucumbers (Cucumis Sativus). https://doi.org/10.1021/jf201355y

Li, F., Fang, X., Zhou, Z., Liao, X., Zou, J., Yuan, B., Sun, W., 2019. Adsorption of perfluorinated acid onto soils: Kinetics, isotherms, and influences of soil properties. https://doi.org/10.1016/j.scitotenv.2018.08.209

Lyu, Y., Brusseau, M.L., Chen, W., Yan, N., Fu, X., Lin, X., 2018. Adsorption of PFOA at the Air-Water Interface during Transport in Unsaturated Porous Media. https://doi.org/10.1021/acs.est.8b02348

Machiwal D., Jha M., Singh V., Mohan C., Assessment and mapping of groundwater vulnerability to pollution: Current status and challenges, Earth-Science Reviews, Volume 185, 2018, https://doi.org/10.1016/j.earscirev.2018.08.009

Ning, C., Ma, h., Pedersen, C.M., Chang, H., Wang, Y., Quiao, Y., 2019. Interaction between environmental contaminant PFOA and PAMAM in water: F and H NMR studies. https://doi.org/10.1016/j.molliq.2019.03.057

Ozekin, K., Fulmer, A., 2019. Per- and Polyfluoroalkyl Substances: Background Technical Information. https://www.waterrf.org/sites/default/files/file/201909/PFCs_StateOfTheScience.pdf

Parise, M., & Gunn, J. (2007). Natural and anthropogenic hazards in karst areas: an introduction. Geological Society, London, Special Publications, 279(1), 1-3.

Piano di Tutela delle Acque. Regione Puglia.

Piccinini L., De Nardo M.T., Filippini M., Segadelli S., Vincenzi V., Gargin A., Hydrogeological protection of non-karstic fractured aquifers, December 2014 Geoingneria Ambientale e Mineraria 143(3):73-92 https://www.researchgate.net/publication/286234363_Hydrogeological_protection_of_non_karstic_fractured_aquifers/related

Ringleb J., Sallwey J., Stefan C., Assessment of Managed Aquifer Recharge through Modeling A Review, 2016, Water 2016, 8, 579; 10.3390/w8120579

Roels S., Vandersteen K., Carmeliet J., Measuring and simulating moisture uptake in a fractured porous medium, Advances in Water Resources 26 (2003) 237–246

Sasidharan, Salini, Scott Bradford, Jiří Šimůnek, and Kraemer. 2019. “Drywell Infiltration and Hydraulic Properties in Heterogeneous Soil Profiles.” Journal of Hydrology 570 (January): 598-611. Accessed May 23, 2019. http://dx.doi.org/10.1016/j.jhydrol.2018.12.073.

Sasidharan, Salini, Scott Bradford, Jiří Šimůnek, Bill DeJong, and Kraemer. 2018. “Evaluating Drywells for Stormwater Management and Enhanced Aquifer Recharge.” Advances in Water Resources 116, no. C (April): 167-77. Accessed May 23, 2019. http://dx.doi.org/10.1016/j.advwatres.2018.04.003.

Scher, D.P., Kelly, J.E., Huset, C.A., Barry, K.M., Hoffbeck, R.W., Yingling, V.L., Messing, R.B., 2018. Occurrence of perfluoroalkyl substances (PFAS) in gar-

dend produce at home with a history of PFAS contaminated drinking water. https://doi.org/10.1016/j.chemosphere.2017.12.179

Squadrone, S., Ciccotelli, V., Prearo, M., Favaro, L., Scanzio, T., Foglini, C., Abete, M.C., 2015. Perfluorooctane sulfonate (PFOS) and perfluorooctanoic acid (PFOA): emerging contaminants of increasing concern in fish from Lake Varese, Italy. https://doi.org/10.1007/s10661-015-4686-0

Standen K., Costa L., Monteiro J., In-Channel Managed Aquifer Recharge: A Review of Current Development Worldwide and Future Potential in Europe, Water 2020, 12, 3099; 10.3390/w12113099

Summerville N.D. (2019) "Simulating colloidal clogging of drywell infiltration devices: assessing strategies to reduce clogging". Thesis presents to the Department of Civil Engineering and Construction Engineering Management. California State University, Long Beach.

Todd, D.K., Mays, L.W., Third Edition. Groundwater Hydrogeology. Wiley.

Torkzaban, Saeed, Scott A. Bradford, Joanne L. Vanderzalm, Bradley M. Patterson, Brett Harris, and Henning Prommer. 2015. "Colloid Release and Clogging in Porous Media: Effects of Solution Ionic Strength and Flow Velocity." Journal of Contaminant Hydrology 181 (October): 161-171. Accessed May 23, 2019. http://dx.doi.org/10.1016/j.jconhyd.2015.06.005.

Torrent Resources. 2012. MaxWell IV Drainage System Drainage System Product Information and Design Features. Phenix Az: Torrent Resources Incorporated. Accessed May 27, 2019. http://www.torrentresources.com/wp-content/uploads/2014/06/MaxWell-IV-Insert- 8-2012_200.pdf.

Touma J., Comparison of different capillary models to predict the hydraulic conductivity from the water retention curve. IRD, UMR LISAH SupAgro-INRA-IRD, B.P. 434, 1004, Tunis, Tunisie

United States Environmental Protection Agency. 2003. Protecting Water Quality from Urban Runoff, by United States Environmental Protection Agency Nonpoint Source Control Branch. EPA 841-F-03-003. Accessed May 27, 2019. https://www3.epa.gov/npdes/pubs/nps_urban-facts_final.pdf

Van Genuchten M., Leij F , Skaggs T., Toride N., Bradford S., Pontedeiro E., Exact analytical solutions for contaminant transport in rivers August 2013 Journal of Hydrology and Hydromechanics 61(3):250-259 10.2478/johh-2013-0032

Voss C., Groundwater modeling fantasies, Hydrogeology Journal (2011) 19: 1281–1284, 10.1007/s10040-011-0789-z

Vurro M., Passarella G., 1998, Groundwater Field Experiences in Porous and Fissured Media

Xiao, F., Simcik, M.F., Halbach T.R., Gulliver, 2015. Perfluorooctane sulfonate (PFOS) and perfluorooctanoate (PFOA) in soil and groundwater of U.S. metropolitan area: Migration and implications for human exposure. https://doi.org/10.1016/j.watres.2014.09.052

Xu M, Eckstein Y (1995) Use of weighted least-squares method in evaluation of the relationship between dispersivity and field scale. Ground Water 33:905–908

Yadav B., Junaid S., Groundwater Vulnerability Assessment to Contamination Using Soil Moisture Flow and Solute Transport Modeling., 2014, American Society of Civil Engineers, 10.1061/(ASCE)IR .1943-4774.0000841

Yeh, T.J., Khaleel, R., Carroll, K.C., 2015. Flow Through Heterogeneous Geologic Media. Cambridge Pinder, G.F., Celia, M.A., 2006. Subsurface Hydrogeology. Wiley.

Zareitalabbad, P., Siemens, J., Hamer, M., Amelung, W., Perfluorooctanoic acid (PFOA) and perfluorooctanesulfonic acid (PFOS) in surface waters, sediments, soils, and wastewater – A review on concentrations and distribution coefficients. https://doi.org/10.1016/j.chemosphere.2013.02.024

Zhang H., Xu Y., Kanyerere T., A review of the managed aquifer recharge: Historical development, current situation and perspectives, Physics and Chemistry of the Earth, Parts A/B/C, Volumes 118–119, 2020, https://doi.org/10.1016/j.pce.2020.102887

Zhu Y., Zha Y., Tong J., Yang J., Method of coupling 1-D unsaturated flow with 3-D saturated flow on large scale, Water Science and Engineering, 2011, 4(4): 357-373 10.3882/j.issn.1674-2370.2011.04.001

APPENDICIES

APPENDIX A

1st SIMULATION OF TRANSPORT UNDER STEADY STATE CONDITIONS

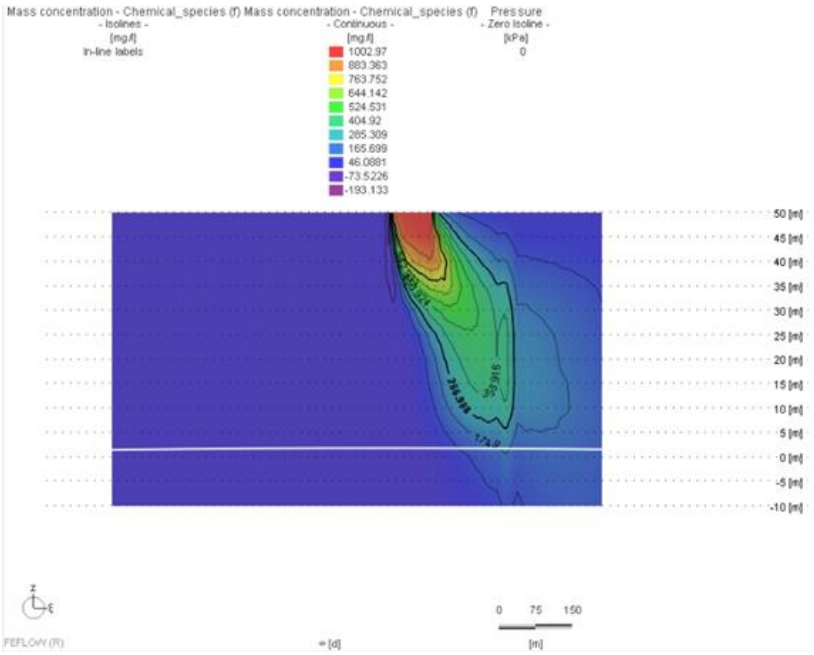

Fig. 7.1 – Mass concentration (aa) - 50% limestone porosity

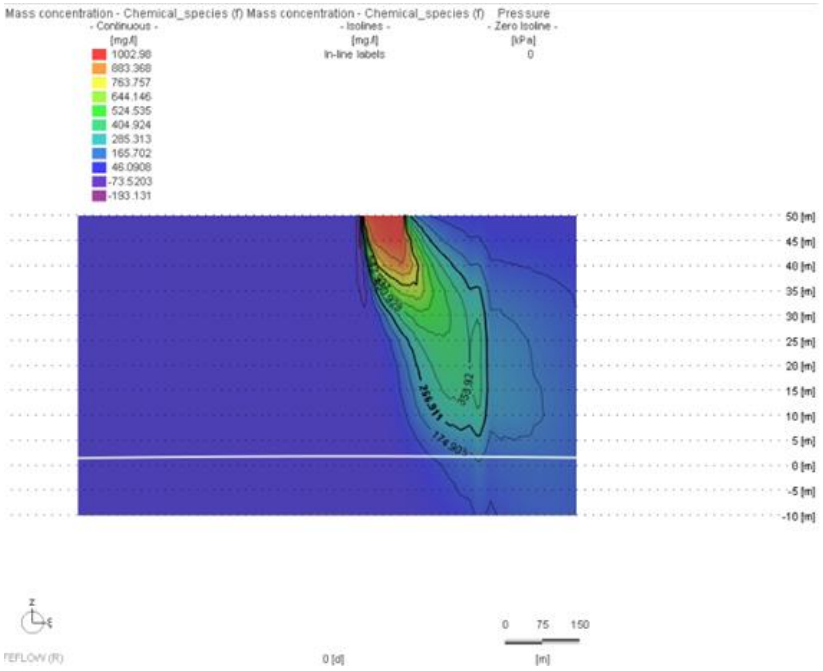

Fig. 7.2 – Mass concentration (aa) - 70% limestone porosity

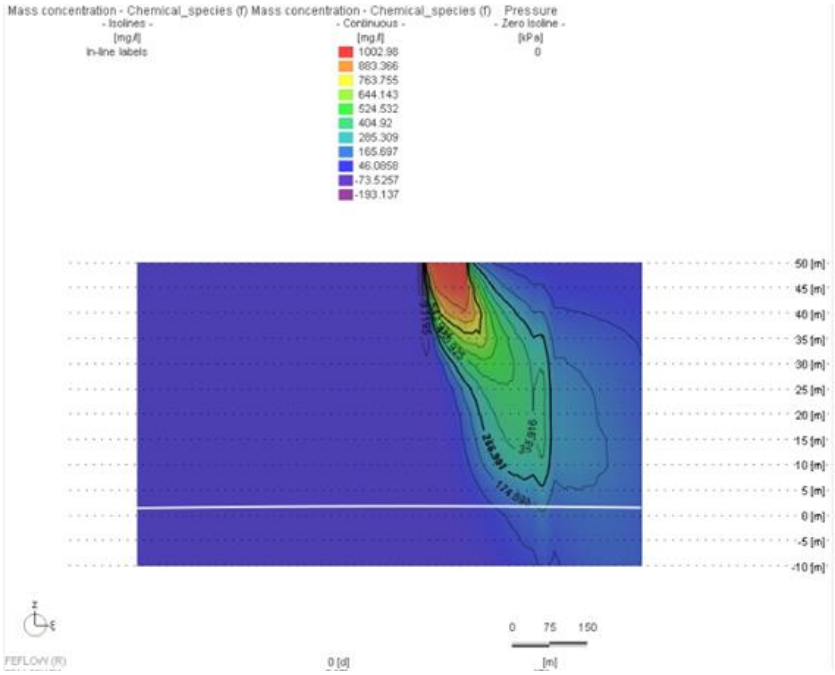

Fig. 7.3 – Mass concentration (aa) - 90% limestone porosity

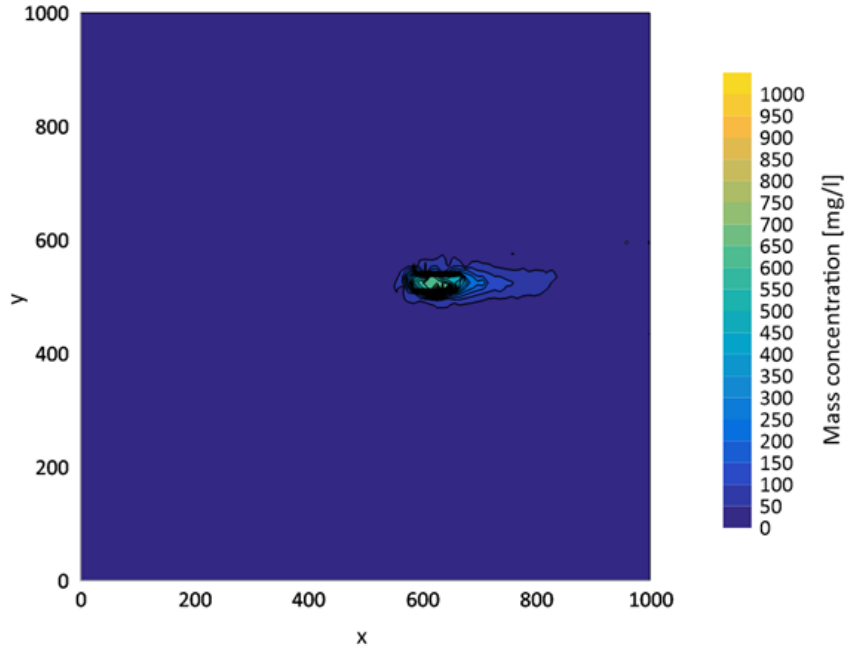

Fig. 7.4 – 50% limestone porosity - slice 2 (45 m s.l.m.)

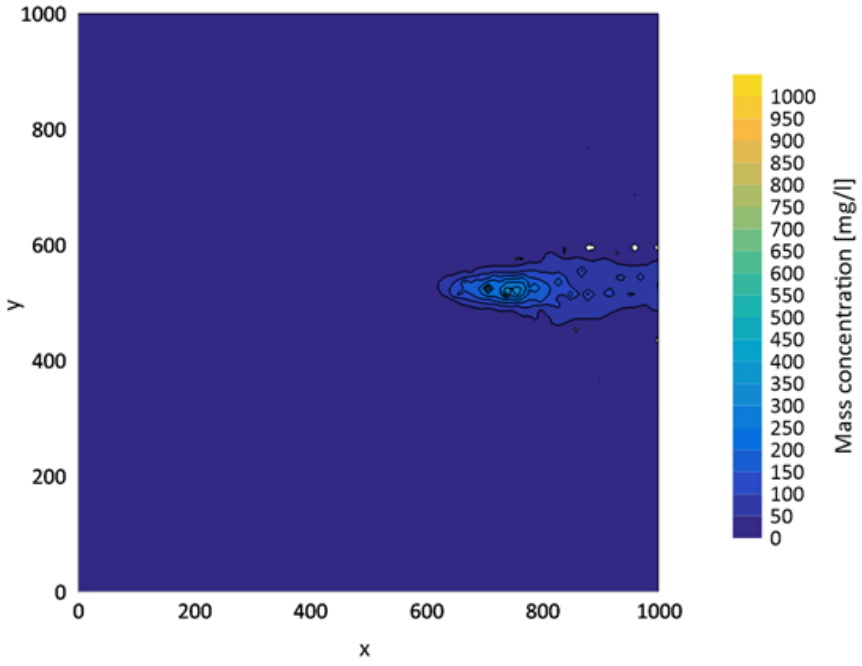

Fig. 7.5 – 50% limestone porosity - slice 5 (30 m s.l.m.)

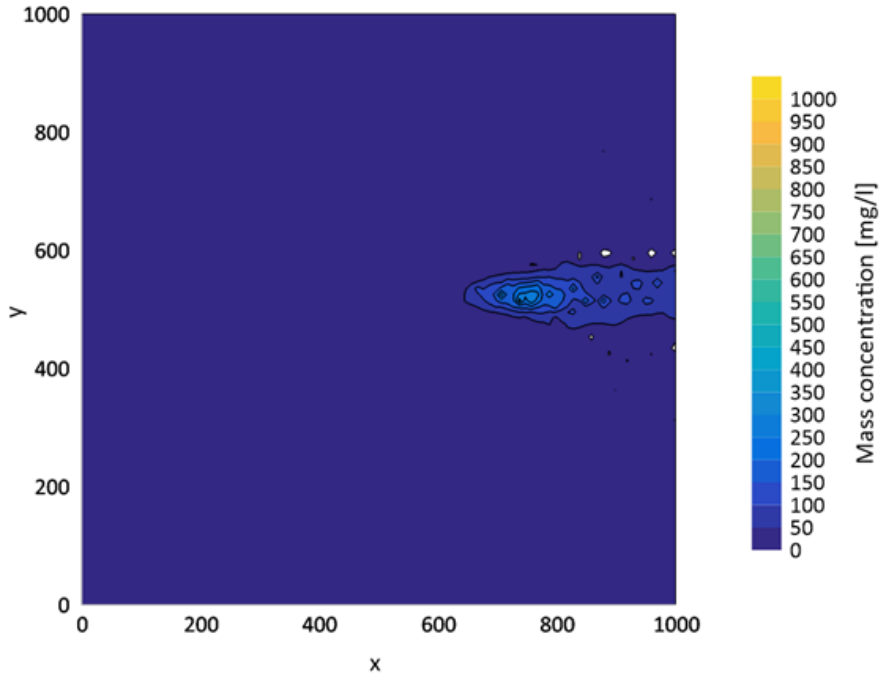

Fig. 7.6 – 50% limestone porosity - slice 7 (30 m s.l.m.)

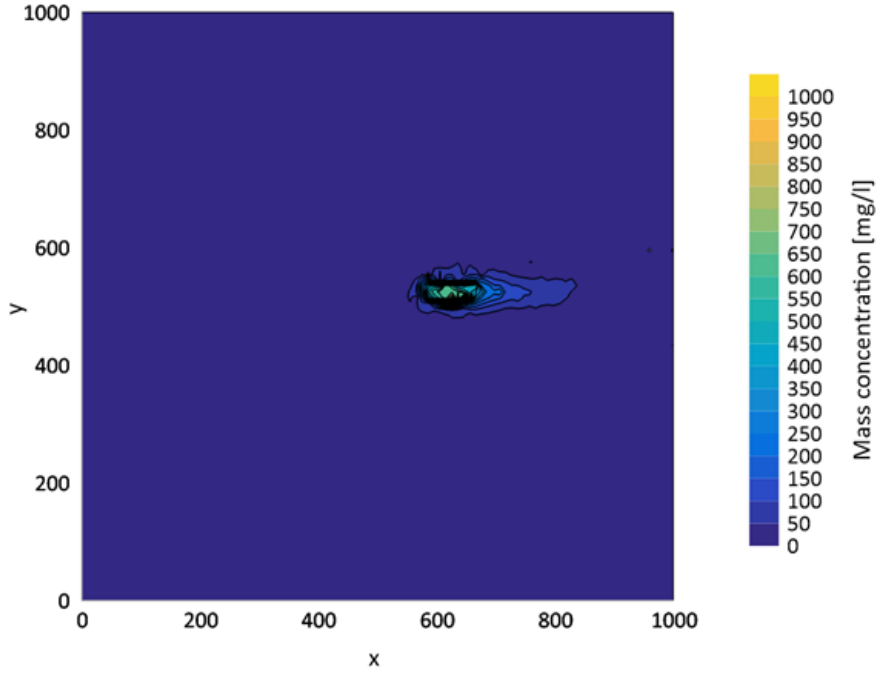

Fig. 7.7 – 70% limestone porosity - slice 2 (45 m s.l.m.)

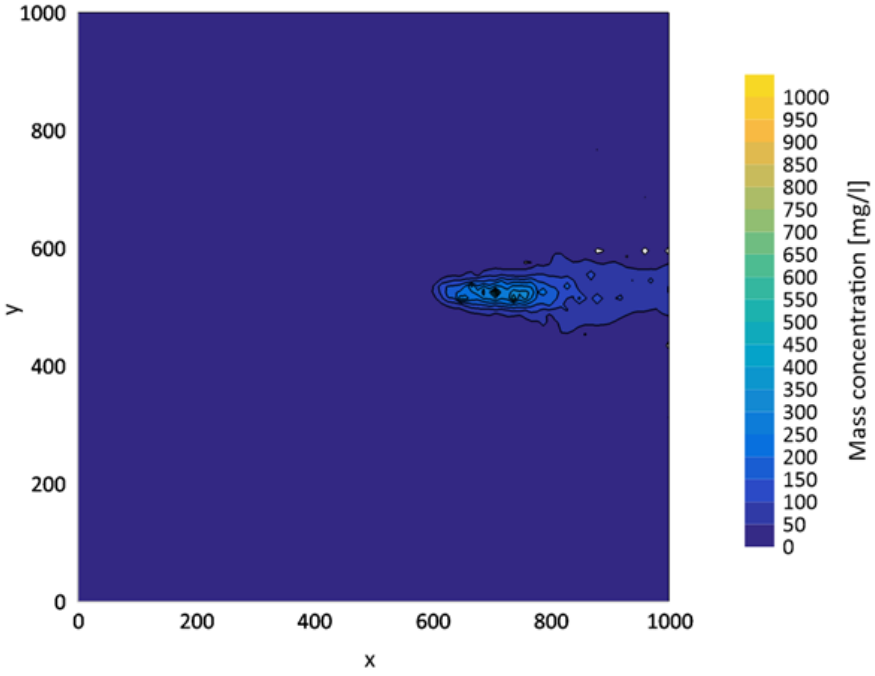

Fig. 7.8 – 70% limestone porosity - slice 5 (30 m s.l.m.)

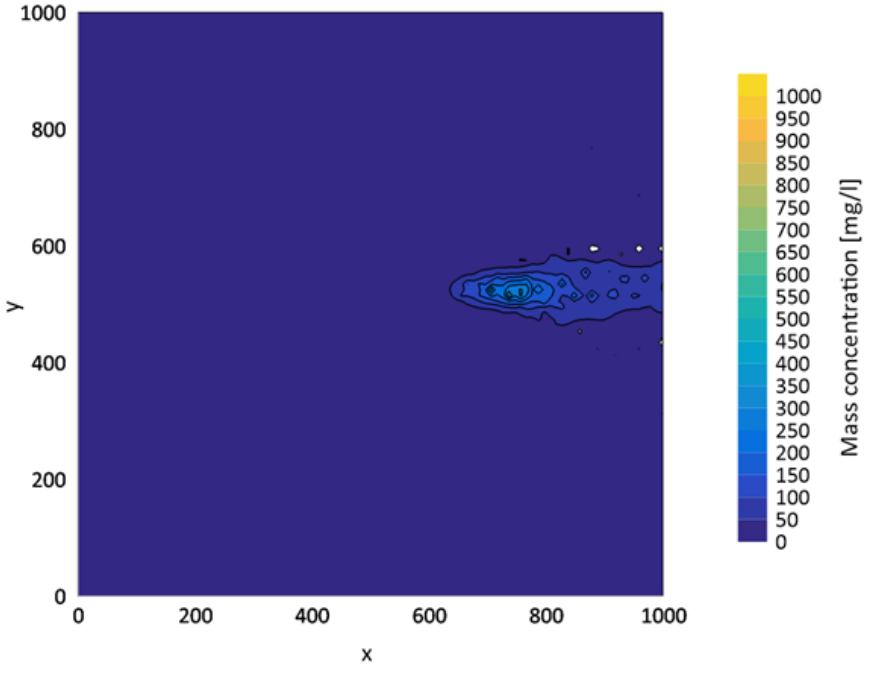

Fig. 7.9 – 70% limestone porosity - slice 7 (20 m s.l.m.)

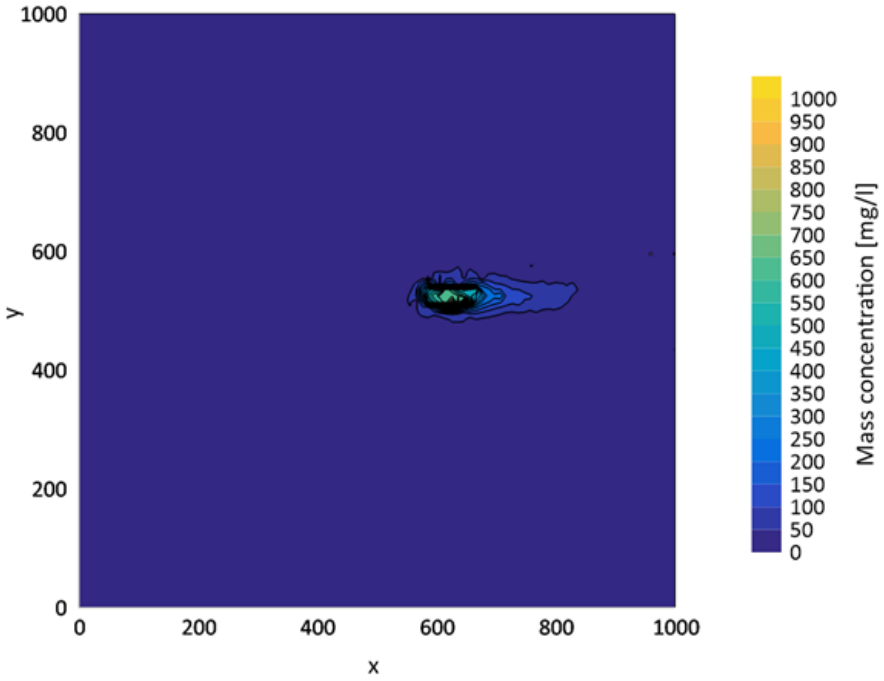

Fig. 7.10 – 90% limestone porosity - slice 2 (45 m s.l.m.)

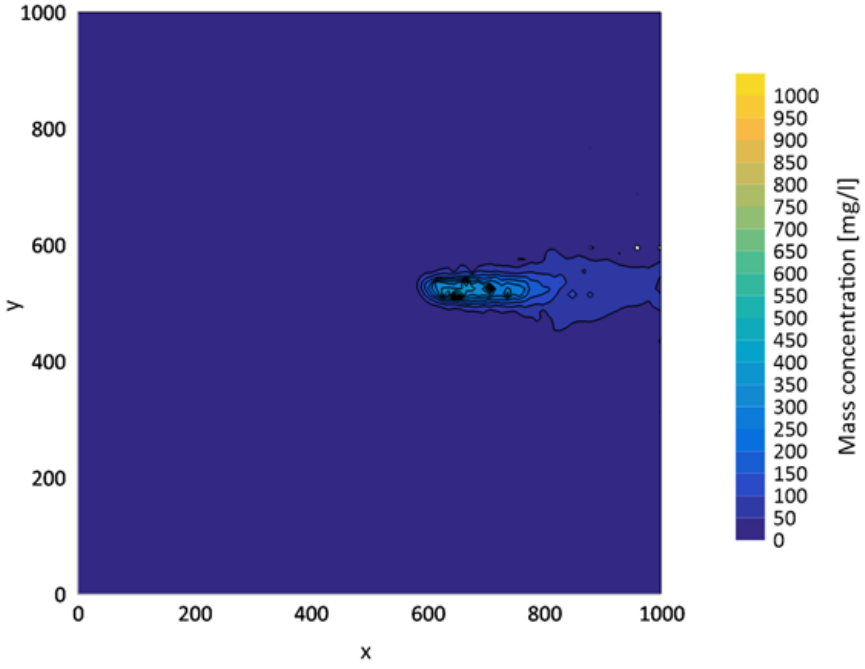

Fig. 7.11 – 90% limestone porosity - slice 5 (30 m s.l.m.)

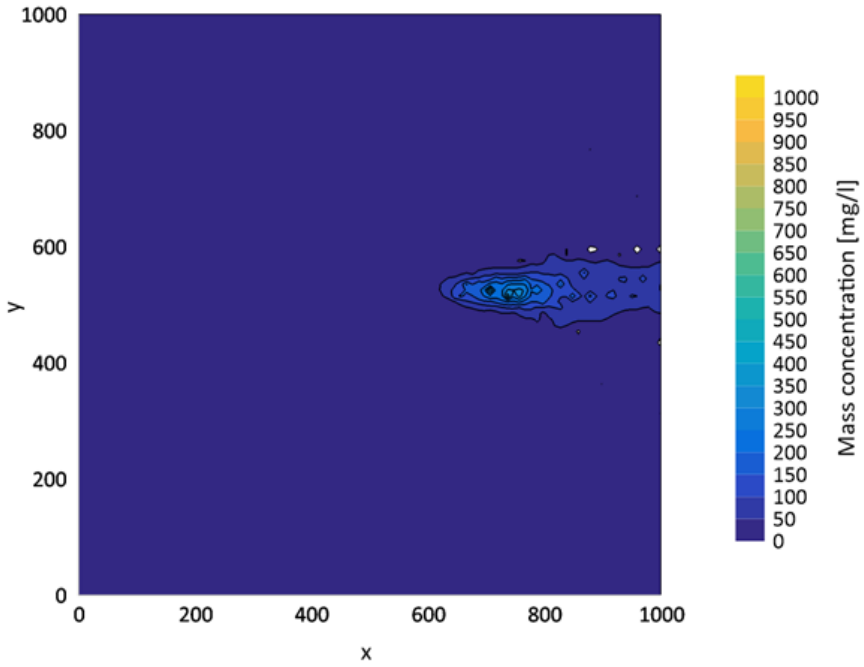

Fig. 7.12 – 90% limestone porosity - slice 7 (20 m s.l.m.)

APPENDIX B

2nd SIMULATION OF TRANSPORT UNDER STEADY STATE CONDITIONS

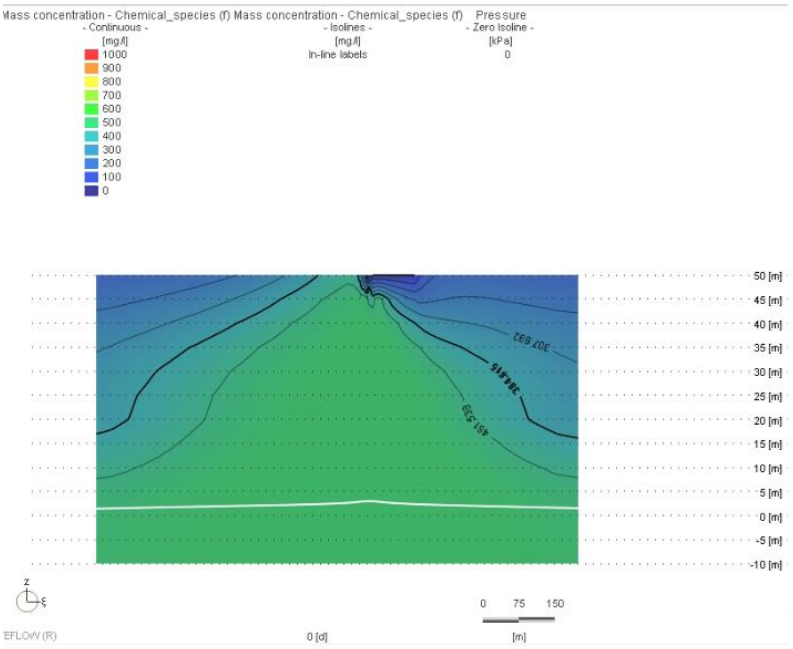

Fig. 7.13 – Mass concentration (aa) - 50% limestone porosity

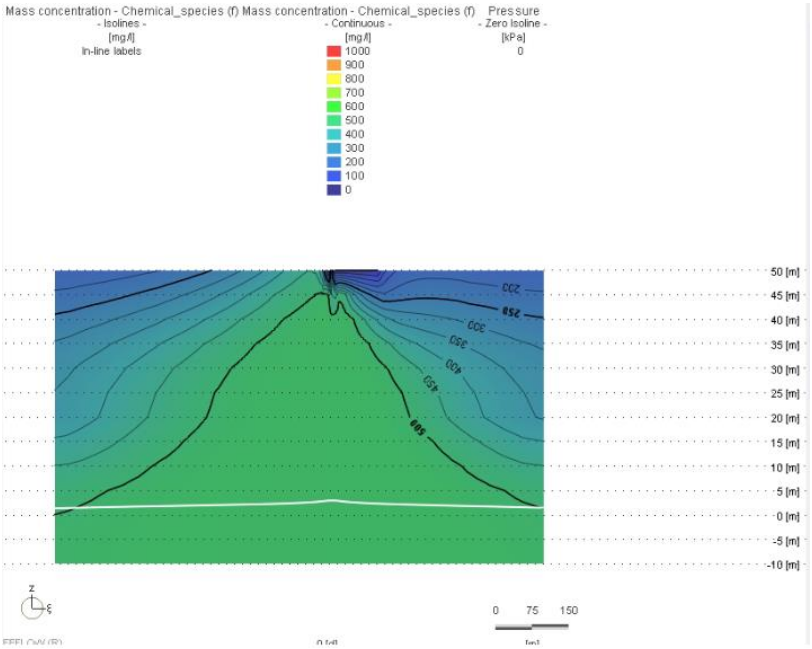

Fig. 7.14 – Mass concentration (aa) - 70% limestone porosity

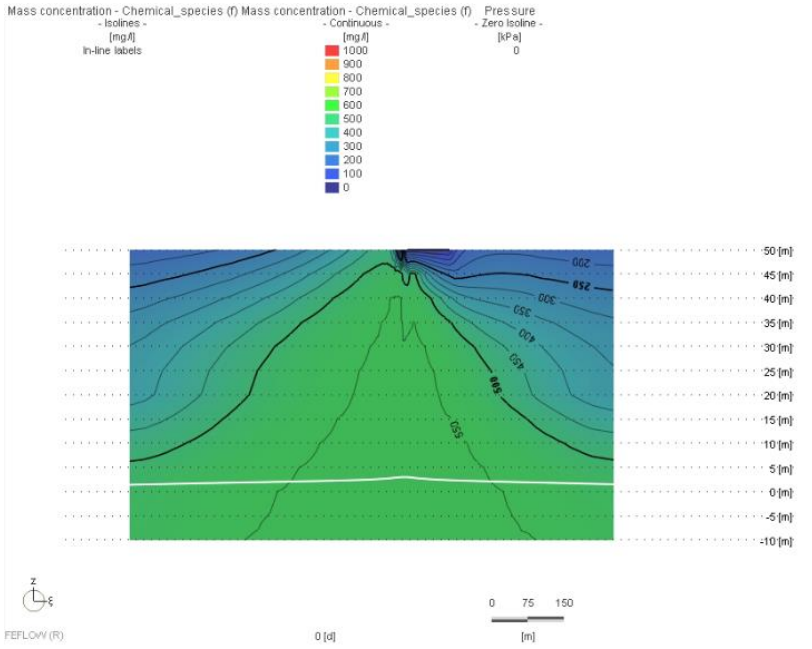

Fig.7.15 – Mass concentration (aa) - 90% limestone porosity

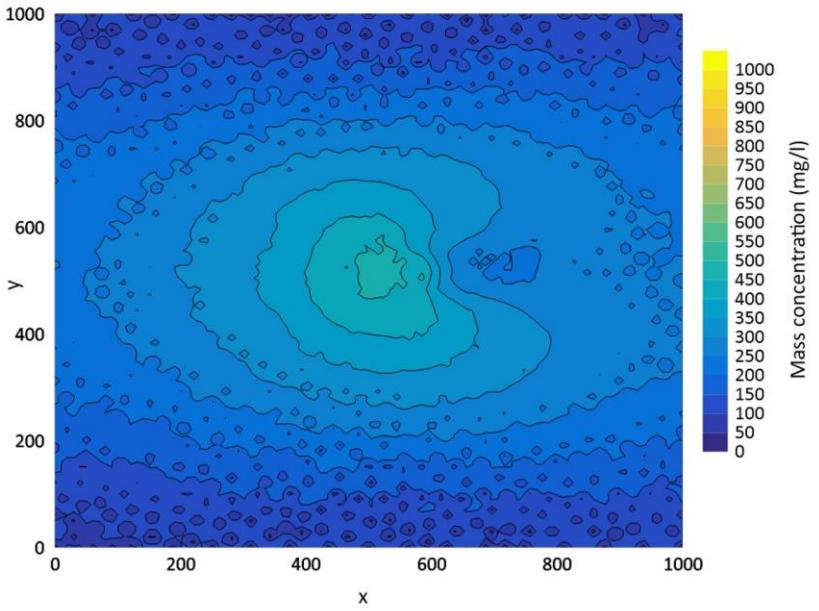

Fig. 7.16 – 50% limestone porosity - slice 2 (45 m s.l.m.)

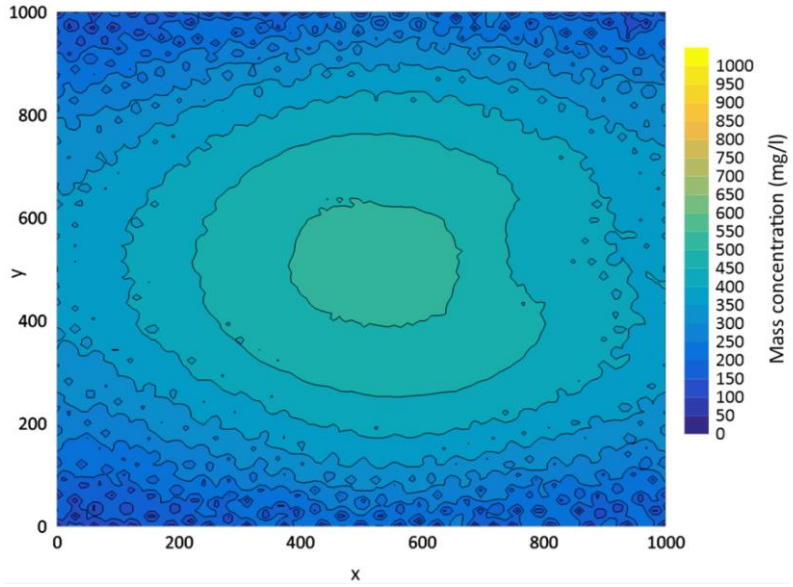

Fig. 7.17 – 50% limestone porosity - slice 5 (30 m s.l.m.)

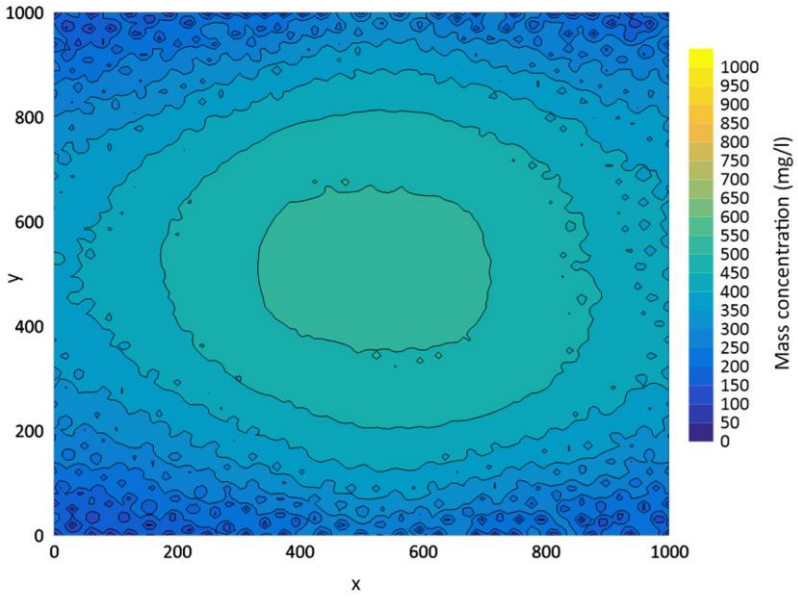

Fig. 7.18 – 50% limestone porosity % - slice 7 (20 m s.l.m.)

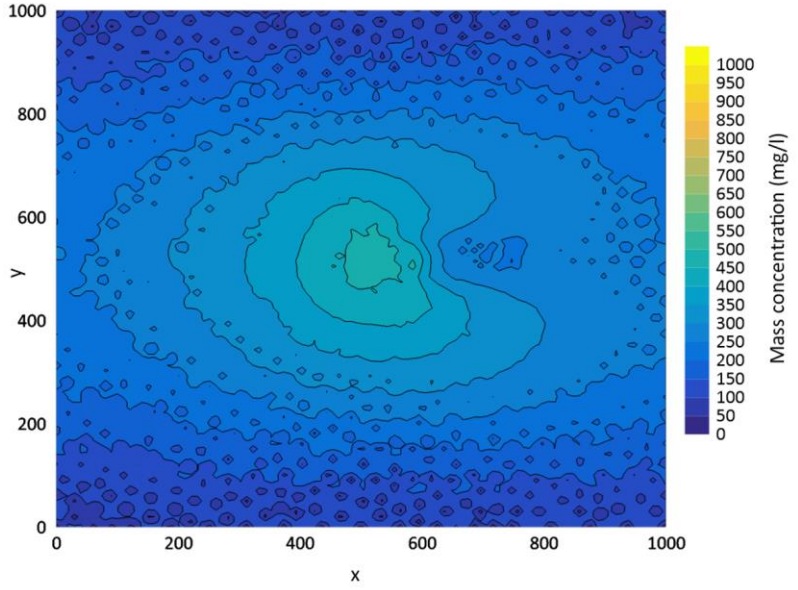

Fig. 7.19 – 70% limestone porosity - slice 2 (45 m s.l.m.)

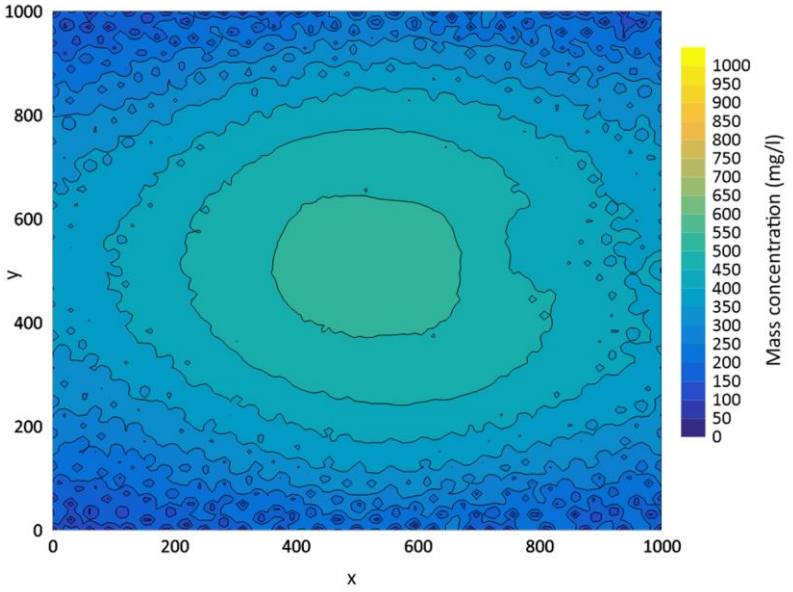

Fig. 7.20 – 70% limestone porosity - slice 5 (30 m s.l.m.)

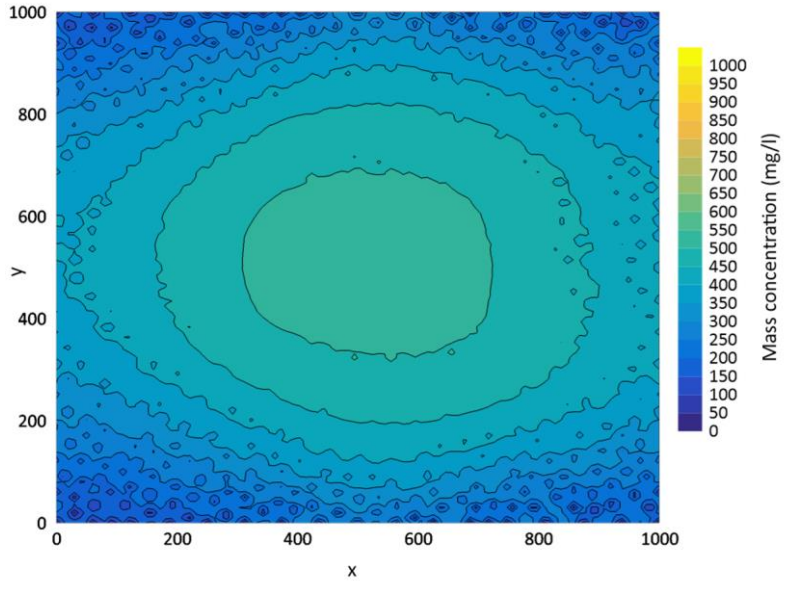

Fig. 7.21 – 70% limestone porosity - slice 7 (20 m s.l.m.)

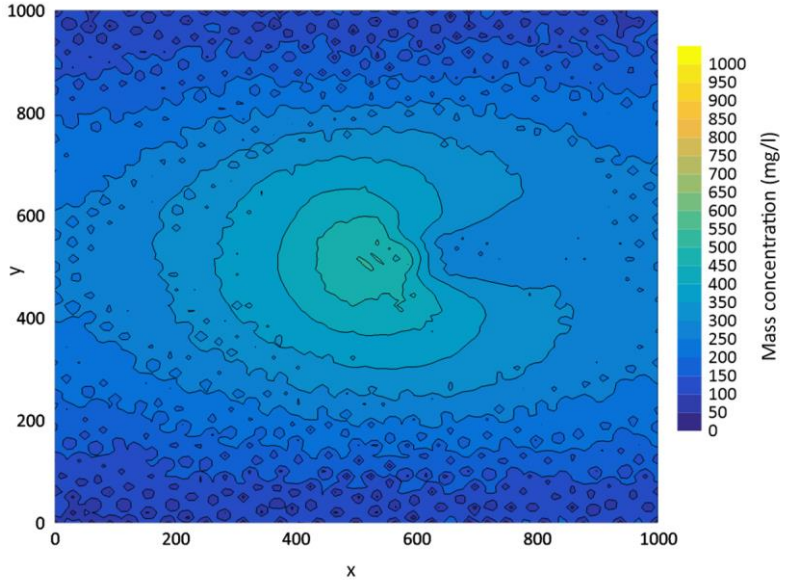

Fig. 7.22 – 90% limestone porosity - slice 2 (45 m s.l.m.)

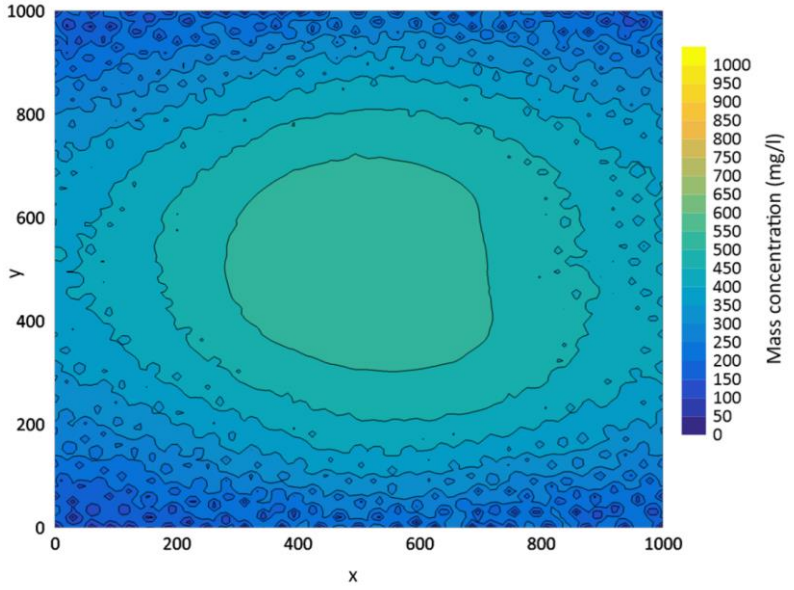

Fig. 7.23 – 90% limestone porosity - slice 5 (30 m s.l.m.)

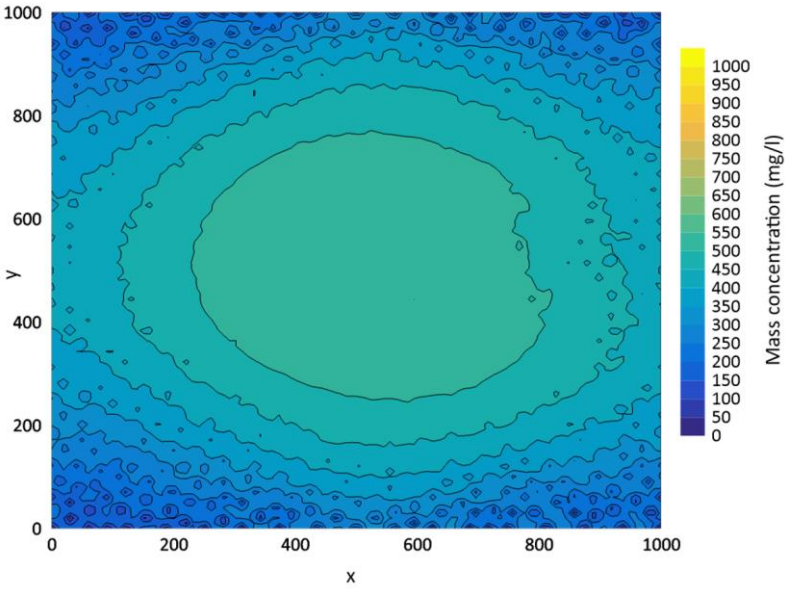

Fig. 7.24 – 90% limestone porosity - slice 7 (20 m s.l.m.)

APPENDIX C

SIMULATION OF TRANSPORT UNDER TRANSIENT CONDITIONS

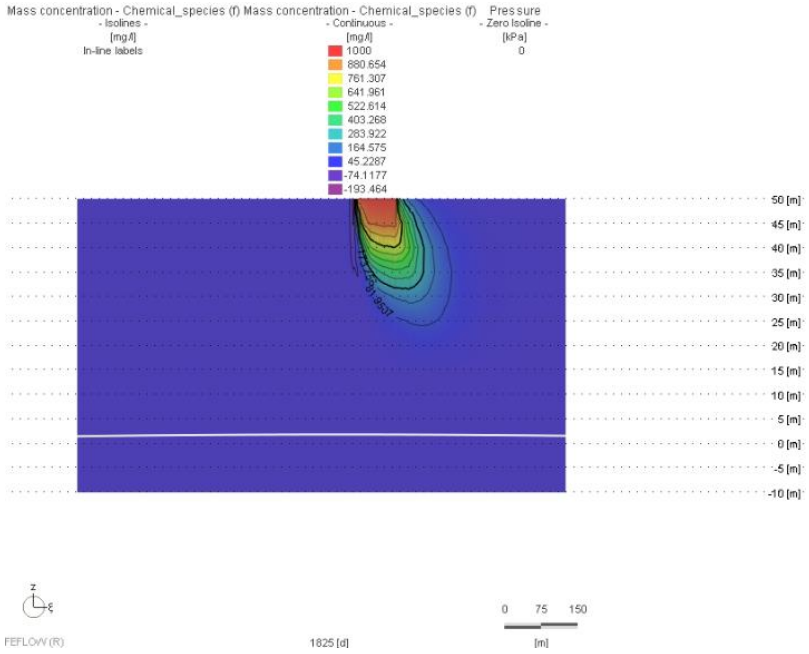

Fig. 7.25 – Mass concentration (aa) - 50% limestone porosity

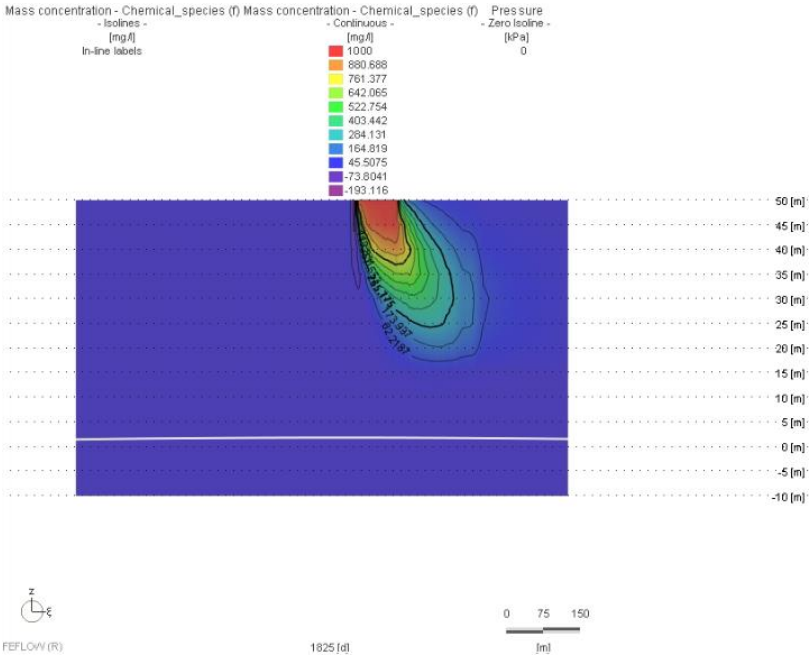

Fig. 7.26 – Mass concentration (aa) - 70% limestone porosity

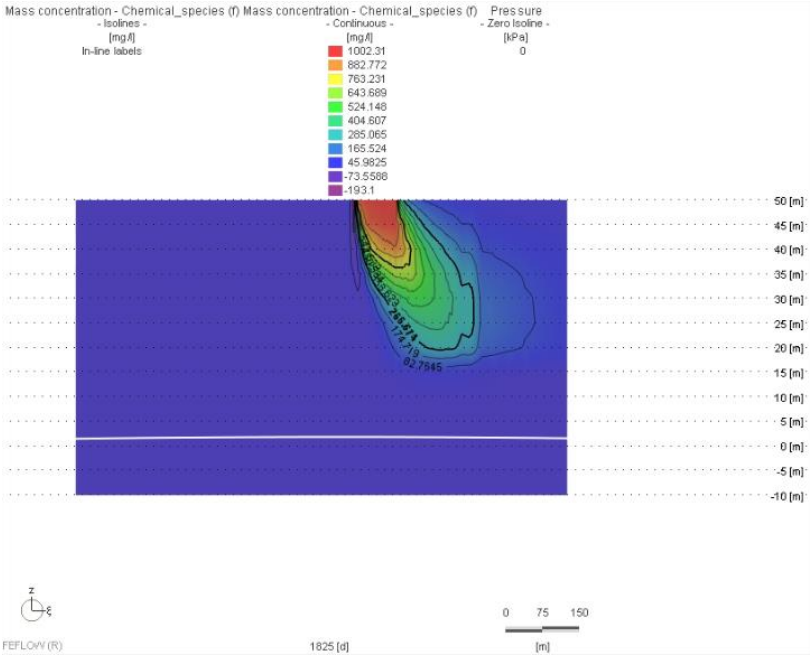

Fig. 7.27 – Mass concentration (aa) - 90% limestone porosity

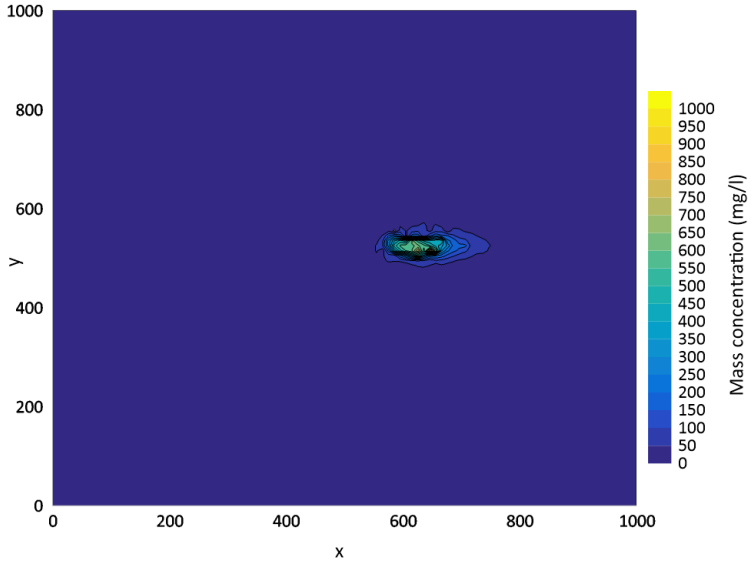

Fig. 7.28 – 50% limestone porosity - slice 2 (45 m s.l.m.)

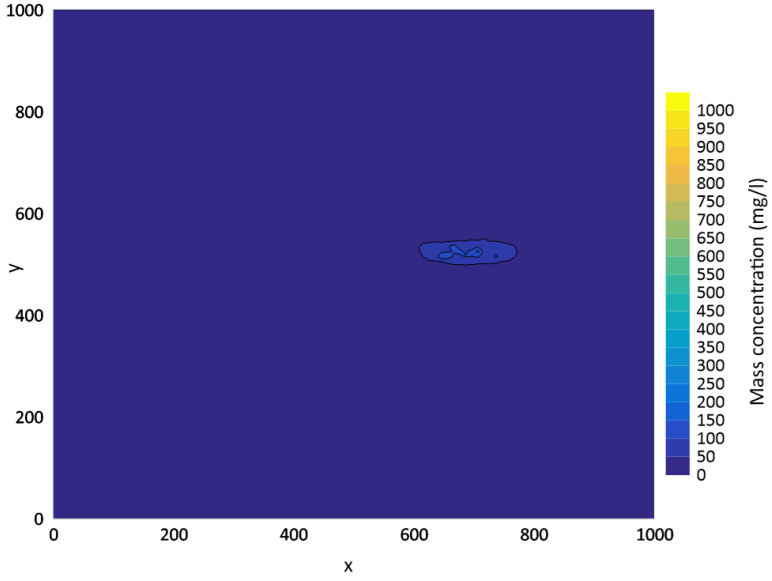

Fig. 7.29 – 50% limestone porosity - slice 5 (30 m s.l.m.)

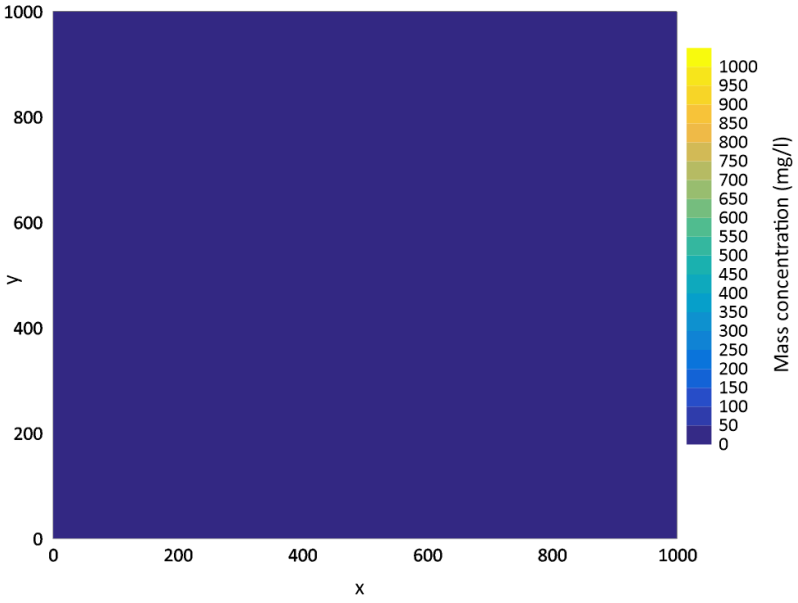

Fig. 7.30 – 50% limestone porosity - slice 7 (20 m s.l.m.)

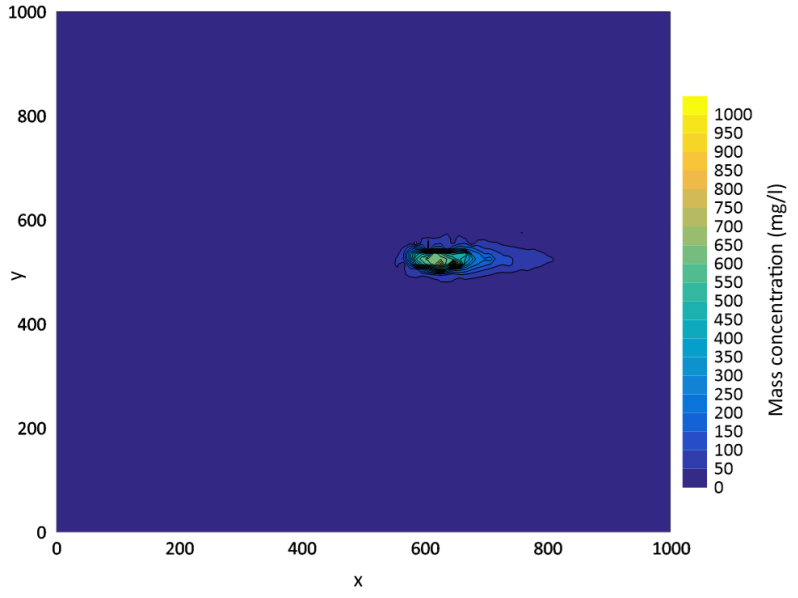

Fig. 7.31 – 70% limestone porosity - slice 2 (45 m s.l.m.)

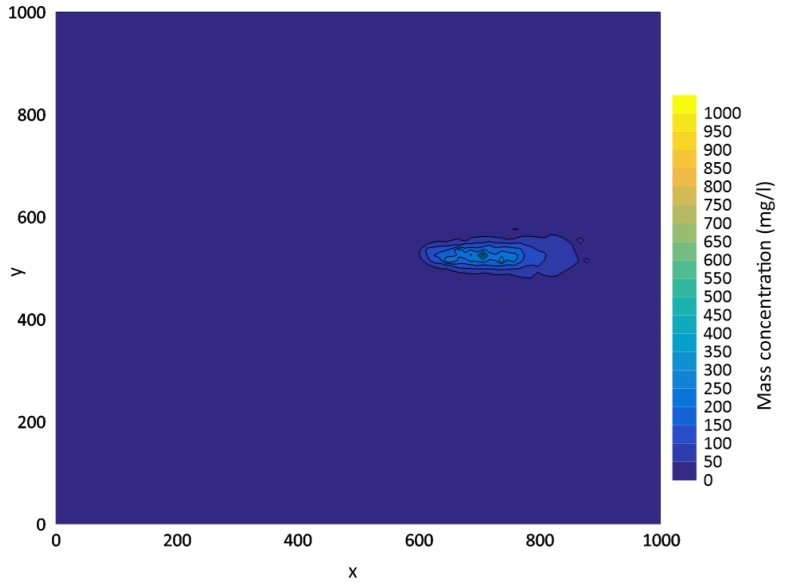

Fig. 7.32 – 70% limestone porosity - slice 5 (30 m s.l.m.)

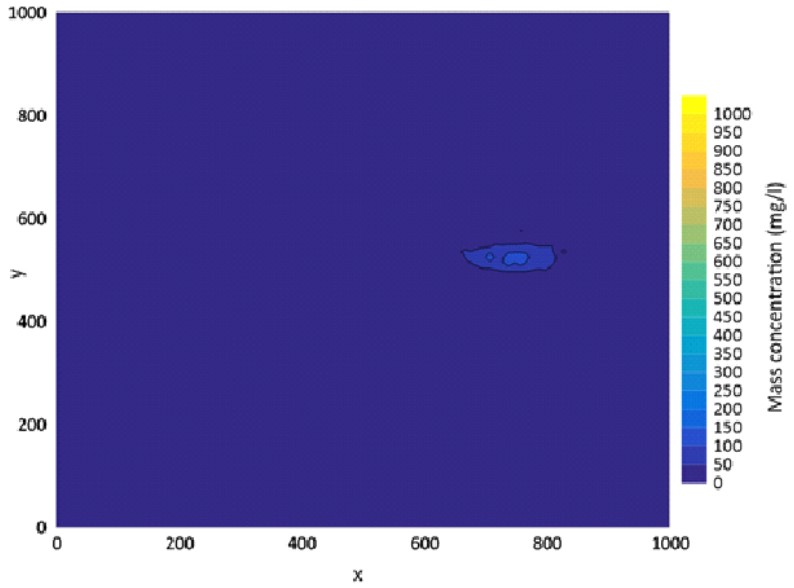

Fig. 7.33 – 70% limestone porosity - slice 7 (20 m s.l.m.)

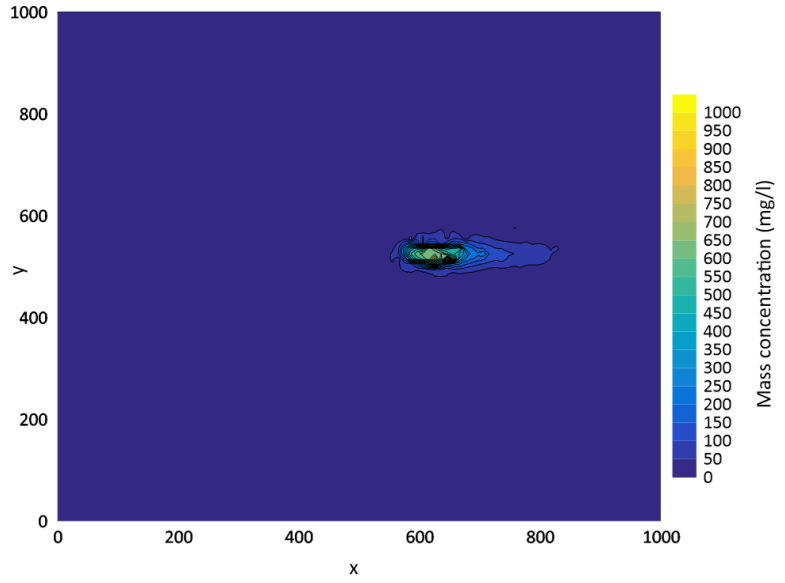

Fig. 7.34 – 90% limestone porosity - slice 2 (45 m s.l.m.)

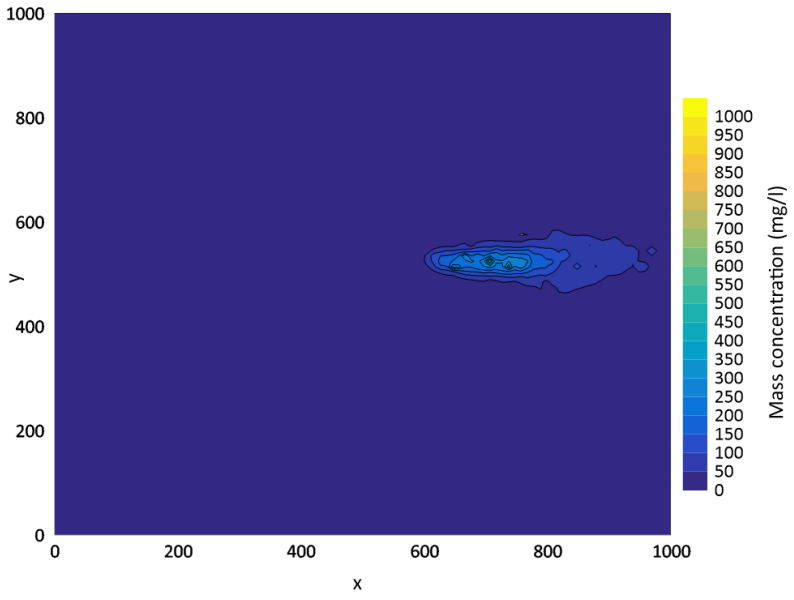

Fig. 7.35 – 90% limestone porosity - slice 5 (30 m s.l.m.)

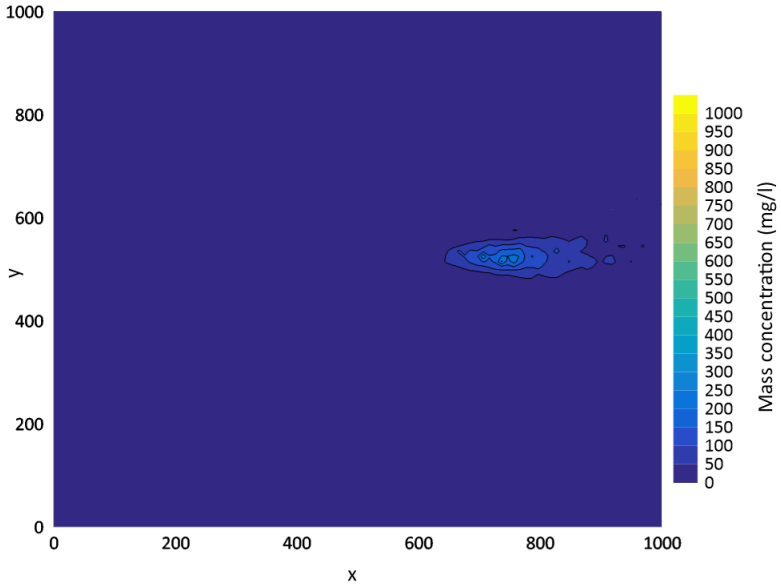

Fig. 7.36 – 90% limestone porosity - slice 7 (20 m s.l.m.)

CURRICULUM VITAE

ALESSANDRA CAMPOBASSO

Bari, 28/08/89
Via Santa Croce, 14
70019, Triggiano, Bari
campobassoalessandra@gmail.com

PROFESSIONAL - EXPERIENCES

October 6, 2021 - in progress:
Professional technical collaborator Civil Engineer at Azienda Ospedaliero - Universitaria Consorziale Policlinico di Bari (Piazza Giulio Cesare 11, Bari).

November 1, 2018 - in progress:
Ph.D. Student at DICATECh – Dpt. Of Civil, Environmental, Land, Building Engineering and Chemistry of Polytechnic University of Bari. (Via Edoardo Orabona, 4, 70126 Bari, ITA)
"Risk and environmental, territorial and building Ph.D." (course no.34)

August 1, 2019 - February 26, 2020:
Visiting Ph.D. Student at California State University Long Beach (1250 Bellflower Blvd, Long Beach, CA 90840, USA)
Study and modelling of contaminant transport mechanisms (PFAS) in groundwater using MODFLOW software.

Master Course in Civil Engineering (45 hours): "Groundwater flow: principles and modelling".

November 1, 2017 - October 31, 2018:
Civil engineer at T&A- Tecnologia & Ambiente s.r.l. (S.P. 237 per Noci, 8 – 70017 Putignano (BA)).
Research activities in the field of environmental development, with particular attention to air and water purification treatments.
Support for statistical processing and interpretation of data related to contamination of groundwater bodies.

November 1, 2016 - September 30, 2017:
Civil engineer at Arkè ingegneria s.r.l. (Via Imperatore Traiano, 4, 70126, Bari).
Design and arrangement of hydraulic works.

Study of analysis and mitigation of hydrogeological risk.

July 18, 2016 - October 31, 2016:
Curricular internship at Acquedotto Pugliese S.p.A. (Via Salvatore Cognetti, 36, 70121 Bari)
Monitoring of effluents discharged on the soil from sewage treatment plants. Work assistance for construction and maintenance of sewage treatment plants.

June 24, 2013 - July 31, 2013:
Curricular internship at Autorità di Bacino Distrettuale dell'Appennino Meridionale Sede Puglia. (SP62, 70010, Bari)
Study assistance of the qualitative and quantitative monitoring system of groundwater bodies in Apulia Region.

EDUCATION

February 19, 2018 - March 18, 2018:
Short master's in "Tutela dell'Ambiente e contrasto a Ecomafie e Eco-reati" at the Department "Ionian in Legal and Economic Systems of the Mediterranean: society, environment, cultures" - Allevi Guardia di Finanza Legion (100 hours).

April 2016 (Second Session State Exams):
Qualification to the exercise of the profession of Engineer.
Registration to the No. A11086 of the Register of Engineers of the Province of Bari, Section A. (Order and date of registration: Bari 26/06/2017)

October 14, 2016:
Master's Degree in Civil Engineering, Hydraulics, at Polytechnic of Bari.
Vote 110/110 cum laude. Thesis title: "Alternative delivery scenarios of effluents from sewage treatment plants", Prof. Ing. U. Fratino.

February 2014:
Bachelor's Degree in civil engineering at Polytechnic of Bari.
Thesis title: "Extension of the groundwater monitoring network in Apulia", Prof. Ing. A. Castorani, Prof. Ing. A. R. Di Santo.

June 2008:
Diploma of classical maturity at the Liceo Quinto Orazio Flacco of Bari.

TECHNICAL SKILLS

ArcGIS: GREAT
AutoCAD: GREAT
MODFLOW: EXCELLENT
FEFLOW: GREAT
FLO-2D: VERY GOOD
Surfer: VERY GOOD

RStudio: VERY GOOD
MATLAB: GOOD
HEC-RAS: GOOD
PAST: GOOD

LANGUAGE SKILLS

ENGLISH: EXCELLENT
English course at Wall Street Institute in Bari

COMPUTER SKILLS

26/05/2009
ECDL CERTIFICATE (N.IT1293684)